Synoptical and mesoscale weather situations associated with tornadoes in Europe

DIPLOMA THESIS

Institute of Geography, University of Zurich (GIUZ)

Supervisor: Dr. Michael Sprenger (IAC ETH)
Co-Supervisor: Dr. Richard W. Moore (IAC ETH)
Faculty representative: Prof. Wilfried Haeberli

Author: Michael Graf

Date: June 28, 2008

Cover photo: *F2 tornado near Tubize (Belgium) recorded on the 1st October 2006 at 1610 UTC (1810 local time) by Karel Holvoet.*

Contents

Chapter 1

Introduction

Tornadoes are mainly associated with the United States, but they occur in the midlatitudes all over the world. Also in Europe many tornado events were recorded in the last years. The main reason for that is the emergence of the internet. But already in the 20th and even 19th century a remarkably number of tornadoes have been recorded in Europe. The reason for that is: tornado research has its origin in Europe. The pioneer of tornado research was Alfred Wegener, who began to investigate tornado events systematically between 1880 and 1916. He built up a first comprehensive climatology. Later, Johannes P. Letzmann continued his research from 1916 until 1940. He stopped his investigations during the Second World War[1]. After the Second World War tornado research in Europe was no longer continued. Only a few works were published about strong tornado events in the second half of the 20th century. After 1950 tornado research was mainly practiced in the United States. Only in the last 10 years, tornado research has been again increasingly practiced in Europe.

1.1 Motivation

Tornadoes are with a maximum horizontal extension of about 2 *km* a rather small-scale phenomena. Nevertheless their impact on economic values and life can be huge, also in Europe where devastating tornadoes occur from time to time. Today, it is nearly impossible to forecast tornadoes in Europe with sufficient accuracy and a warning system does not exist. So, an improvement of forecast quality is needed. For that, a climatology can be very usefull, because it shows typical weather situations associated with tornadoes which are not necessarily the same as in the United States. Further, it is important to obtain a better understanding of the mechanism producing such storms, also in view of the coming climate change which will possibly have a large influence on them.

[1] from http://de.wikipedia.org/wiki/Tornado#Tornadoforschung

Damage: f scale	Little Damage	Minor Damage	Roof Gone	Walls Collapse	Blown Down	Blown Away	
	f0	f1	f2	f3	f4	f5	
Windspeed: F scale	18 m/s 65 km/h	33 119	51 184	71 256	93 335	117 421	143 515
	F0	F1	F2	F3	F4	F5	
To convert f scale into F scale, add the appropriate number							
Weak Outbuilding	-3	f3	f4	f5	f5	f5	f5
Strong Outbuilding	-2	f2	f3	f4	f5	f5	f5
Weak Framehouse	-1	f1	f2	f3	f4	f5	f5
Strong Framehouse	0	F0	F1	F2	F3	F4	F5
Brick Structure	1	-	f0	f1	f2	f3	f4
Concrete Building	2	-	-	f0	f1	f2	f3

Figure 1.1: The original F-scale shown with corrections for building strength (Fujita, 1992).

1.2 Literature

1.2.1 Definition

A *tornado* is a violently rotating column of air, in contact with the ground, either pendant from a cumuliform cloud or underneath a cumuliform cloud, and is often (but not always) visible as a funnel cloud[2]. Tornadoes occur always together with convective cells. This leads to the assumption that tornadoes are a convective caused phenomena. Commonly, but not always, they are accompanied by thunderstorms (Wegener, 1917). Obviously, high innercloud vertical windspeeds, which are occurring typically in thunderstorm cells, are not necessary for the tornado genesis.

1.2.2 Intensity scales

In order to determine the intensity of a tornado wind damages need to be investigated and finally classified. The most common used method is the Fujita scale. In Europe also the compatible TORRO scale with a doubled resolution compared to the Fujita scale is used.

Fujita scale

The Fujita scale (also called F-Scale) was developed by Fujita and Pearson (1973). The original scale as derived by Fujita was a 13-level scale (F0-F12) designed to smoothly

[2]taken from http://amsglossary.allenpress.com/glossary

connect the Beaufort scale and the Mach number scale. The gap between F0 and F1 corresponds to the eleventh and twelfth levels of the Beaufort scale, marked by the threshold value for hurricane force winds. On the original scale, the wind speeds for F11 and F12 corresponded to Mach numbers 0.9 and 1.0 respectively.

Fujita intended that only F0-F5 will be used in practice (see figure 1.1), as this covered all possible levels of damage to frame homes as well as the expected estimated bounds of wind speeds. He did, however, add a description for F6, which he phrased as "inconceivable tornado", to allow for wind speeds exceeding F5 and for possible future advancements in damage analysis which might show it[3].

The F-scale wind speeds are computed from

$$V_F = 6.30(F+2)^{1.5} \tag{1.1}$$

where V_F denotes the F-Scale wind speed ($m\ s^{-1}$)

Fujita (1992) recognized that residences were not homogeneously constructed and he devised corrections to compensate for assigning an F-scale rating. Recently, the Fujita scale has been replaced in the USA as the official system for rating tornado intensity by the so-called Enhanced Fujita scale (EF-scale) (Doswell III et al., 2007). The enhanced Fujita (EF) scale was introduced by McDonald (2002). The EF-scale was not used in this work.

TORRO scale

The TORRO scale was developed in England by Meaden (1976). It has a double resolution (see figure 1.2) compared to the F-scale. It is mainly used in the UK and in parts of Europe. The T-scale wind speeds are computed from

$$V_T = 2.36(T+4)^{1.5} \tag{1.2}$$

where V_T denotes the T-Scale wind speed ($m\ s^{-1}$)

1.2.3 Theories of tornadogenesis

Burgess and Donaldson (1979) distinguish between 2 types of tornadoes supercell and non-supercell tornadoes.

Non-supercell tornadoes

On the basis of numeric simulations it was formerly accepted that the tornado results primarily from the concentration of vorticity by horizontal convergence. Thus, vertical vorticity from the environment is amplified by values within the range of the tornado

[3] from http://en.wikipedia.org/wiki/Fujita_scale

	Unterkritisch (Sub–critical)				Schwach (Weak)			
Fujita	F-2		F-1		F0		F1	
TORRO	T-4	T-3	T-2	T-1	T0	T1	T2	T3
Beaufort	B0, B1	B2, B3	B4, B5	B6, B7	B8, B9	B10, B11	B12, B13	B14, B15
v in m s^{-1}	0 – 3	3 – 7	7 – 12	12 – 18	18 – 25	25 – 33	33 – 42	42 – 51
v in km h^{-1}	0 – 11	11 – 25	25 – 43	43 – 65	65 – 90	90 – 119	119 – 151	151 – 184
Δv in m s^{-1}	3	4	5	6	7	8	9	9
$\bar{S}_-$ in %	0.0	0.0	0.0	0.01	0.05	0.10	0.25	0.80
$\bar{S}_+$ in %	0.0	0.0	0.0	0.0	0.01	0.05	0.10	0.25
	Signifikant (Significant)							
	Stark (Strong)				Verheerend (Violent)			
Fujita	F2		F3		F4		F5	
TORRO	T4	T5	T6	T7	T8	T9	T10	T11
Beaufort	B16, B17	B18, B19	B20, B21	B22, B23	B24, B25	B26, B27	B28, B29	B30, B31
v in m s^{-1}	51 – 61	61 – 71	71 – 82	82 – 93	93 – 105	105 – 117	117 – 130	130 – 143
v in km h^{-1}	184 – 220	220 – 256	256 – 295	295 – 335	335 – 378	378 – 421	421 – 468	468 – 515
Δv in m s^{-1}	10	10	11	11	12	12	13	13
$\bar{S}_-$ in %	3.0	10.0	30.0	90.0	100	100	100	100
$\bar{S}_+$ in %	0.80	3.0	10.0	30.0	60.0	80.0	90.0	95.0

Figure 1.2: A comparison between Fujita and TORRO intensity scale according to Meaden (1976) and Fujita and Pearson (1973). The table was published by Hubrig (2004).

(Ward, 1972; Lewellen, 1993). Stretching of vorticity under the updraft of a convective cell (see figure 1.3) seems to be the main development mechanism for non-supercell tornadoes. It is probably similar to that of a waterspout and so-called “cold air funnels“ (Cooley, 1978; Burgess and Donaldson, 1979).

Supercell tornadoes

In the case of supercell tornadoes, there’s a mesoscale circulation (mesocyclone) embedded in the midlevel region of the convective cell. This circulation can propagate towards the ground during or shortly before the tornado develops (Dowell and Bluestein, 1997). This type of tornado is generally larger, stronger and more long-lived than non-supercell tornadoes. It turned out that this type of tornado develops not directly under the updraft region of the supercell, but in a zone with high horizontal gradients of environmental vertical vorticity (Ray et al., 1976; Lemon and Doswell III, 1979; Rotunno and Klemp, 1985). This contradicts the mechanism in non-supercell tornadoes, where maximum environmental vorticity values should be situated under the tornado.

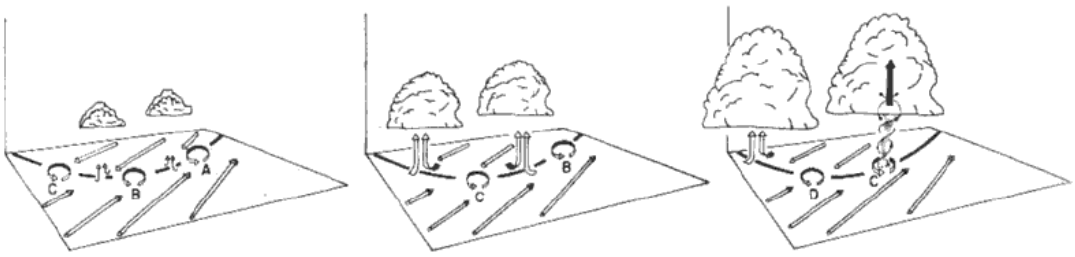

Figure 1.3: Development of non-supercell tornadoes along a convergent shearzone according to Wakimoto and Wilson (1989). The arrows indicates wind direction, the solid line the shear zone. The letters mark zones with high values of vorticity which can be amplified under an updraft of a convective cell leading to an tornado.

Generally, it is accepted that the tilting of horizontal vorticity into the vertical causes the rotation of the mesocyclone in the middle part of the supercell. The horizontal vorticity is caused in this case by vertical wind shear (Barnes, 1970; Rotunno and Klemp, 1985). However, the emergence of rotation in the lower layers is disputed. Numerical simulations of Rotunno and Klemp (1985) points out that for a rotation in the lower layers evaporative cooled air must be present at ground level. As soon as this pool of cold air has developed, horizontal vorticity is produced by baroclinic effects. If this zone comes under the upwind range, horizontal vorticy is tilted into vertical vorticity ('tilting') and under the upwind by acceleration stretched. Contrary to the work of Rotunno and Klemp (1985), simulations of Walko (1993) showed that horizontal vorticity could be the cause for the low level circulation.

On the doppler radar image a *tornadic vortex signature (TVS)* is visible in certain cases. A TVS is a Doppler weather radar detected rotation algorithm that indicates a strong possibility of a tornado. In most cases, the TVS is a tornado cyclone aloft, not a tornadic circulation[4]. However, many tornadoes show no signature of a mesocyclone or TVS (Wilson, 1986). Davies-Jones (1985) assumes that almost all TVS are connected with a tornado, but not each tornado shows a TVS. The TVS develops typically at midlevel and spreads then upwards and downwards. It can however also first appear at low levels or develop over large vertical distance at the same time. Usually the tornado develops only when a TVS is detected at low level (Brown et al., 1978). This contradicts the general assumption that the tornado develops at ground level (Rotunno, 1986; Rasmussen et al., 1994).

The *rear flank downdraft (RFD)* seems to play an important role for the genesis of supercell tornadoes (Ludlam, 1963; Fujita, 1975; Burgess et al., 1977; Barnes, 1978; Lemon and Doswell III, 1979) (see figure 1.4). The tornado develops normally between the storm inflow and the RFD (Dowell and Bluestein, 1997). The temperature of the

[4]from http://en.wikipedia.org/wiki/Tornado_vortex_signature

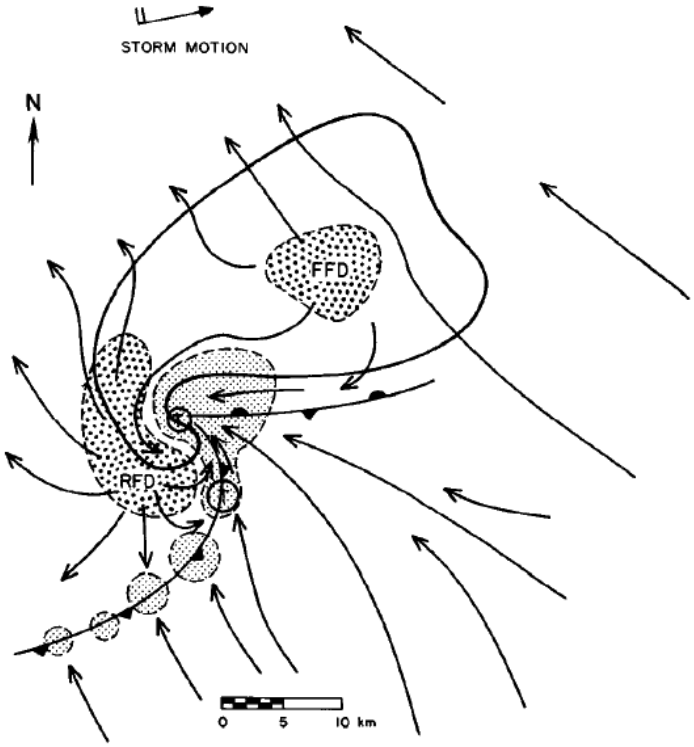

Figure 1.4: Schematical plan view of a tornadic thunderstorm near the surface. The thick line encompasses the radar echo. The barbed line denotes the boundary between the warm inflow and cold outflow and illustrates the occluding gust front. Low-level position of the updraft is finely stippled, while the forward-flank(FFD) and rear-flank (RFD) downdrafts are coarsely stippled. Storm-relative surface flow is shown along with the likely location of tornadoes (encircled T's) (from Lemon and Doswell III (1979) and adapted by Davies-Jones (1985)).

RFD obviously plays an important role during tornado genesis. On the average the temperatures of the RFD are in tornadic supercells only slightly lower (-1.5°C) than in the warm inflow section of the cell, while in non-tornadic supercells the temperature difference of -4.5°C is clearly more pronounced (Markowski, 2001; Grzych et al., 2006).

1.2.4 European climatology

In Europe (without UK) tornadoes occur mainly in summer (46.9%), followed by autumn (24.4%). Their occurrence is most rare during winter (12.7%) and spring (16.0%), however, there is also in this season still a considerable number of events. The most active time lies between May and September, the smallest activity takes place in December, March and April. A strong reduction of the events in October and a significant increase in January are found. In the USA the largest activity occurs in spring (54%) followed by summer with 27%. The minimal activity is in the autumn and winter (19%) (Schaefer et al., 1980). The seasonal distribution in the USA differs thus clearly

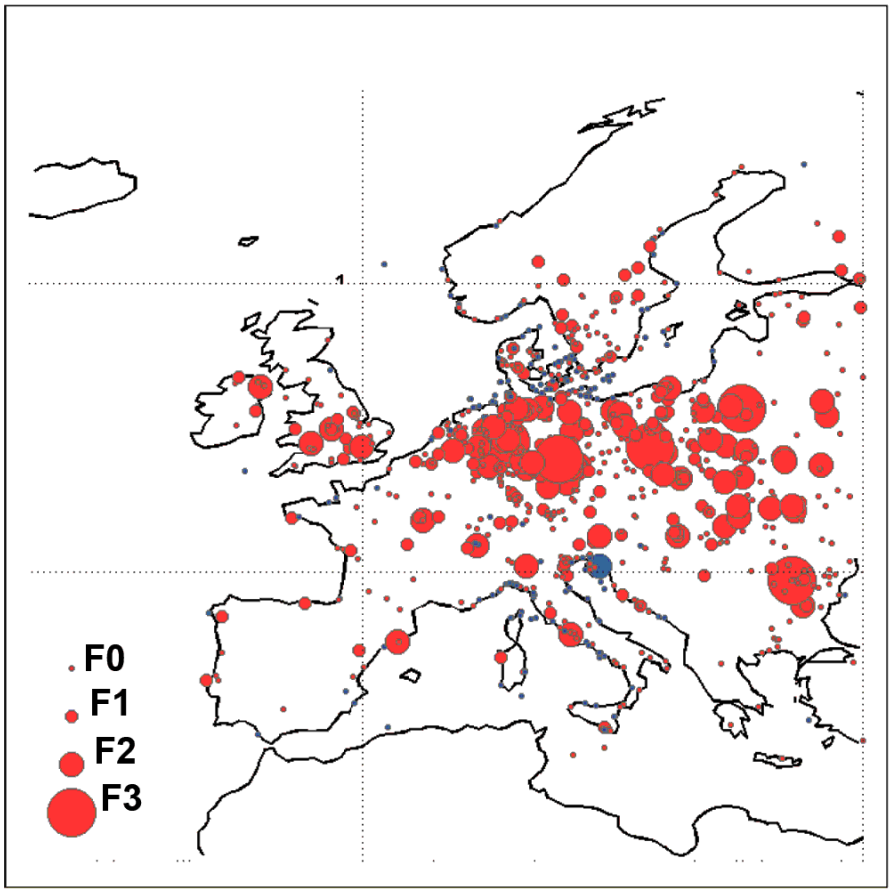

Figure 1.5: Spatial distribution of tornadoes over land (red dots) and waterspouts (blue dots) within Europe in 2005 and 2006. The size of dots describes the intensity with Fujita scale.

from that in Europe (Reynolds, 1999) (see figure 1.6) The spatial distribution of tornado events in 2005 and 2006 shows many cases between 45°N and 55°N. Towards the north tornadic activity decreases rapidly whereas towards the south locally stronger events are visible. Also in the southeastern part of Europe an accumulation of stronger tornadoes can be observed (see figure 1.5).

Great Britain: According to Reynolds (1999) most tornadoes in Great Britain (approx. 2/3 of all cases) occur in autumn (37.2%) or winter and thus later than over the European mainland. The high number seems to be due to a frequent occurrence of tornado outbreaks during the period between September and January. 7 of 8 outbreaks between 1960 and 1989 took place during this period. Only one case occurred in February. Most cases (92%) are weak (T0-T3), 8% are strong (T4-T7) and 0,1% of the cases can be classified as destructive (T8 and greater). In Great Britain meanwhile only two cases can be classified as T8. The activity minimum is in spring (10,7%) (Reynolds, 1999).

Ireland: Tyrell (2005) provided a tornado climatology for Ireland. He considered all

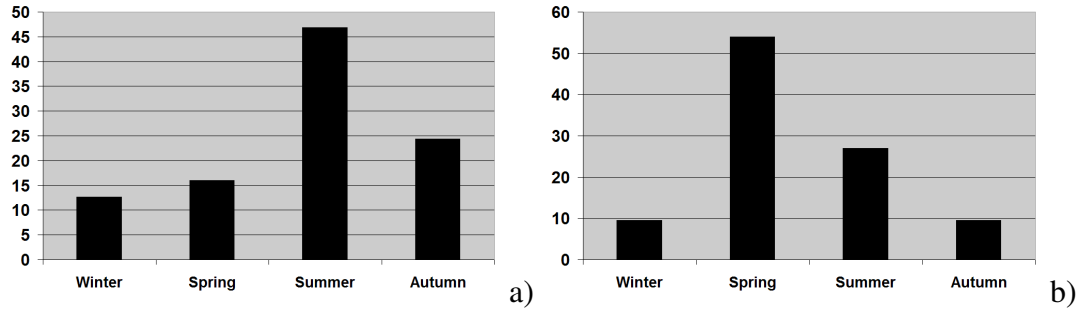

Figure 1.6: Seasonal distribution of tornado events in a) Europe and b) USA. The y-axis describes the frequency of tornadoes in percent (Reynolds, 1999).

tornado events between 1984 and 2004. He found a maximum number of events in August (see figure 1.7a). However, all F2/T5 events and 50% the F2/T4 events take place during wintertime. This is indicating that the frequency could be clearly higher in the winter and only due to the meager daylight weaker events are not observed. This would be in agreement with the climatology of Reynolds (1999), which stated a higher activity in the autumn and winter.

France: In France tornadoes occur mainly in the northwestern part and in a small section in the extreme south (Dessens and Snow, 1993). Only few events take place in the mountainous terrain with the exception of the Jura mountains, where tornadoes are quite frequent. The maximum number of tornadoes is recorded in August. Most events occur between May and September (see figure 1.7b). Tornadoes occur also in wintertime, mainly in the western part of France. They constitute even 20% of all events between November and March. The maximum daily activity is between 17 an 18 UTC. Nocturnal tornadoes are rarely observed. The favorite movement direction is SW to NE or W to E (79% of all cases). In France there are two F5-cases noted (Paul, 2000).

Germany: The tornadoes in Germany are usually connected with the passage of strong low pressure systems. Often there's a strong wind occurring at upper level. Frequent occurrence of tornadoes is remarkable near the coast and over hilly terrain. This could be attributed to changes of the surface roughness, which leads to the production of horizontal vorticity in the boundary layer (Dotzek, 2000). Particularly in the wintertime, tornadoes develop in situations with advection of relatively warm and moist air from the North Sea. Most tornadoes in Germany exhibit F1 intensity. With exception of the F0 cases all cases between F1 and F4 are lying approximately on a lin-log distribution. Brooks and Doswell III (2000) assume that with detection of all tornado events the intensity distribution would correspond to a linear-logarithmic probability density function.

Comparison France/Germany: The tornado climatologies of France and Germany are systematically different from each other. The correlation of the two time series is small (R=0.28) for the period between 1800 and 1999. The largest frequency of tornadoes in

Germany occurs during July (27%) (see figure 1.7c). 2/3 of all cases happen between June and August, only few cases take place during wintertime (Dotzek, 2000). The seasonal frequency distribution is rather representative for continental regions of Central Europe and follows the annual trend of the thunderstorm activity (Finke and Hauf, 1996; Hagen et al., 1999). July and August point out the most probable time for the occurrence of waterspouts (Dotzek, 2000).

The maximum daily activity is between 14 and 18 UTC and correlates thus with the maximum of the convective activity. More than 50% of all cases occur during this period. (Wegener, 1917; Finke and Hauf, 1996; Hagen et al., 1999). A secondary maximum is found between 6 and 7 UTC because of several waterspout outbreaks. With waterspout events usually several waterspouts are involved (Dotzek, 2000).

Austria: Austria exhibits like Germany the largest tornado frequency in July. Most cases occur between May and August. The daily maximum takes place around 17 LST (16 UTC). 45% of the cases are classified as F1 tornadoes, 24% as F2 and 14% as F3 (Holzer, 2000). The high portion of F3 cases speaks for the fact that many weaker cases were not classified.

Italy: Italy registers the largest tornado frequency in August, the maximal activity lies between August and November (see figure 1.7d). Italy's tornado climatology shows regional differences. While in the northern part of Italy most cases were noted in the summer, in central and southern Italy many cases occur only in autumn. Between 1991 and 2000 six F3 tornadoes occurred. All F3 events had energy helicity index (EHI) values under 1. This would speak against a link to supercells, although tornadoes of this magnitude are normally mesocyclonic induced. Three of the six F3 cases occur with storm-relative helicity (SRH) values around 0 $J\ kg^{-1}$, 2 exhibits 200 $J\ kg^{-1}$, a case took place even with negative helicity. However F3 cases exhibits in comparison to weaker events a higher 0-1km shear, which could be due to the small number of events. It is in addition remarkable that most of the tornadoes occur with convective available potential energy (CAPE) values under 1000 $J\ kg^{-1}$. Tornadoes took place in Italy preferentially over flat area (Giaiottia et al., 2005). F5 events were already registered in Italy.

In Italy two cases are known, in which a strong tornado passed by close to a weather station. On 24th July 1930, in 3 *km* distance of the tornado path a brief decrease of pressure of 9 *hPa* was recorded, which shows that strong tornadoes are embedded into a mesoscale low. The translation speed of the Tornado reached 57 $km\ h^{-1}$. On 11 September 1970, a strong tornado in Lido lead to a sudden decrease of pressure from 1008 *hPa* to 986 *hPa*, followed by a rapid relaxation to on 1001 *hPa*. In this case however at the same measuring station wind velocities of about 220 $km\ h^{-1}$ were measured, indicating that the tornado passed nearby the station. In this case the translation speed was estimated to 54 $km\ h^{-1}$. Both tornadoes were several hundreds of *m* wide and their path length amounts to 70 to 80 *km*.

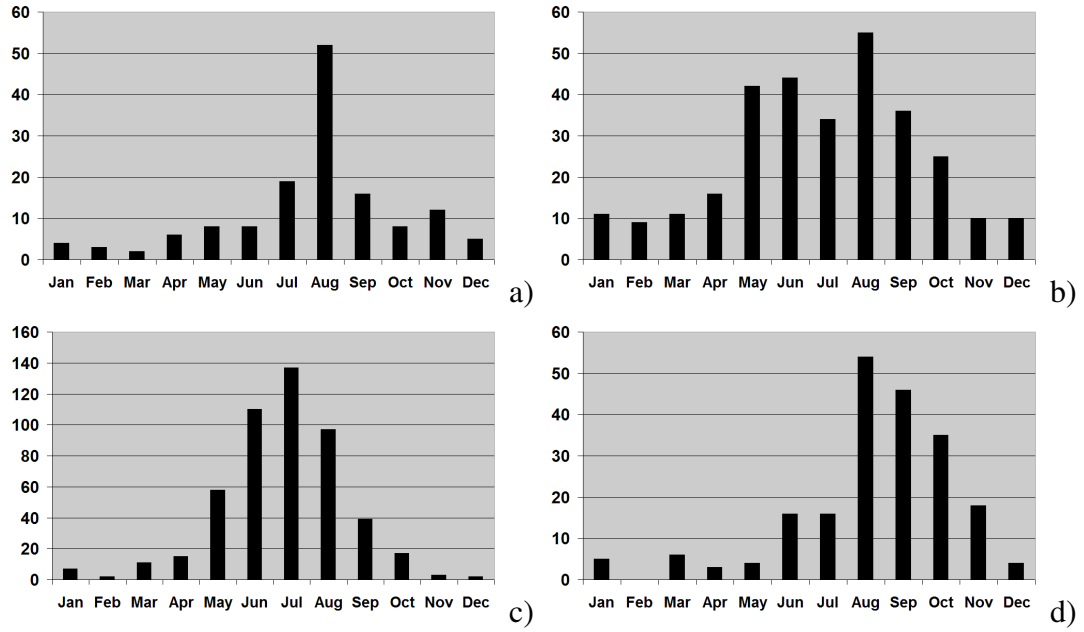

Figure 1.7: Monthly distribution of tornado events in a) Ireland, b) France, c) Germany and d) Italy (Tyrell, 2005; Paul, 2000; Dotzek, 2000; Giaiottia et al., 2005). The y-axis describes the number of tornadoes per month.

Greece/Eastern Mediterranean: The largest tornado activity in Greece is in July. If waterspout events are added the activity is largest in September. Therefore also the waterspout activity is largest in September. The maximum daily activity is reached already around 7 UTC, because of the large number of waterspout events in the data. The most frequent path direction is SW-NW (84.2% of the cases). In 2002 waterspouts are mainly observed in the Adria from July to October, while the season in the Ägais from August until November was retarded a little bit.

The average CAPE values exhibits 575 $J\ kg^{-1}$, the average EHI amounts only 0.05 and the 0-3 km SRH exhibits on average 23 $J\ kg^{-1}$. Sioutas (2003) has distinguished in his work between tornadic waterspouts (during a thunderstorm with lightnings) and fair-weather waterspouts (with no lightnings accompanied). He stated, that when tornadic waterspouts occur the average CAPE values are higher (726 $J\ kg^{-1}$), while fair weather waterspouts occur with much lower average values of 64 $J\ kg^{-1}$ (Sioutas, 2003).

Balearic Islands: Also on the Balearic Islands a maximum of waterspouts and tornadoes is registered in September. A secondary maximum of waterspouts take place in April. The CAPE values vary strongly depending upon event and amounts between 0 to 5400 $J\ kg^{-1}$ with tornadoes and 0 to 4000 $J\ kg^{-1}$ with waterspouts. The SRH values amount between -50 and 120 $J\ kg^{-1}$, only one tornado occurred with 380 $J\ kg^{-1}$ Helicity (Gayà et al., 2000).

Summary: Most events in Eastern Europe are limited to the summer half-year. In contrast to it a maximum of tornado outbreaks (with several tornadoes within short time) occur only in autumn or early wintertime in Great Britain. These winter tornado outbreaks concerns also parts of north and west France, as well as Belgium, the Netherlands and parts of Germany and Denmark. Smaller tornado outbreaks occur during the summer also in innercontinental areas, usually with clearly smaller number of tornadoes in these cases. Also in south Europe tornadoes occur clearly later than on European average where maximal tornado activity is in July. There, usually the maximum is registered in September. However the activity decreases more rapidly than in the rest of Europe. Winter tornadoes are rare in southern Europe.

The most frequent path direction of tornadoes in Europe is from SW (37.7% of the cases). Altogether 85.3% move from direction west to south (Reynolds, 1999). This is comparable with values from the USA. There 87% of the tornadoes move from south to west (Schaefer et al., 1980).

Romero et al. (2007) built up a climatology for Europe of various parameters used by the forecast of severe convective storms. For that, reanalysis data base from ERA-40 was used for the period from 1971-2000 and out of these data, fields like CAPE, convective inhibition (CIN), mid-tropospheric lapse rate, low-tropospheric moisture content and storm-relative helicity were calculated. Further, the results were compared with a collection of existing reports of significant (at least F2) tornadoes in Europe during the period 1971-2003. The tornado climatology was used to test the appropriateness of the parameters selected for the climatology.
It results that convective available potential energy, low-tropospheric moisture content and environmental shear were all quite useful for identifying significant tornado environments, but only when they were expressed in relation to the monthly climatological values. That is, they become useful indicators of the likelihood for tornadoes when the monthly climatological mean is substantially exceeded, regardless of the absolute values which are clearly lower than they are typically in the US (Romero et al., 2007).

1.2.5 Typical synoptical situations (in UK)

Tornadoes in Great Britain occur usually with the following synoptical situations: during cyclonic SW-situations, closed with passages of a short or a long wave trough or directly under a low pressure system. Often areas are lying near the Jetstreams. (Sioutas, 2003; Tyrell, 2005) Bolton et al. (2003) differentiated 3 typical synoptic situations for Great Britain associated with tornadoes.

Type A (see figure 1.9a and figure 1.9b) is associated with a strong cold front which belongs to a rapidly developing low. This type produces usually several tornadoes and also tornado outbreaks. It is responsible for the largest number of tornadoes. They are however in most cases short-lived and weak (Bolton et al., 2003). Often these situations are connected with strong horizontal and vertical wind shear ('Veering'). A case study shows that these situations can be connected with high vorticity advection.

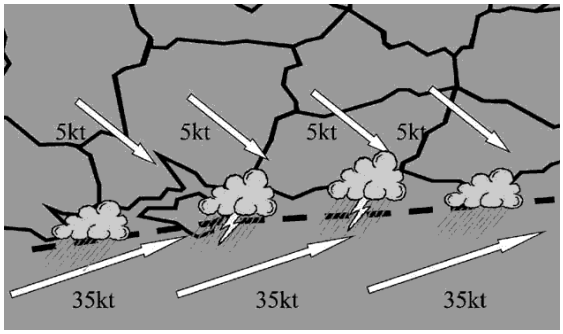

Figure 1.8: Shear zone along the south coast of England caused by interaction of light land breeze off of the cold land with a strong gradient wind over the warm sea during the autumn and winter. This effectively produces a coastal front marked by the dashed line (Bolton et al., 2003). This front has similar characteristics to the shear zone described by Wakimoto and Wilson (1989) (see figure 1.3).

Type B (see figure 1.8) is defined by a zone with strongly increased horizontal wind shear. This can possibly still be forced by the topography. This type can also be connected with an active cold front or stand in connection with the advection of cold, unstable air masses from W to SW. Different friction over land and water can induce convergent flow at the southern coast of England; this might enhance the conditions for tornadoes in these situations. In addition such a shear zone can result from the Outflow of thunderstorm cells (Bolton et al., 2003).

Type C (see figure 1.9c and figure 1.9d) is linked to a weak depression in late spring or summer. This is connected with a upper level cold air vortex and increased cyclonic vorticity at upper levels. In accordance with Bolton et al. (2003), this leads to an increased convective instability.

Quite often the wind shear is large in the lower troposphere, particularly when strong tornadoes occur. This is however not inevitably the case, as different works show. (Gayà et al., 2000; Groenemeijer, 2005). Note also that for waterspouts shearing is usually small in lower layers.

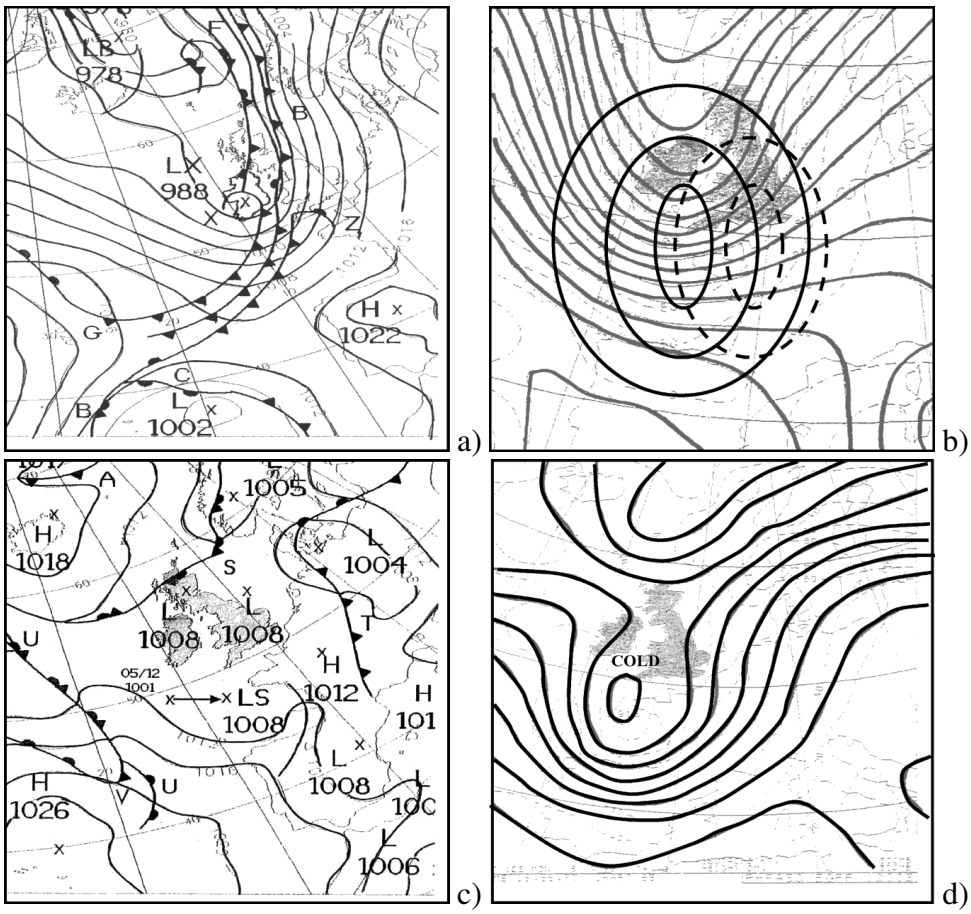

Figure 1.9: a) Synoptic situation at 0000Z on 5th November 1999 showing a rapidly deepening area of low pressure and its associated weather fronts over the United Kingdom. The three cold fronts to the southwest of the low merged into one by midday with a subsequent increase of air-mass change across the front. b) Profile of the forecast 300 hPa chart based for midday on the 5th November 1999. It clearly shows a sharpening upper trough moving in from the west with tight contour gradients around the base of the trough. The solid ellipses show the area of maximum positive vorticity. The dotted ellipses show the area of maximum positive vorticity advection, the area where most ascent will take place. c) Synoptic situation at 0000Z on 5th July 1999 showing a slack area of low pressure covering the United Kingdom. d) Chart showing the upper air pattern over the United Kingdom at 0000Z on the 5th July 1999 showing a slack, slow moving upper cold trough and cold pool in the vicinity of the United Kingdom. Note also, the strong flow around the periphery of the cold pool (Bolton et al., 2003).

1.2.6 Vertical layering (comparison of USA with Netherlands)

Rasmussen and Blanchard (1998) have examined different convection parameters to find out which parameter is most suitable for the forecast of tornadoes. To this aim, they differentiated 3 types of thunderstorms: ORD are called usual thunderstorm cells without mesocyclone and tornado, SUP are called supercells without or with weak tornadoes (<F2 intensity) and TOR are called supercells with significant Tornadoes (>=F2 intensity). For all cases the most representative sounding was selected.

While ORD exhibits on average a SRH of 55 $J\ kg^{-1}$, type SUP reaches 124 $J\ kg^{-1}$ and TOR reaches 180 $J\ kg^{-1}$. This seems to be a very clear result, however, there is a strong overlap between the frequency distribution of SUP and TOR (see figure 1.10b). The mean CAPE values are significant lower with type ORD (537 $J\ kg^{-1}$) than that with SUP (1152 $J\ kg^{-1}$) or TOR (1314 $J\ kg^{-1}$). The lowest value of all ORD and SUP amounts to 0 $J\ kg^{-1}$, that of TOR 66 $J\ kg^{-1}$. There is also a large lap between SUP and TOR (see figure 1.10a).

The EHI, which combines SRH and CAPE, supplies clearly better results, but also here the overlapping range is large (see figure 1.11). ORD exhibit on the average 0.16, while SUP and TOR with 0.64 respectively 1.48 clearly differ from each other (see figure 1.10c). In accordance with the Heidke skill score[5] (HSS) the EHI is the best parameter for distinction between supercells and non-supercells. For the distinction of tornadoes and supercells however the Lifted Condensation level (LCL) is suitable best in accordance with HSS. While with SUP the mean LCL lies on 1.23 *km* height, it is significant lower with 0.78 *km* height on the average with type TOR (see figure 1.10d). Interestingly, Groenemeijer (2005) in a similar work notices for the Netherlands that the LCL is not particularly useful for the distinction between thunderstorms (0.79 *km*) and tornadoes (0.6 *km* with tornadoes > F0). This could possibly be due to a smaller number of supercells in this region or due to a generally lower LCL in the climatological mean.

However, wind shear and SRH seem to play also in Europe an important role for the development of stronger tornadoes. Thus, the middle SRH for tornadoes in the Netherlands amounts to 59 for F0, 105 for F1 and 210 for F2 tornados. Also with 0-1 *km* shear this connection is to be recognized. F1 occur on the average with 9 $m\ s^{-1}$, F2 tornadoes with 20.3 $m\ s^{-1}$ 0-1 *km* shear (Groenemeijer, 2005).

[5]Measures the fraction of correct forecasts after eliminating those forecasts which would be correct due purely to random chance. This is a form of the generalized skill score, where the score in the numerator is the number of correct forecasts, and the reference forecast in this case is random chance. In meteorology, at least, random chance is usually not the best forecast to compare to - it may be better to use climatology (long-term average value) or persistence (forecast = most recent observation, i.e., no change) or some other standard (taken from http://www.bom.gov.au)

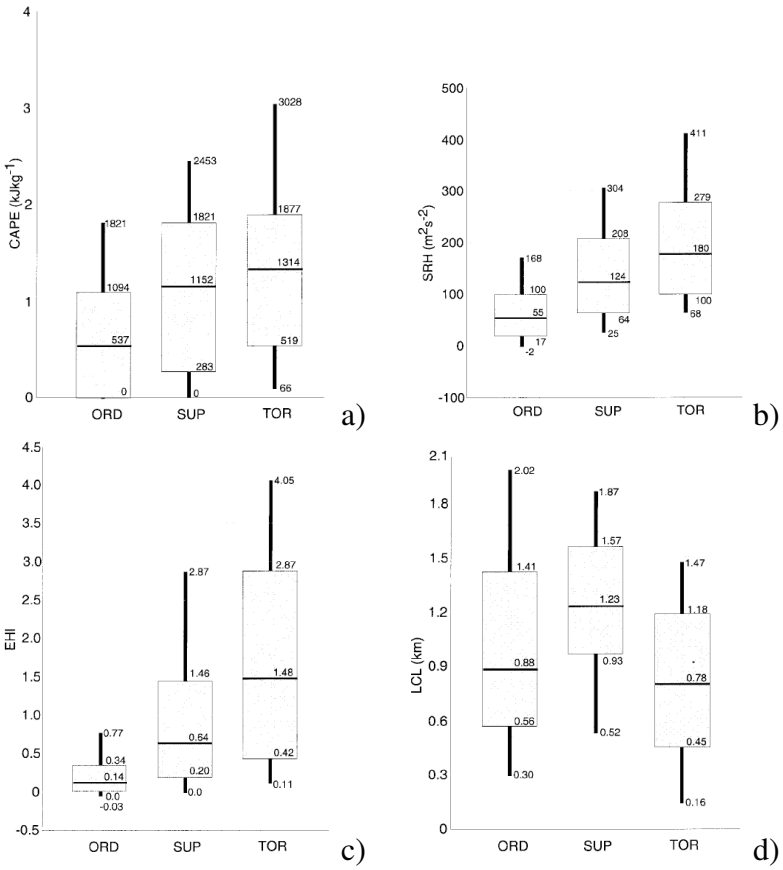

Figure 1.10: This figure indicates distribution of a) CAPE b) SRH c) EHI and d) LCL for the types ORD, SUP and TOR according to Rasmussen and Blanchard (1998). The boxes denote the 25th to 75th percentiles, with heavy horizontal bar at the median value. Thin vertical lines extend to the 10th and 90th percentiles.

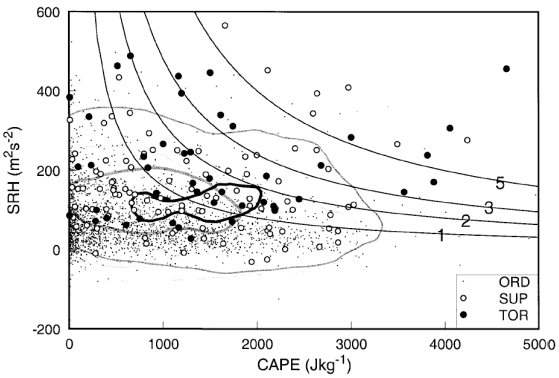

Figure 1.11: This figure indicates a distribution of CAPE and SRH for ordinary thunderstorm (ORD), supercells (SUP) without or with weak tornadoes (<F2) and tornadic supercells (TOR) with significant tornadoes (>=F2) according to Rasmussen and Blanchard (1998).

Chapter 2

Data

2.1 ECMWF data

The European Center for Medium-Range Weather Forecasts (ECMWF) is an international organization based at Reading, England, which was founded in 1975.

In order to analyse the weather situations during tornado events and to build up a climatology ECMWF analysis data were used. "ECMWF produces routine global analyses for the four main synoptic hours 00, 06, 12 and 18 UTC. The data were interpolated from a spectral grid with a resolution of T511 truncation respectively T799 truncation to a gaussian grid with a spatial resolution of 1°x 1° and 60 vertical levels[1]."

This data set contains the primary fields temperature, absolute humidity, pressure, geopotential height and wind velocity in zonal, meridional and vertical direction. From these fields secondary fields are extracted by different FORTRAN-routines e.g. potential and equivalent-potential temperature, relative humidity, vorticity and potential vorticity, instability and shear parameter (for more details see section 3.1) Mainly surface observations and sounding measurements flow into analysis data, further satellite and aircraft data were used for data assimilation. Because of the dense meteorological network over Europe the analysis of ECMWF should represent conditions in this area relatively well.

2.2 ESWD data

"Tornado data were taken from the European Severe Weather Database (ESWD), which was built up and supervised by the European Severe Storm Laboratory (ESSL). The ESSL started as an informal network of European scientists in 2002. On 28 September 2006, the ESSL was formally founded as an association, acquiring full legal status on 8 December 2006 following entry to the register of associations. Non-profit status was granted on 21 December 2006. The ESSL is a non-profit research organization with legal type e. V. (eingetragener Verein, registered association) under German law[2]."

[1] taken from http://www.ecmwf.int/products/data/

[2] taken from http://essl.org/ESWD/

2.2.1 Development and quality-control

”The ESWD was initiated by Fulvio Stel and Dario Giaiotti of ARPA-FVG in Italy, who first proposed a text-based database of severe weather events covering Europe during the 2nd ECSS Conference in Prague, August 2002. The ESWD was further enhanced by its present graphical user interface (GUI) in 2004. Pieter Groenemeijer then brought together a working group of experts to advise on a data format adapted for storage of severe weather data. This led to the present data format (version 1.40) which was first presented at the 3rd ECSS Conference in Léon, Spain, 2004. In 2005, the ESWD was established at the European Severe Storms Laboratory, then still an informal network of European scientists initiated by Nikolai Dotzek of the German Aerospace Center DLR. After two years of test operations, 2006 was the first year with operational ESWD service. In the same year, also the ESSL was formally established as a non-profit research organization.

Despite all the achievements over the last years, there is still a long way to go until the ESWD can be called a truly mature database. For instance, underreporting of specific events is still notable in a number of regions in Europe. One option to overcome this is to extend ESSL’s collaboration with national weather services (NMHS) in Europe to augment and homogenize the database. Another point, and in fact one of the major strengths of the ESWD is to involve the public in the data reporting. The public ESWD web interface at www.eswd.eu encourages submission of reports from all over Europe and the Mediterranean region.

The input to the ESWD by the public and the ESWD maintenance has led to a large increase in reports over the last years. This poses a challenge for an appropriate quality-control (QC) procedure, which is currently one of the most important tasks of the ESSL in operating the ESWD. The basic procedure foresees that the ESSL is responsible for QC of all reports coming in via the public interface while the cooperating NMHSs are responsible for QC of the severe weather reports they enter in their own installations of the ESWD software.

Both ESSL and the NMHSs are expected to follow a 3-level QC process during which an initial report to the database usually receives the lowest QC-level 0, or if the initial information is already reliable, QC-level 1. Further verification of the report including editing of the information contained therein can lead to an upgrade to QC-levels 1 (partially verified) or 2 (verified). The ESWD data format also contains fields with metadata information. For instance, aside from the pure tornado or straight-line wind intensity rating, there are also fields describing on what kind of information this intensity rating was based. In case of no information available for an intensity rating, then the event remains unrated - contrary to some other severe storm databases, there are no "default intensity ratings" in the ESWD.

The ESWD data format allows for both detailed event information and thorough quality-control. Enhancing earlier voluntary efforts, in 2007 the first part-time ESSL staff have

begun to enter and quality-control reports. There are close contacts with colleagues at the cooperating NMHSs concerning the QC of events reported from their countries and in merging double reports of events which were entered to the database both by the NMHS and the public interface. These first years of ESWD operations are a learning period for developing best practices in handling the QC challenge. But taking this challenge is definitely a worthwhile task[3].“

The most ESWD data used in this work are rated by QC-level 0. The experience made using public input has shown, that only few of them required later corrections by the ESWD quality-control process (Kaltenböck et al., 2007). The data also were randomly checked and unreliable events were taken out.

2.3 Lightning data

Europe's primary lightning network consists of seven stations, unmanned automatic lightning sensors, at different locations in Europe. This allows a continuous registration of the lightning activity.

The commonly available British spherics bulletin (SFUK) has a domain of 40°W to 40°E and 30°N to 70°N. SFUK data are publically available on the Internet. The SFUK is based on the World Meteorological Organization (WMO) FM 32-I SFLOC code form. For this work SFUK30 and SFUK31-files were used.

- SFUK30 contains data at every full hour
- SFUK31 contains data at every full hour plus 30 minutes

The files have a spatial resolution of 0.5°x 0.5°. The data contain the number of lightnings during a 10 minute period before a full or half hour.

2.4 Sounding data

On the homepage of the University of Wyoming[4] sounding data are freely available. This data sets were used for validating ECMWF analysis data over Europe. Radiosoundings are commonly available at 0 and at 12 UTC, some of them also at 6 and at 18 UTC. The sounding data contain the parameters: pressure [hPa], height [m], temperature [$^{\circ}C$], dewpoint [$^{\circ}C$], relative humidity [%], mixing ratio [$g\ kg^{-1}$], wind direction [°] and speed [kt], potential temperature [K], equivalent potential temperature [K], virtual potential temperature [K], CAPE [$J\ kg^{-1}$] and more.

[3] taken from http://essl.org/ESWD/

[4] http://weather.uwyo.edu/upperair/sounding.html

Chapter 3

Methodology

Forecast parameters are an important instrument for a US-forecaster to recognize a potential tornado situation. But often the quality of such a parameter depends on geographical position. It is not necessarily the case, that a "good" forecast parameter in the US also works in Europe. So, it is meaningful to check them for Europe. For this reason the most common used forecast parameter in the US for the prediction of supercells and tornadoes were tested.

3.1 Forecast parameters

3.1.1 Convective available potential energy

Convective available potential energy (CAPE) is one of the most important instability parameters to recognize the potential for moist convection. It is a measure for the amount of latent instability (Emanuel, 1995). CAPE is calculated from ECMWF-fields with a program in common use at the Swiss meteorological service (www.meteoswiss.ch). The program was originally written by the German weather service (DWD) and reorganized by Marco Stoll and Daniel Leuenberger (MeteoSwiss). The routine is calculating the most unstable CAPE (MUCAPE) and the mixed-layer CAPE (MLCAPE) as well. It was originally tested for the COSMO model and adapted to ECMWF fields by Schlemmer (2007).

CAPE is defined as

$$CAPE = \int_{LFC}^{EL} g(T_{v_{parcel}} - T_{v_{env}}/T_{v_{env}}) \cdot dz \tag{3.1}$$

where LFC is the level of free convection, EL denotes the equilibrium level, $T_{v_{parcel}}$ stands for the virtual temperature of a rising parcel and $T_{v_{env}}$ denotes the virtual temperature of the environmental air

Above the level of free convection (LFC) and below the equilibrium level (EL) a rising air parcel is warmer than environmental air because of the disposal of latent heat. In this area it is accelerated and reaches theoretically maximum vertical motion on the EL. In reality, lower maximum upward motion will be reached, because of frictional processes.

The difference between $T_{v_{parcel}}$ (virtual temperature of parcel) and (virtual temperature of environmental air) in relation to $T_{v_{env}}$ determinates the acceleration of an air parcel. Hence, CAPE is the integration of this difference between LFC and EL.

The vertical motion of air above the LCL leads to a convergence in the boundary layer which can concentrate vorticity from the environment. Furthermore, the acceleration of air over the LCL can induce vortex stretching (see section 1.2.3). So, CAPE can be termed as an important factor for tornado genesis.

3.1.2 Convective inhibition

CIN is describing convective inhibition (Emanuel, 1995). It can be important, because it may prevent convection even in a highly unstable airmass. It can also delay convection and lead to higher instability because of more heating due to insolation. Such weather situations are called ”loaded gun“ in the US and can produce severe convective events (Fawbush and Miller, 1952).

CIN is defined as

$$CIN = \int_{SL}^{LFC} g(T_{v_{parcel}} - T_{v_{env}}/T_{v_{env}}) \cdot dz \tag{3.2}$$

where SL is the surface layer and LFC the level of free convection, $T_{v_{parcel}}$ stands for the virtual temperature of a rising parcel and $T_{v_{env}}$ denotes the virtual temperature of the environmental air

CIN is calculated between the source layer and the level of free convection (see section 3.1.1). SL is describing the source layer of a rising air parcel. CIN is calculated in the same way as CAPE (see section 3.1.1), but the integration is resulting in negative values. It specifies the amount of kinetic energy that an air parcel is needing to overcome this stable air layer.

3.1.3 Storm-relative helicity

The storm-relative helicity (SRH) (Davies-Jones et al., 1990) is an important predictor for supercells and tornadoes. Values over 100 $J\ kg^{-1}$ are supportive for development of supercells and also tornadoes. The physical mechanism associated with SRH is the tilting of horizontal vorticity into vertical orientation (see section 1.2.3).

The SRH is an integration of streamwise vorticity between 2 levels. In order to calculate the SRH the vector product of storm-relative wind vectors from 0 to 3 km height

(H) was used which is a good approximation of SRH. v stands for the horizontal wind velocity and ω for the horizontal vorticity. c describes storm motion velocity which is calculated using the average over all model levels between 3 and 10 km. This weights the wind velocity on lower levels higher because vertical distance between model levels (σ-coordinates) grows with height. This was done because of the assumption that winds on upper levels do not have much influence on storm motion velocity.

Storm-relative helicity (SRH) is defined as

$$SRH = \int_0^H (v - c) \cdot \omega \cdot dz \tag{3.3}$$

where H decribes a height, v is the horizontal wind velocity, c the storm motion velocity and ω denotes horizontal vorticity

3.1.4 Energy helicity index

The EHI is an empirically combination of CAPE and SRH. It is build up by the assumption that an environment of high SRH- and low CAPE-values can be also supportive for the generation of supercell like an environment with low SRH- and high CAPE-values. This relation was observed in statistical analysis. Further it is also a quiet good predictor for tornadoes.

The energy helicity index (EHI) is defined as

$$EHI = \frac{CAPE \cdot SRH}{1.6 \cdot 10^5} \tag{3.4}$$

where $CAPE$ is a convective available potential energy and SRH denotes a storm-relative helicity.

All these parameters work in the US more or less. In Europe, they were also used for the forecast of severe convection, but experience with the reliability is rather scarce.

3.2 Frontal zones

In order to determ fronts a dataset calculated by Jenkner (2008) out of ECMWF-data was used. Basically, he takes the gradient of equivalent-potential temperature on 850 hPa and 700 hPa and determines a threshold value, which describes frontal zones. For this work the data on the 700 hPa level were used. For this reason fronts with larger vertical extension were focused in this work, because they are usually a trigger for convective storms whereas shallow fronts lead to stabilization and suppress convection.

3.3 Potential vorticity (PV)

Potential vorticity (PV) is a useful utility for analysing mid-latitude synoptic systems (Hoskins, 1990). It was developed by Ertel (1942).

Ertel's potential vorticity is defined as

$$PV = (\zeta_\Theta + f)(-g\frac{\delta\Theta}{\delta p}) \tag{3.5}$$

where ζ_Θ describes the vertical component of the relative vorticity on an isentropic surface, f is the coriolis parameter. In other words, PV depends on absolute vertical vorticity $(\zeta_\Theta + f)$ and stratification $(\frac{\delta\Theta}{\delta p})$. PV is a conservative value as long as no diabatic or frictional effects occur.

3.3.1 Streamer

Potential vorticity (PV) streamers are meso- or synoptic-scale upper-level features, which can have an impact on surface weather (Hoskins et al., 1985). PV-streamers can produce strong vertical ascent and destabilize the atmospheric stratification. Therefore a streamer can act as a trigger for convection and so have also an indirect influence on tornadoes.

Wernli and Sprenger (2005) developed an algorithm which detects such streamer on different levels. Streamer data on the 320K and on the 330K isentropic level were used, because they are mainly visible in this region. For the calculation also ECMWF-data were used.

3.4 Lagrangian trajectories

In order to determine weather classes, lagrangian trajectories were used. Backward-trajectories were calculated with the three-dimensional trajectory tool LAGRANTO developed by Wernli and Davies (1997). As data basis serves ECMWF analysis data.

3.4.1 Cluster analysis

The cluster analysis was used to obtain an objective way to classify different weather situations from backward-trajectories. The routine for clustering trajectories was taken from StatLib[1]. The tool does a hierarchical clustering using (user-specified) criterion. It was written by F. Murtagh (ESA) in 1986 and was adapted for trajectory calculations.

In order to determine distances between trajectories, spherical distances were calculated. Because of different starting points of the trajectories, they had to be centered, so that only their shape is included in the calculations.

[1] http://lib.stat.cmu.edu

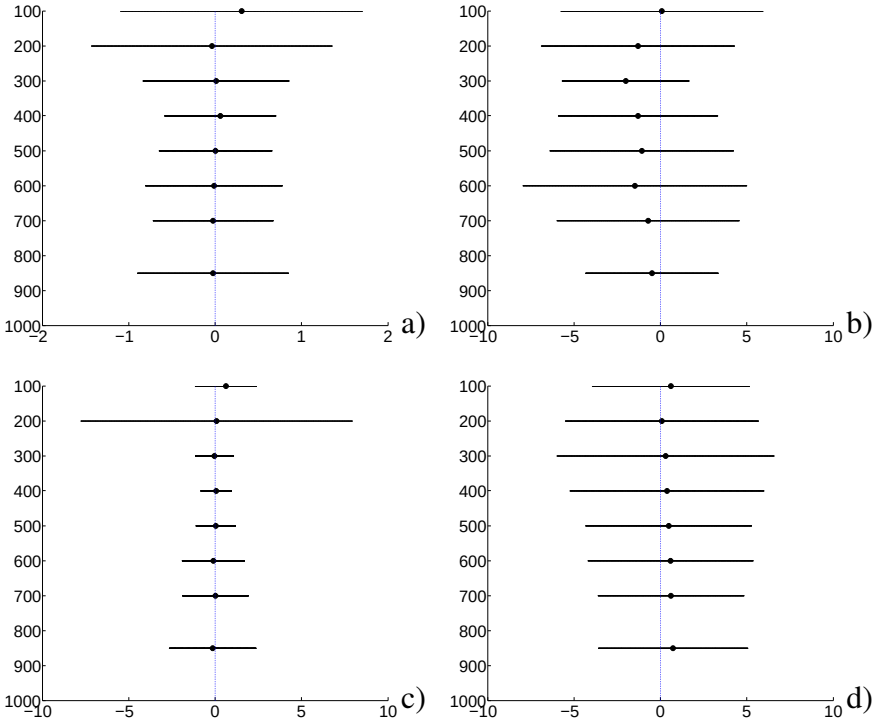

Figure 3.1: The dots show the mean difference (sounding data minus ECMWF-data) of a) temperature in °C, b) dewpoint in °C, c) equivalent-potential temperature in K and d) wind velocity in ms^{-1} in x-direction. The line shows the range of standard deviation. The y-axis describes the pressure level in hPa.

Ward's method

For the cluster analysis, the usage of average linkage and ward's method were discussed. It was decided to use the second method. Ward's method has a tendency to split data in groups of roughly the same size. This can be a disadvantage, but that is not a problem for this study, because small classes are not representative anyway and not useful in a climatology. Further, Ward's method seems subjectively clustering better than other methods.

In statistics, Ward's method is a widely used technique of cluster analysis that begins with isolated individuals or cases and progressively combines them into clusters until every individual is in the same cluster. At each stage of the analysis, individuals or clusters that merge are those, that result in the smallest increase in the sum of the squared distances of each individual from the mean of its cluster (Stohl, 1998). Ward's method is a form of agglomerative hierarchical clustering[2].

3.5 Validation of ECMWF data

The **temperature** in the ECMWF-analysis seems to be a excellent representation of the actual conditions. The mean temperature (denoted as dot in figure 3.1) does not differ more then $0.1°C$ except for the 100 *hPa* level (see figure 3.1a). On this height, it it possible that measurement errors in the sounding data are contaminating the dataset. Also the standard deviation (denoted as horizontal line in figure 3.1), which lies below $1°C$ on most levels, shows the high accuracy of the ECMWF-temperature data. However, it should be kept in mind that sounding data were assimilated directly into the ECMWF analysis which explains partly the high data accuracy of ECMWF.

The **dewpoints** are slightly overestimated in the ECMWF-analysis data (see figure 3.1b). The standard deviations is rather high with several degrees. This problem is generated by large variations of atmospheric water content over small distances. The bias and especially the large distribution can produce large errors in the calculations of convective indices, but this will not be a larger problem for a climatology, because random errors will be averaged out.

The **equivalent-potential (θ_e) temperature** are well described by ECMWF (see figure 3.1c). Only the large standard deviation on the 200 *hPa* level peaks out. Because this level lies close to the tropopause, it is possible that convective events produce large variation of θ_e-values.

The **wind velocity** is marginally underestimated in the ECMWF-analysis with about 1 $m\ s^{-1}$ (see figure 3.1d). The standard deviation amounts to 5 $m\ s^{-1}$. This is also an excellent result and speaks for the high quality of ECMWF-data.

3.5.1 CAPE

In order to check if ECMWF-data were indicating CAPE-values well, already calculated mixed-layer CAPE-values in the sounding dataset (see section 2.4) were used. All available soundings for Europe from the year 2005 and 2006 were compared with the CAPE-output of the ECMWF-dataset in the same period of time.

In figure 3.2 it is visible that MLCAPE is also underestimated by the CAPE-routine, if you take sounding values as a reference. The difference grows linearly with higher values. Because the scatter plot shows a linear distribution and primary values like equivalent-potential temperature does not indicate a large bias, the differences can be explained by different calculation methods.

[2] taken from http://en.wikipedia.org/

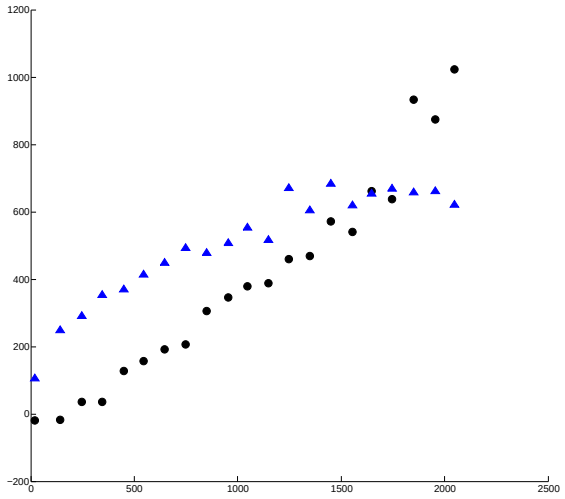

*Figure 3.2: The x-axis shows the mean of a set of soundings. The y-axis describes the difference (mean mixed-layer CAPE of soundings minus mean **mixed-layer CAPE (MLCAPE)** calculated from ECMWF. Black dots indicate the mean difference of CAPE between soundings and ECMWF data. Blue triangles describe the standard deviation of ECMWF-CAPE compared to sounding measurements.*

3.5.2 Validation in the closer environment of tornadoes

Measurement values were checked if they are also according well to the ECMWF-analysis data in the closer environment of tornadoes. For that, sounding data within a range of max. 400 km around the tornado event were used.

In the closer environment of tornadoes the mean temperature of ECMWF-data match very well with the sounding measurements (see figure 3.3a). The standard deviation is also low except for the levels above 400 hPa. Probably, convection produces this deviations in temperature and ECMWF cannot get such small-scale temperature variations.

Figure 3.3b shows a overestimation of the dewpoint by ECMWF at upper levels. This can be due to parameterization problems of convection in ECMWF. The standard deviation increases with height which can be explained by smaller water content at higher levels. This generates automatically larger uncertainty especially in regions with forced deep convection.

Figure 3.3c indicate, that windvelocity is represented well by ECMWF. The standard deviation increases slightly with height. This can explained by generally higher windspeed at the upper levels especially around the jetstream level.

The winddirection (see figure 3.3d) is the parameter with the largest uncertainty. The mean values of ECMWF represents the sounding measurements quiet well. But standard deviation is rather high, especially at lower levels. This can produce problems

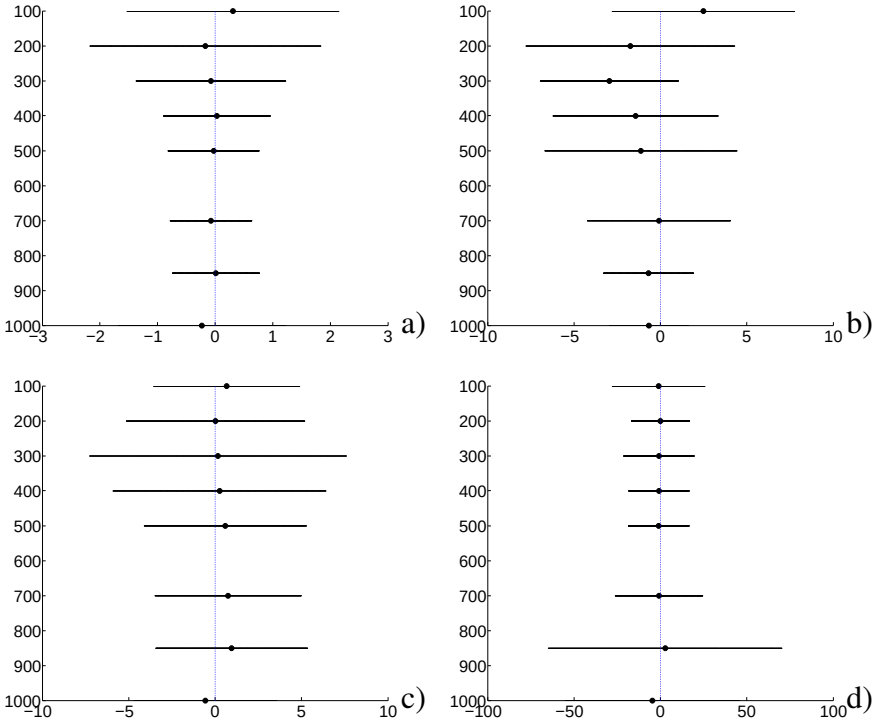

Figure 3.3: The dots show the mean difference (sounding data minus ECMWF-data) of a) temperature in °C, b) dewpoint in °C, c) wind velocity in m s^{-1} and d) wind direction in ° in x-direction within a 400 km range around the tornado. The line shows the range of standard deviation. The y-axis describes the pressure level in hPa.

in calculating storm-relative helicity from ECMWF. For the forecast, this can be a difficulty. For a climatological study it is not a problem because random errors will be averaged out in a larger data sample.

Chapter 4

Climatology

Because of the difficulty to determine relevant synoptic and mesoscale signals out of a few cases, it was chosen to make composites for different parameters and for a distinct period of time prior and after the tornado event takes place. The disadvantage of this method is that eventually smaller structures are smoothed out because of the time resolution from ECMWF of six hours.

4.1 Temporal evolution

The temporal evolution of composites from parameters shows clearly which synoptic and mesoscale systems and parameters are playing a relevant role in tornado genesis. Furthermore, it is a method to check if ECMWF is representing well specific tornado forecast parameters like CAPE and SRH which should reach higher values near tornadoes.

In this section, composites of damaging tornadoes (F1 and stronger) were used because these data are more reliable and contain events of higher importance.

4.1.1 Vorticity

On the 850 *hPa* pressure level, already 24 hours before the tornado event, a zone with high vorticity level is present about 20°W of the later affected area. 12 hours before the event, it is visible around 15°W and during the tornado case it is reaching the affected area with values up to $2 \cdot 10^{-5} s^{-1}$. The strengthening of the vorticity signal is likely to be produced by convergence. Even if winds on the 700 *hPa* level were taken, the fast motion of the vorticity signal on that level cannot be explained by advection. Interestingly, it seems to be connected with the upper tropospheric PV anomaly shown below in figure 4.3a and b.

On the 250 *hPa* pressure level the same vorticity anomaly is visible, but larger in extent and with significant higher vorticity values (see figure 4.2). The vorticity anomaly is intensifying till the tornado event and is weakening significantly after it. The maximum

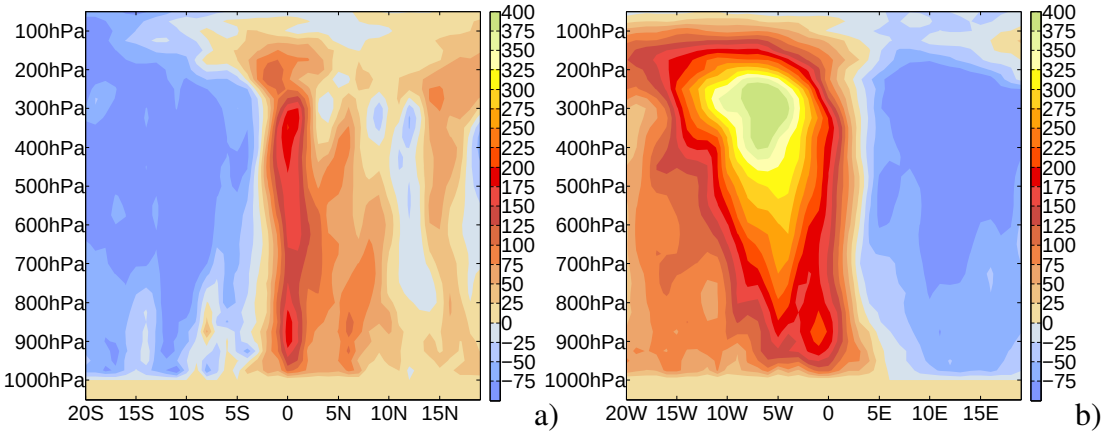

Figure 4.1: a) Cross section in north-south direction through a composite of mean vorticity in $10^{-6}\ s^{-1}$ *averaged over all cases which have at least F1 strength during the tornado event. b) Same as figure a in west-east direction.*

vorticity values during the event were reached at 7°W of the affected area with values up to $4 \cdot 10^{-5} s^{-1}$. This is twice as high as on the 850 *hPa* pressure level.

The north-south vertical cross section shows a significant rising of the vorticity values during a tornado event between 900 and 300 *hPa* (see figure 4.1a). 12 hours after the tornado event, a maximum of vorticity is present on jetstream level.

The west-east vertical cross section shows the vorticity anomaly moving from west to east. It strengthens between 900 *hPa* and 200 *hPa* (see figure 4.1b). During the tornado event a vorticity maximum is visible slightly west on 900 *hPa* pressure level. It is likely to be produced by convergence at the low levels. The deep vorticity anomaly 5°W is likely to be connected with deepening of the 1 and 1.5 *PVU* layer (shown in figure 4.3b). Possibly, this signal is produced by a stratospheric intrusion of high PV air. (see also figures in section B.1 for more information)

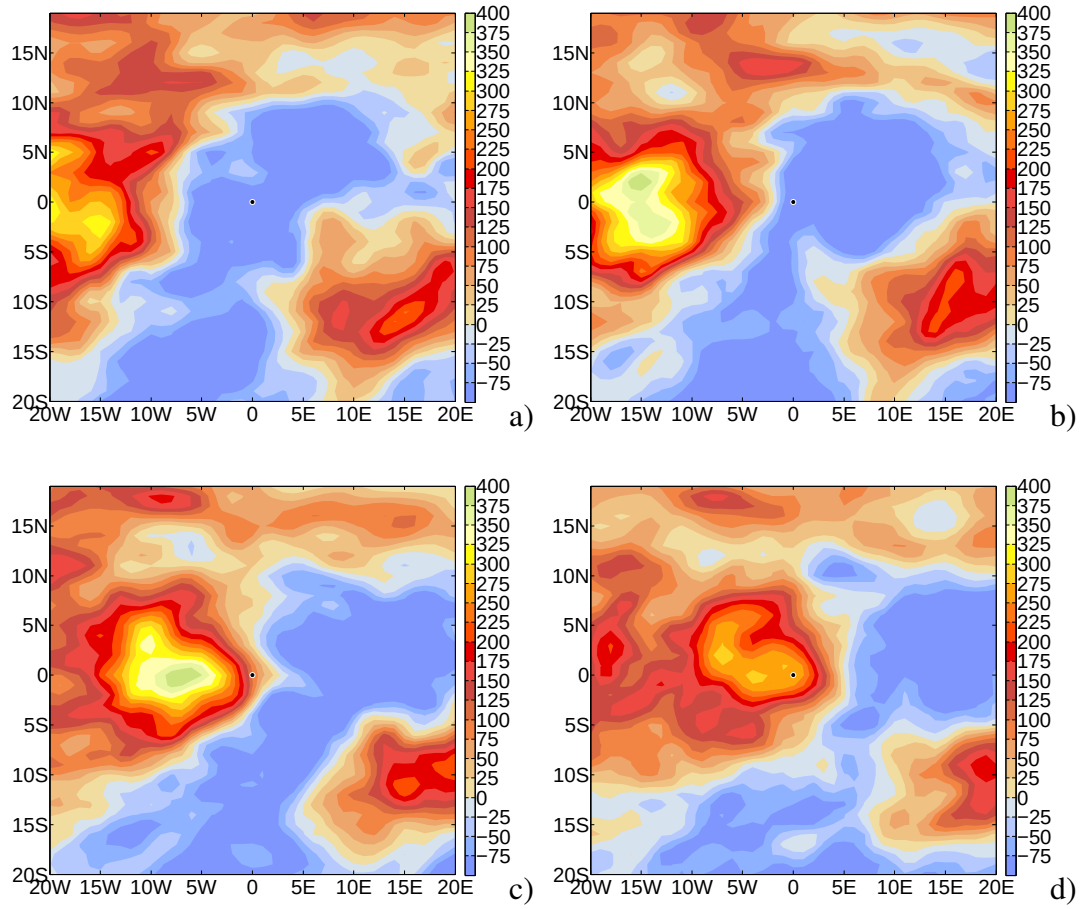

Figure 4.2: Composite of mean vorticity on the 850 hPa level in 10^{-6} s^{-1} *averaged over all cases which have at least F1 strength a) 24 h before b) 12 h before c) during the tornado event and d) 12 h after the event. The black dots mark the position of the tornado events.*

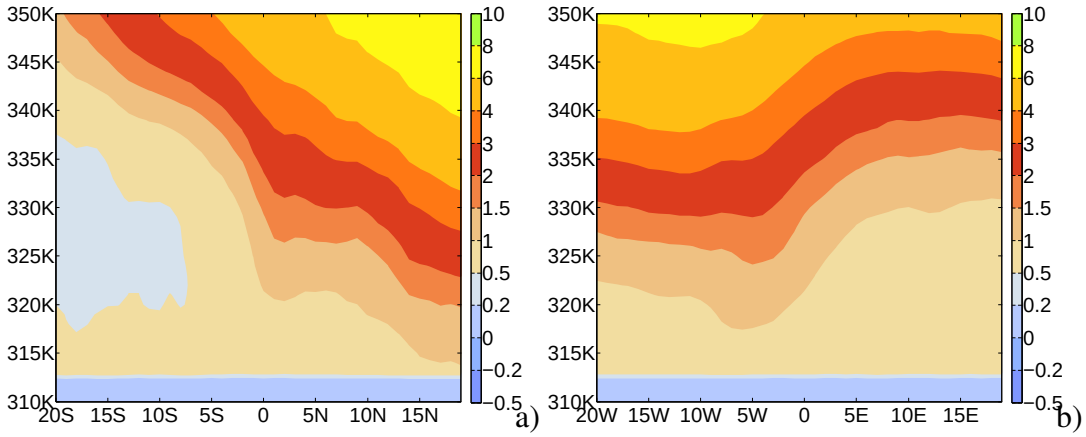

Figure 4.3: a) Cross section in north-south direction through a composite of mean potential vorticity in PVU averaged over all cases which have at least F1 strength during the tornado event. b) Cross section in west-east direction through a composite of mean potential vorticity in PVU averaged over all cases which have at least F1 strength during the tornado event.

4.1.2 Potential vorticity

In the PV field on the 320 K isentropic level, 24 hours prior to the tornado event, a PV trough is present at 20° west of the later affected area. This PV anomaly is moving towards east. It is producing a zone with high PV gradients just west of the struck area during the tornado event. The values are rising from 0.5 to 1.0 PVU 24 hours before to 1.5 to 2.0 PVU 12 hours after the tornado event on the 320 K isentropic level. It is possible that the PV leads to a destabilization of the stratification which enhances the potential for convection. A high PV gradient also produces strong winds which matches well to the intensification of the wind field (see figure 4.6a, b and c).

In the north-south cross section, the high PV gradient is also visible well (see figure 4.3a). Also a rising of PV values during and after the tornado event is present above the affected region and slightly north of it. During the tornado event some kind of PV fold can be observed between the 320 K and 335 K potential temperature level.

In the west-east cross section a strong descent of the dynamical tropopause (2 PVU) is visible to the west (see figure 4.3b). During the event under the PV anomaly a smaller anomaly can be noticed at about 5°W of the tornado region between the 315 K and 330 K level of potential temperature.

The descent of the dynamical tropopause indicates an incoming upper-level trough from the west. This system causes probably a destabilization of the air mass which enhances the evolution of convective cells. It also produces a wind field with southerly component, so that warm and moist air can be advected, which is improving additionally the conditions for convection. The role of the PV fold is not clear. Possibly, it is indicating a zone of high baroclinity.

4.1.3 CAPE

The spatial and temporal CAPE-distribution shows a distinct maximum in the region where tornadoes occur (see figure 4.4). However, the absolute CAPE values are rather low with around 400 $J\ kg^{-1}$ compared to typical CAPE values in the United States around 1'300 $J\ kg^{-1}$ in tornadic environments (see figure 1.10a).

24 hours before the event, a broad sector with relatively high CAPE values is present in the SW of the later affected area. This indicates that an unstable airmass is sometimes originating from more southwestern regions. Northwest of this zone is a high gradient of CAPE visible, indicating a frontal zone or a region with high gradient of low level moisture. After the tornado events a strong decay of CAPE from NW can be observed in the affected area. This also suggests that after a tornado event often a cold front is passing by or at least a colder air mass is flowing in and leads to stabilization.

4.1.4 SRH

The storm-relative helicity shows 24 h before the event a maximum west and west-southwest of the later affected area moving to the east (see figure 4.5). The signal strengthens 12 h prior to the tornado case reaching values up to 90 $J\ kg^{-1}$ at 8°W and at 5°S. During the tornado event, the signal is lying slightly southern of it with maximum values between 80 and 90 $J\ kg^{-1}$ and values around 70 $J\ kg^{-1}$ in the struck region. The values are also rather low compared to the United States, where typical values average around 180 $J\ kg^{-1}$ (see figure 1.10b). Nevertheless, the SRH shows a clear signal associated with tornadoes in Europe.

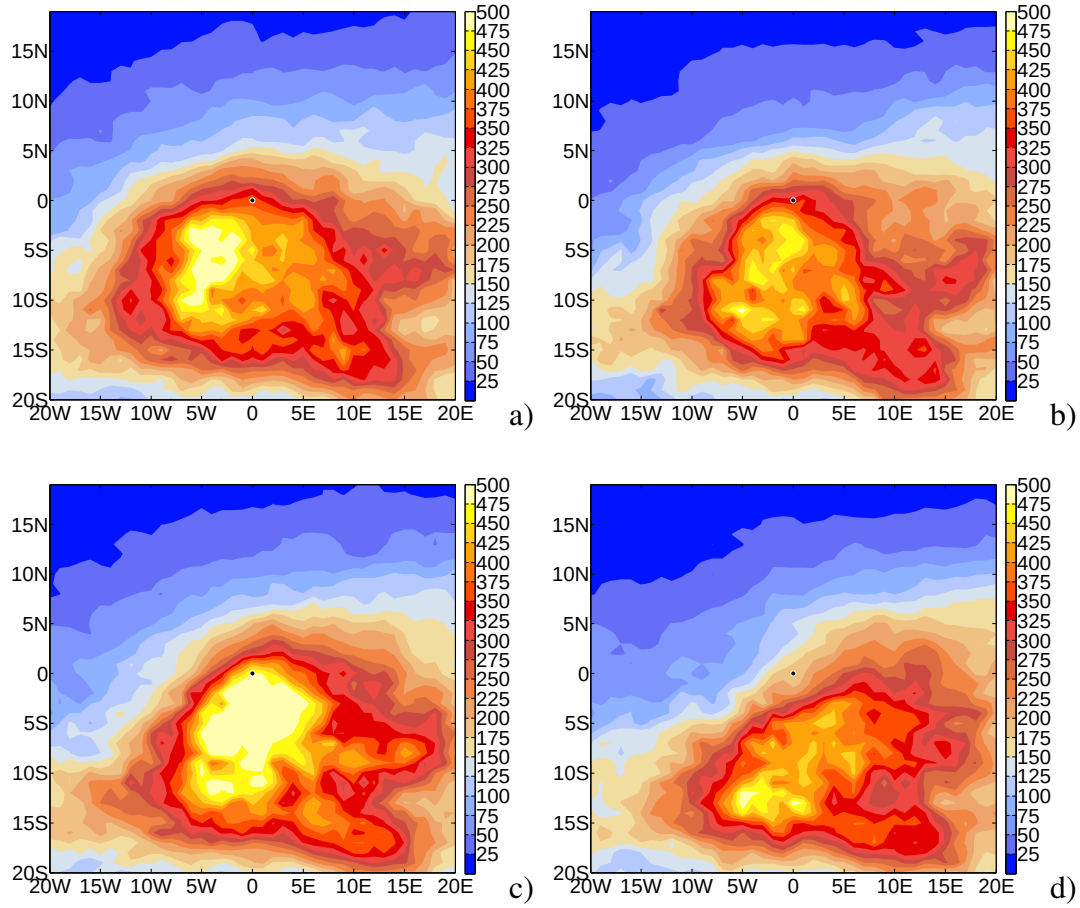

Figure 4.4: Composite of mean mixed-layer CAPE in J kg^{-1} averaged over all cases which have at least F1-strength a) 24 h before b) 12 h before c) during the tornado event and d) 12 h after the event. The black dots mark the position of the tornado events.

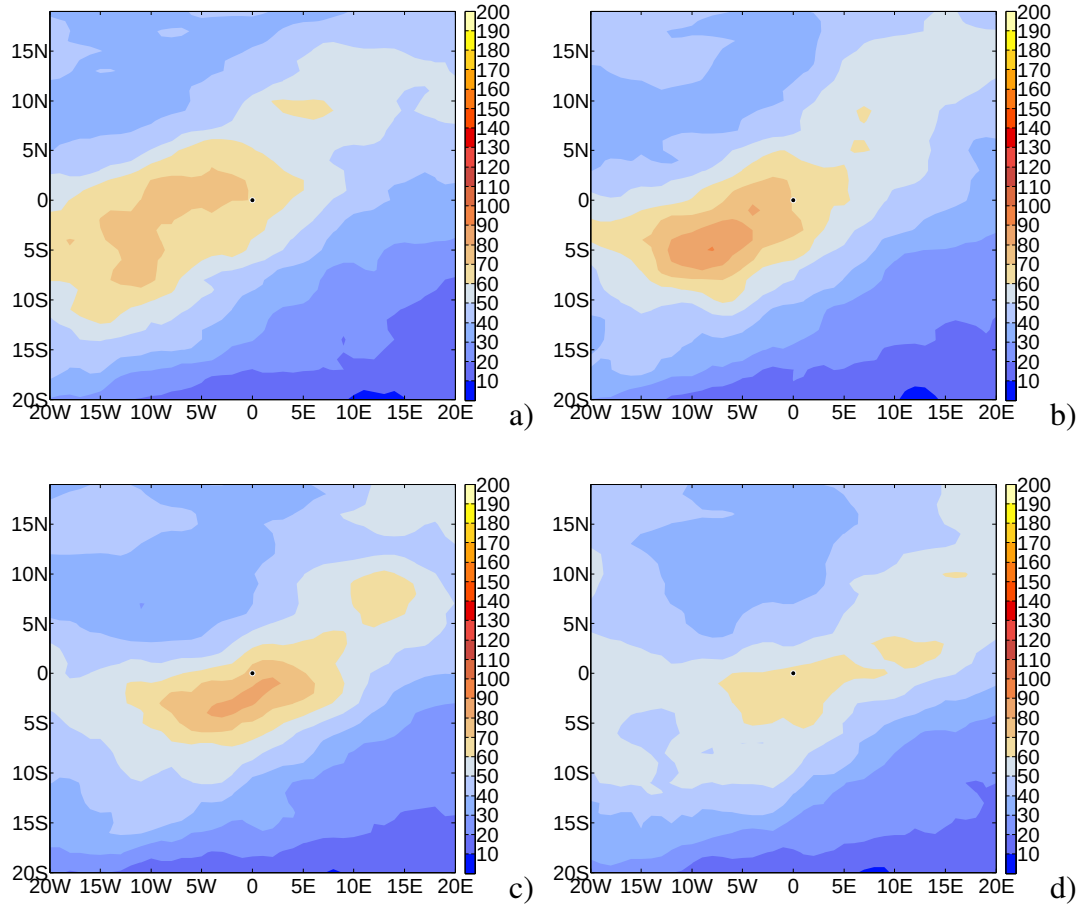

Figure 4.5: Composite of mean storm-relative helicity (SRH) in J kg^{-1} averaged over all cases which have at least F1-strength a) 24 h before b) 12 h before c) during the tornado event and d) 12 h after the event. The black dots mark the position of the tornado events.

4.1.5 Wind velocity

The wind field on the 700 *hPa* pressure level shows a low level jet west of the affected area 24 h before (see figure 4.6a). It is moving to the east and lying over the region during the tornado case with mean winds around 13 $m\,s^{-1}$ (47 $km\,h^{-1}$). Further, it is also showing a slightly cyclonic wind field over the affected region. This is indicating that stronger winds on the 700 *hPa* level can boost the development of tornadoes. Possibly, the low level jet enhances the probability of supercells with the production of horizontal vorticity. It's remarkable that the low level jet maximum on 700 *hPa* is lying north of the SRH maximum.

The wind field on the 250 *hPa* level indicates a jet streak with a maximum wind velocity of 30 $m\,s^{-1}$ (108 $km\,h^{-1}$) in the SW of the later affected area 24 h before (see figure 4.6b). The cyclonic curved jet is moving towards east. During the tornado event, the wind velocity maximum is lying at about 5°W and 5°S with maximum winds reaching 28 $m\,s^{-1}$. The tornadoes are spinning up under the left-exit region of jet streak which is consistent with observations from the United States.

The cross section through the wind field shows a broad area with strong winds between 200 and 300 *hPa* 24 h before the event (see figure 4.6c). The area with maximum wind-speed is sinking slightly from south to north. During the tornado event, a significant strengthening of the wind velocity between 900 and 200 *hPa* is visible, reaching maximum values slightly south of the affected area. This is indicating that wind fields and jetstreams are playing an important role for tornado genesis.

4.1.6 Vertical velocity

The vertical motion shows a maximum of lifting 24 h before the event in the west of the later struck area (see figure 4.6d). This area is moving towards east under intensification and is reaching maximum values during the tornado event. Also a maximum of sinking is visible at about 15° to 20° south of the area. This is indicating a strong ageostrophic circulation, which is possibly an additional trigger of convection and partly responsible for the moisture transport from southerly regions.

In the vertical north-south oriented cross section, already 24 hours before the tornado event a strong ageostrophic circulation is visible. The circulation is overlaid by convective lifting during the tornado event.

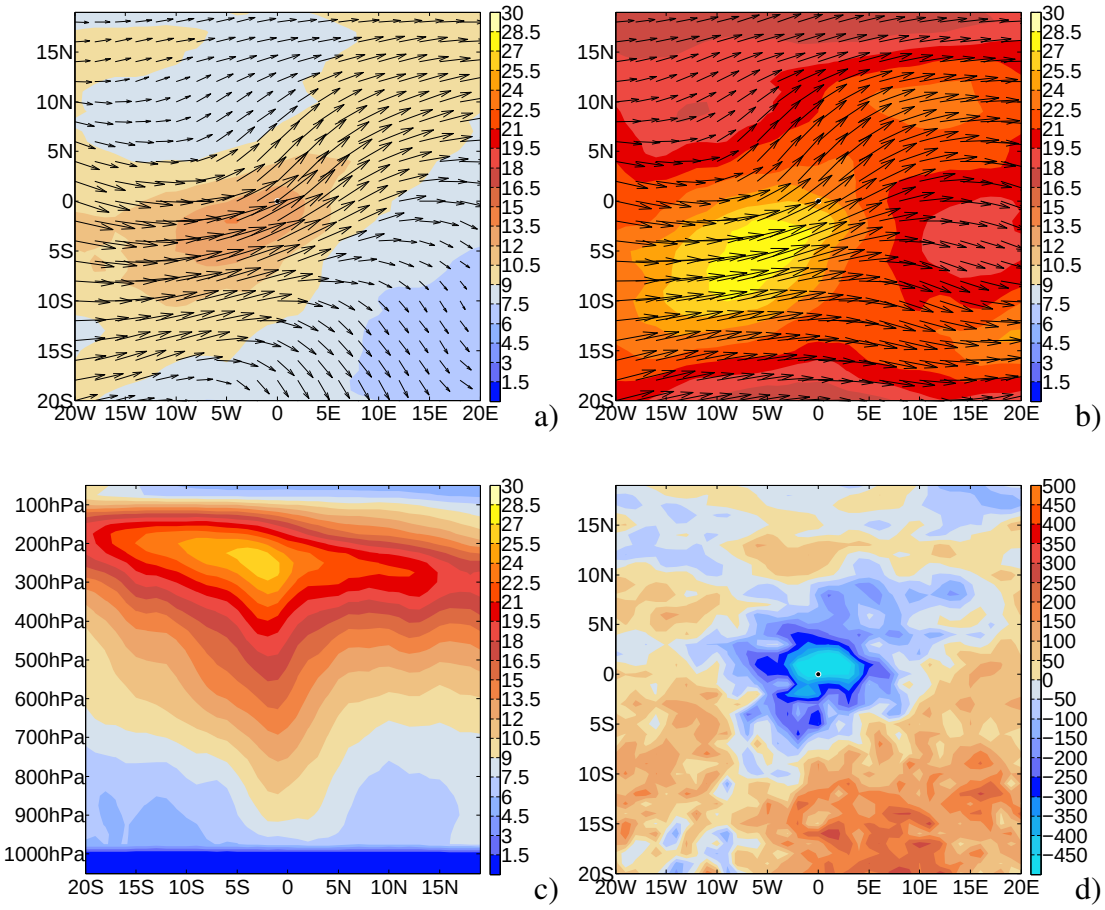

Figure 4.6: a) Composite of mean wind velocity on the 700 hPa pressure level in m s^{-1} averaged over all cases which have at least F1 strength during the tornado event. b) Like figure a) with wind velocity on the 250 hPa level. c) Vertical cross section in north-south direction through a composite of mean wind velocity in m s^{-1} averaged over all cases which have at least F1 strength during the tornado event. d) Composite of mean vertical velocity on the 700 hPa level in hPa h^{-1} averaged over all cases which have at least F1-strength during the tornado event. The black dots mark the position of the tornado events.

4.1.7 Divergence

In divergence field associated with the vertical motion, a convergence is visible near the ground already 24 hours before the tornado develops meanwhile on the tropopause level a divergent wind field is visible. Simultaneously, a convergent wind field exists on the tropopause level at 15°S and a divergent wind field is present near the ground. This leads to a southerly wind in the lower troposphere which can transport moisture from this southerly regions where evaporation is higher due to higher temperatures and lower cloud cover because of sinking motion. During the tornado event, the divergence/convergence field in the upper/lower troposphere is placed over the affected area. It can be assumed that they are associated mainly with the upward motion produced by convection. However, an additional component of ageostrophic upward motion is likely to be involved.

4.1.8 Moisture flux

24 h prior the tornado event, on the 850 *hPa* level, a strong moisture flux is visible west of the affected area. The zone with high moisture flux is moving to the east and lying exactly over the struck region during the event (see figure 4.7a). The moisture flux is strengthening till the event reaches values up to 10^{-3} $kg\ m\ s^{-1}$. The moisture flux has a strong westerly and only a weak southerly component. This leads to the assumption that the main moisture source in Europe is the Atlantic. The north-south cross section shows that moisture flux also strengthens with the height till the tornado event occurs (see figure 4.7b). Eventually, moisture advection at higher levels play also a role in tornado genesis. Markowski (2001) and Grzych et al. (2006) detected that warmer rear flank downdraft favor tornadogenesis. Probably, a higher moisture content in the mid troposphere leads to a lower evaporation of precipitation and so heats up the downdraft.

4.1.9 Moisture flux convergence

Moisture flux convergence on the 850 *hPa* level show a zone with high moisture advection in the west/northwest of the affected area 24 hours before. It is moving from west to east and reaches its maximum over the affected area during the tornado event (see figure 4.7c). It is known that moisture flux convergence is showing strong signals in the convective area, so it is not clear whether this parameter can also be used for tornado prediction.

In the north-south vertical cross section significant higher values of moisture flux convergence were observed up to 600 *hPa* (see figure 4.7d). Also here, it is not clear whether this is typical for convective areas. Further research will be necessary. (see also figures in section B.1 for more detailed information)

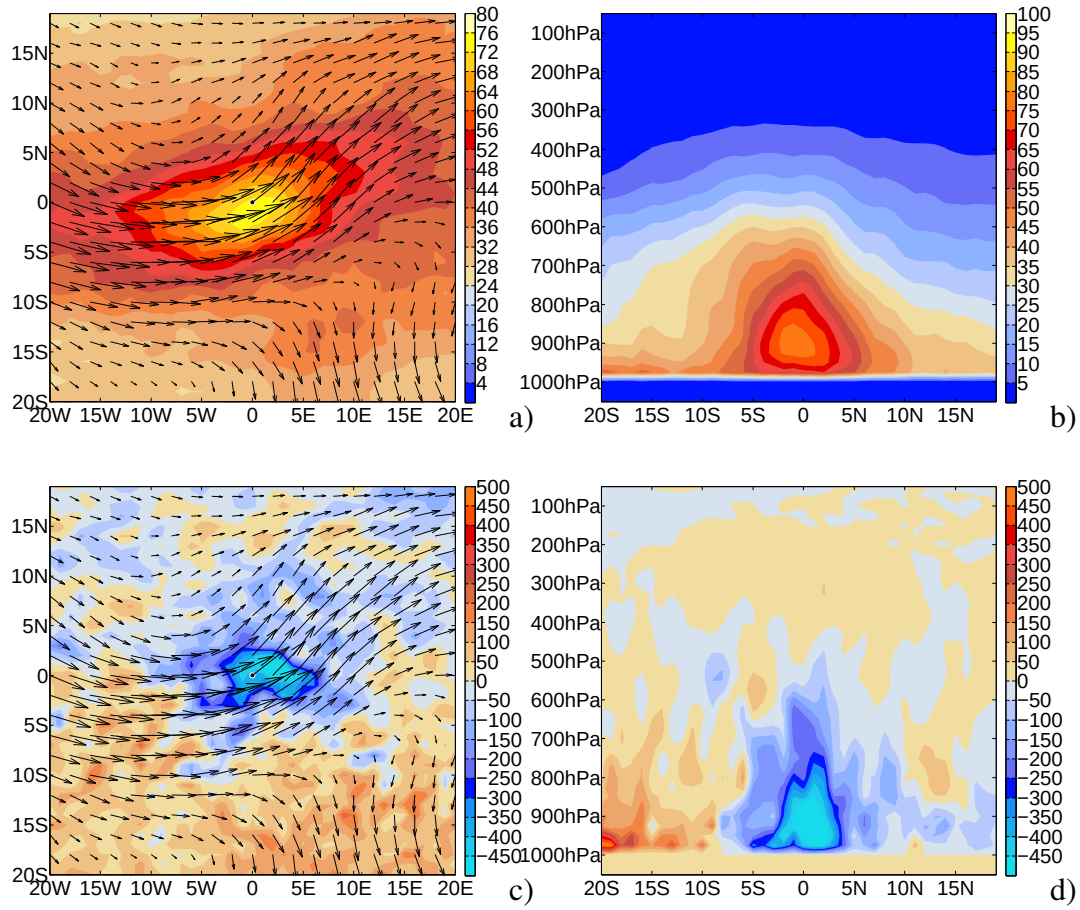

Figure 4.7: a) Composite of mean moisture flux on 850 hPa in 10^{-3} *kg m* s^{-1} *averaged over all cases which have at least F1 strength during the tornado event. b) Cross section in north-south direction through a composite of mean moisture flux in* 10^{-3} *kg m* s^{-1} *averaged over all cases which have at least F1 strength during the tornado event. c) Composite of mean moisture flux divergence on the 850 hPa level in* 10^{-3} *kg m* s^{-1} *averaged over all cases which have at least F1 strength during the tornado event. Negative values stand for moisture flux convergence. d) Cross section in north-south direction through a composite of mean moisture flux divergence in* 10^{-3} *kg m* s^{-1} *averaged over all cases which have at least F1 strength during the tornado event. Negative values are standing for moisture flux convergence. The black dots mark the position of the tornado events.*

4.2 Comparison of types

4.2.1 Waterspouts and land tornadoes

In this section, tornadoes and waterspouts were compared with each other. Because waterspouts are generally weak events, and in order to get a better comparability, only land tornadoes with F0 strength were compared with them. In the composites, 236 waterspout cases and 416 F0 land tornadoes were averaged.

Both types show a pronounced **CAPE** signal, but with lesser values and higher spatial variability for waterspouts (see figure 4.8a and c). Possibly over relatively warm sea surface locally higher CAPE values are present which cannot be represent well by ECMWF analysis data. Especially near the coast, where most waterspouts were observed, small-scale land-sea wind systems can lead to convergence zones and locally warmer water can produce higher CAPE values. Such small-scale processes are not resolvable by a global weather model like ECMWF.

The mean **SRH** is low in both cases, but signals were visible (see figure 4.8b and d). For tornadoes over land, a weak maximum is present over the affected area whereas in waterspout cases the signal is localized at about 5°W and 5°S. This indicates that SRH is not playing a large role in the evolution of waterspouts. Possibly this is because waterspouts are normally non-supercellular. Also for F0 land tornadoes, SRH does not seem to be an important parameter, although a weak signal is present. This also indicates that most weak tornadoes in Europe are non-supercellular. (for more details see also figures in section B.2.1)

The results lead to the assumption, that SRH is not a useful forecast parameter for weak tornadoes. CAPE seems to be more important, but the signal is not very distinct as well. Because CAPE is also a predictor for convection, it does not seem to be not a useful discriminator between convective cells and weak tornadic storms.

The **wind velocity** field on the 700 *hPa* pressure level shows a cyclonic curved wind field nearby for both tornado types, but more curved for waterspout types. In case of waterspouts, a significantly pronounced low level jet (LLJ) is visible about 5° to 10° south of the affected area, whereas for land tornadoes a LLJ is only weakly indicated.

On the 250 *hPa* pressure level for both types, a jetstreak is present in the south of the tornado position(see figure 4.9a and c), but more pronounced and stronger for waterspout events. The maximum wind speed in the land type was reached SSW of the affected area whereas for waterspouts it is positioned more to the WSW. A secondary wind speed maximum is visible SE of the waterspout cases.

The **vorticity** on 850 *hPa* level shows a maximum above and slightly to the west of the affected area. The values are only slightly higher in waterspout cases. On the 250 hPa pressure level vorticity values are higher and the maximum is shifted to the west(see

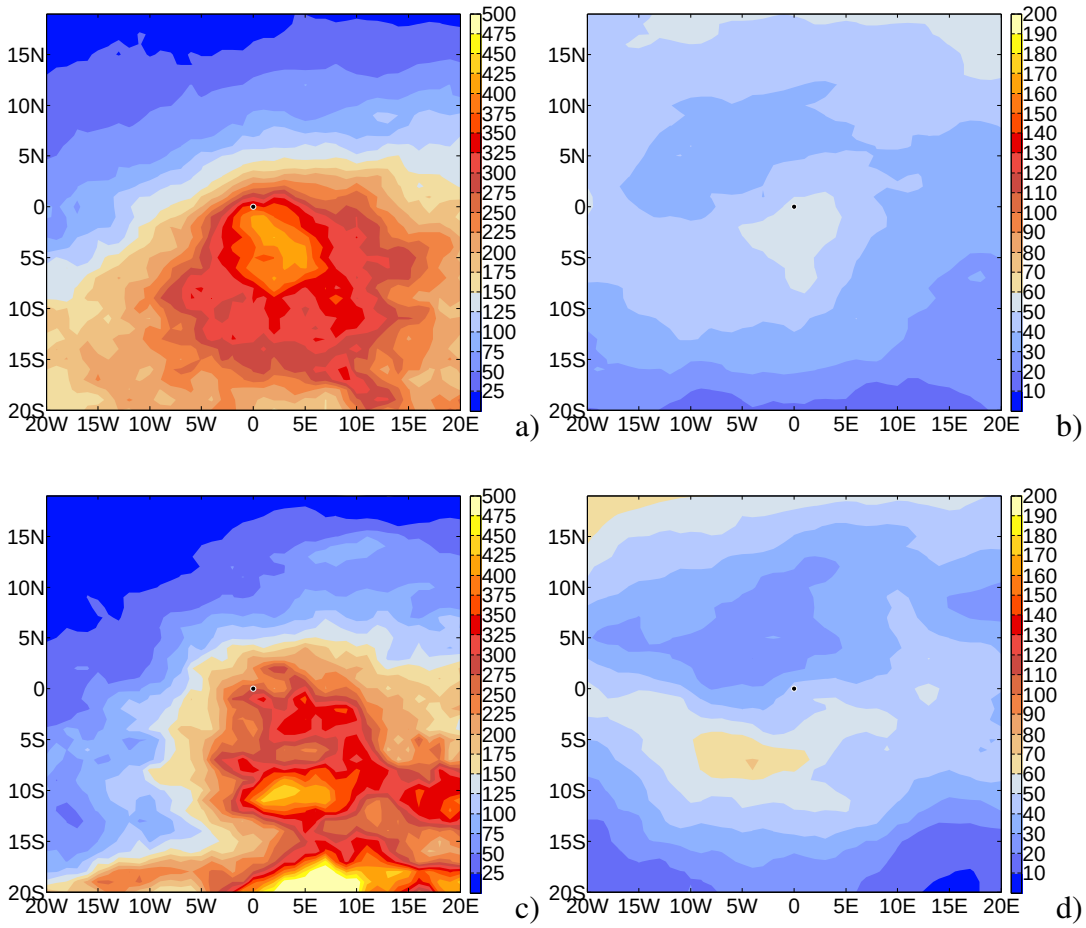

Figure 4.8: Comparison between tornadoes over land (upper row) and waterspout type (lower row) for CAPE (left side) and SRH (right side) during the event. The black dots mark the position of the tornado events.

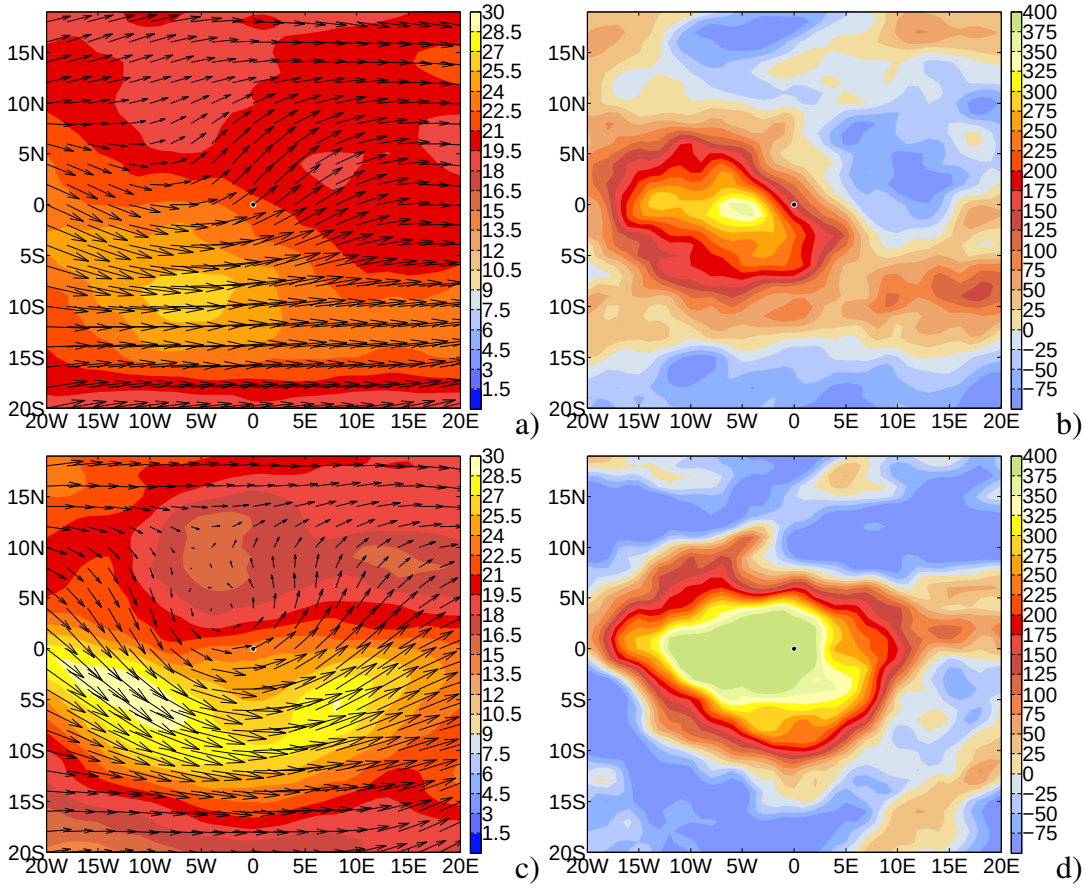

Figure 4.9: Comparison between tornadoes over land (upper row) and waterspout type (lower row) for wind velocity (left side) in m s^{-1} on the 250 hPa level and for vorticity (right side)in 10^{-6} s^{-1} during the event. The black dots mark the position of the tornado events.

figure 4.9b and d). Significantly higher values are present in the environmental area of waterspouts, especially in the upper troposphere.

High vorticity values seem to be important in both cases. The stronger signal for waterspouts is surprising. Obviously, in case of waterspouts an overlying strong cyclonic circulation is playing an important role in their evolution. This contradicts the idea that waterspouts are a purely small-scale phenomena which develops independently from synoptic systems. Because vorticity is not necessarily connected with convection, it is maybe a good discriminator between convection and weak tornadic storms.

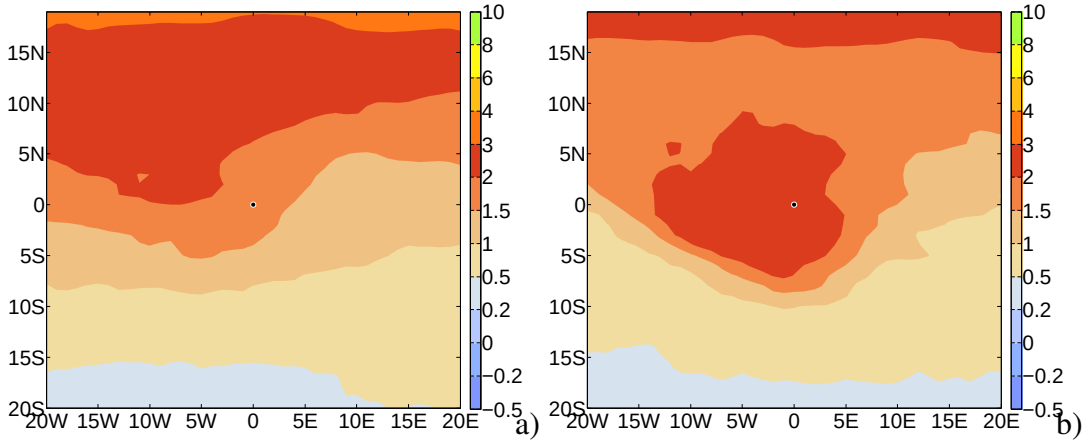

Figure 4.10: Comparison between tornadoes over land (figure a) and waterspout type (figure b) for PV in PVU on the 320 K Θ-level during the event. The black dots mark the position of the tornado events.

The **PV** pattern on the 320 *K* level of potential temperature indicates that both cases are affected by the influence of an upper-level trough (see figure 4.10). But the PV values are clearly higher during waterspout cases. This is also an explanation for higher vorticity values seen in waterspout types, especially in the higher troposphere. This is also visible in the vertical cross sections (see figure 4.11a and c). Further, it can be observed that in waterspout cases, the PV signal is more distinctive and is lying closer to the affected region. This indicates that a PV anomaly is an important trigger for waterspouts.

Because in waterspout cases generally lower moisture advection is present, the PV anomaly can destabilize the atmosphere by cooling the upper troposphere and thus leading to sufficient instability for moist convection above the water surface. Also the PV anomaly produces a cyclonic wind field below it, which explains high vorticity values especially in case of waterspouts.

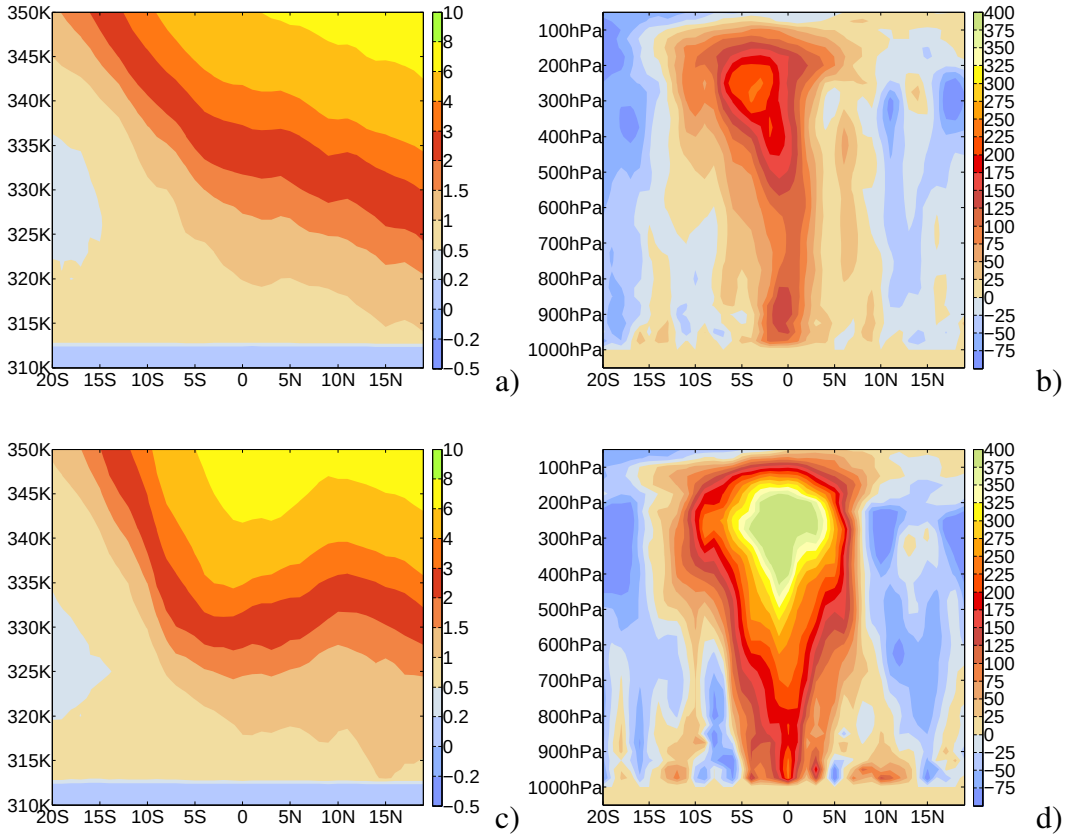

Figure 4.11: Comparison between tornadoes over land (upper row) and waterspout type (lower row) for a north-south PV [PVU] cross section (left side) and a north-south vorticity [10^{-6} s^{-1}] cross section (right side) during the event.

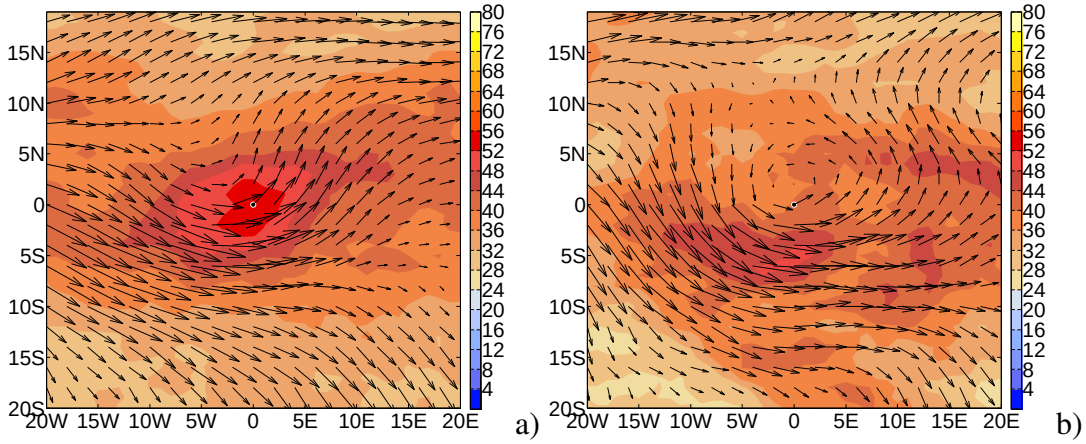

Figure 4.12: Comparison between tornadoes over land (figure a) and waterspout type (figure b) for moisture flux in 10^{-3} *kg m* s^{-1} *on 850 hPa (left side) during the event. The black dots mark the position of the tornado events.*

The **moisture flux** is maximal over the affected area of land tornadoes (see figure 4.12a and c), whereas over water the signal is less distinct (see figure 4.12b and d). So, it can be supposed that moisture flux is more important over land than over water, where evaporative processes at least sometimes are playing a major role. However, moisture flux convergence is visible in both tornado types.

Summary

Waterspouts and land tornadoes seem to occur in quiet different synoptic environments. CAPE and SRH values are significantly lower in case of waterspouts. However, the absolute values of CAPE and SRH are relatively low. In both cases, a distinct vorticity signal is visible, especially in the upper troposphere. This indicates that synoptic-mesoscale systems have an important influence on weak tornadic storms over water and land as well. Especially in case of waterspouts, overlying PV anomalies are a factor in their evolution. Possibly, the strong vorticity in the upper troposphere is caused partly by this PV anomaly. Moisture fluxes are higher in case of land tornadoes. It can be supposed that evaporative processes compensate the lower moisture flux over water at least partly. (for more details see also figures in section B.2.1)

4.2.2 Winter and summer

In this section, winter and summer season types were compared with each other. Waterspouts and tornadoes over land were put together. The winter season types contain events in the months October, November, December, January, February and March. The other events were termed as summer season types. In the composites, 118 winter cases and 803 summer cases were averaged.

Both types show a maximal **CAPE** signal in the south of the affected area (see figure 4.13a and c). But CAPE values are much lesser (around 150 $J\ kg^{-1}$) for the winter season type due to a lower insolation whereas summer season types occur with values around 400 $J\ kg^{-1}$. However, it can be recognized that in winter CAPE values are lying significantly over the climatological mean, whereas in summer, this is not the case. This indicates that eventually CAPE is a better predictor for tornadoes in winter.

The mean **SRH** is low in summer season cases, but a weak signal with values around 50 $J\ kg^{-1}$ is visible in the south and in the southwest of the affected area. For the winter season case a more distinct maximum can be observed in the south of the tornado point (see figure 4.13b and d). The values are higher with values around 110 $J\ kg^{-1}$. This indicates that eventually storm-relative helicity is more important in wintertime for the generation of tornadoes. However, average wind speeds are higher during winter in the climatological mean which leads to higher probability for high SRH values. Nevertheless, the SRH signal is quiet distinct, so that it can be assumed that it is a useful predictor for tornadoes.

The **wind velocity** on the 700 *hPa* level shows a maximum in the south and in the south-west of the affected area. For both types, a trough is indicated at around 5° west to the tornado events, but the wind field shows a stronger cyclonic curvature in winter. Wind speed ranges around 10 $m\ s^{-1}$ for summer season types and around 15 $m\ s^{-1}$ for cases in winter. This is consistent with the higher storm-relative helicity observed in winter (see figure 4.13b and d). Thus, more horizontal vorticity is available in the lower troposphere.

The trough positioned to the west is also visible in both 250 hPa level wind fields (see figure 4.14a and c). The wind field shows also a stronger cyclonic curvature on this level in wintertime. In both types, a jet streak is present in the south of the affected area. The average wind speed amounts to 22 $m\ s^{-1}$ in summer and to 30 $m\ s^{-1}$ in winter. It is also remarkable that the region with strong winds is much broader in winter whereas in summer the region with maximum winds is situated quite close to the tornado point. (for more details see also figures in section B.2.2)

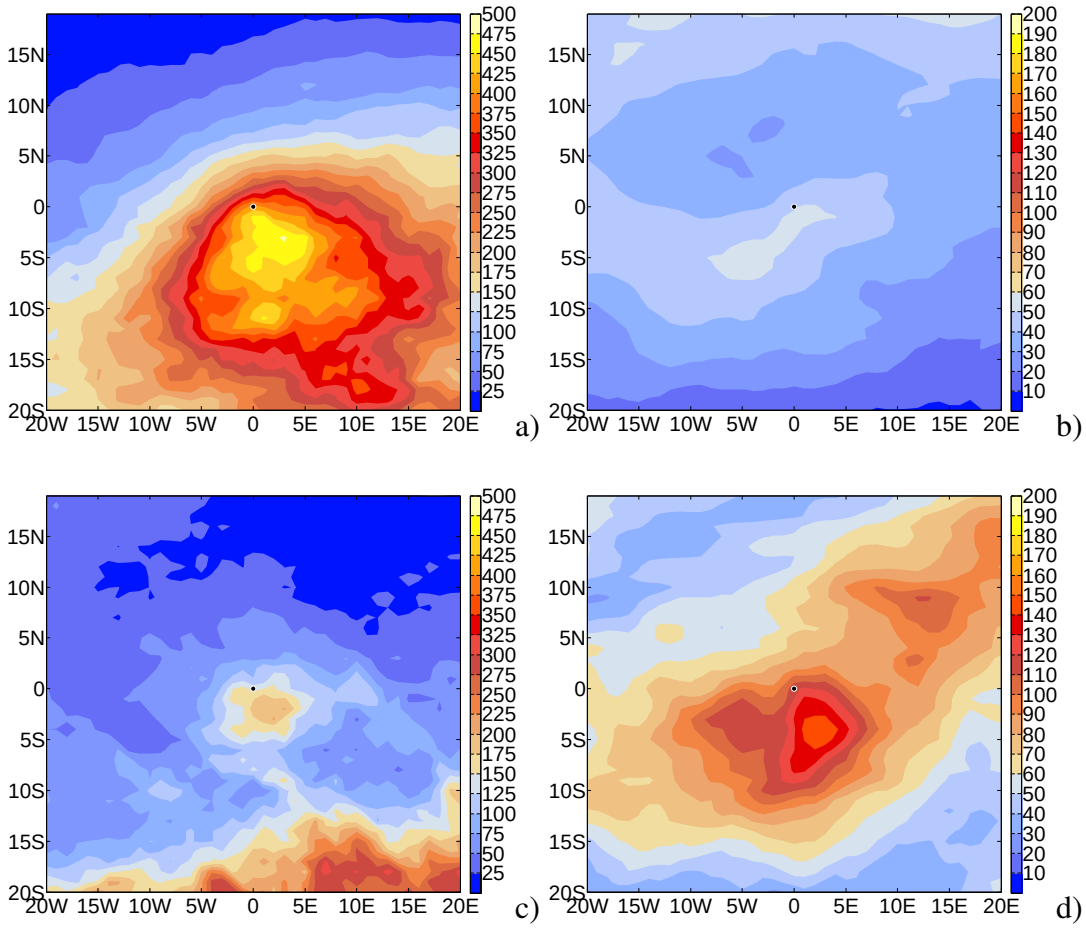

Figure 4.13: Comparison between summer season type (upper row) and winter season type (lower row) for CAPE (left side) and SRH (right side) during the event. The black dots mark the position of the tornado events.

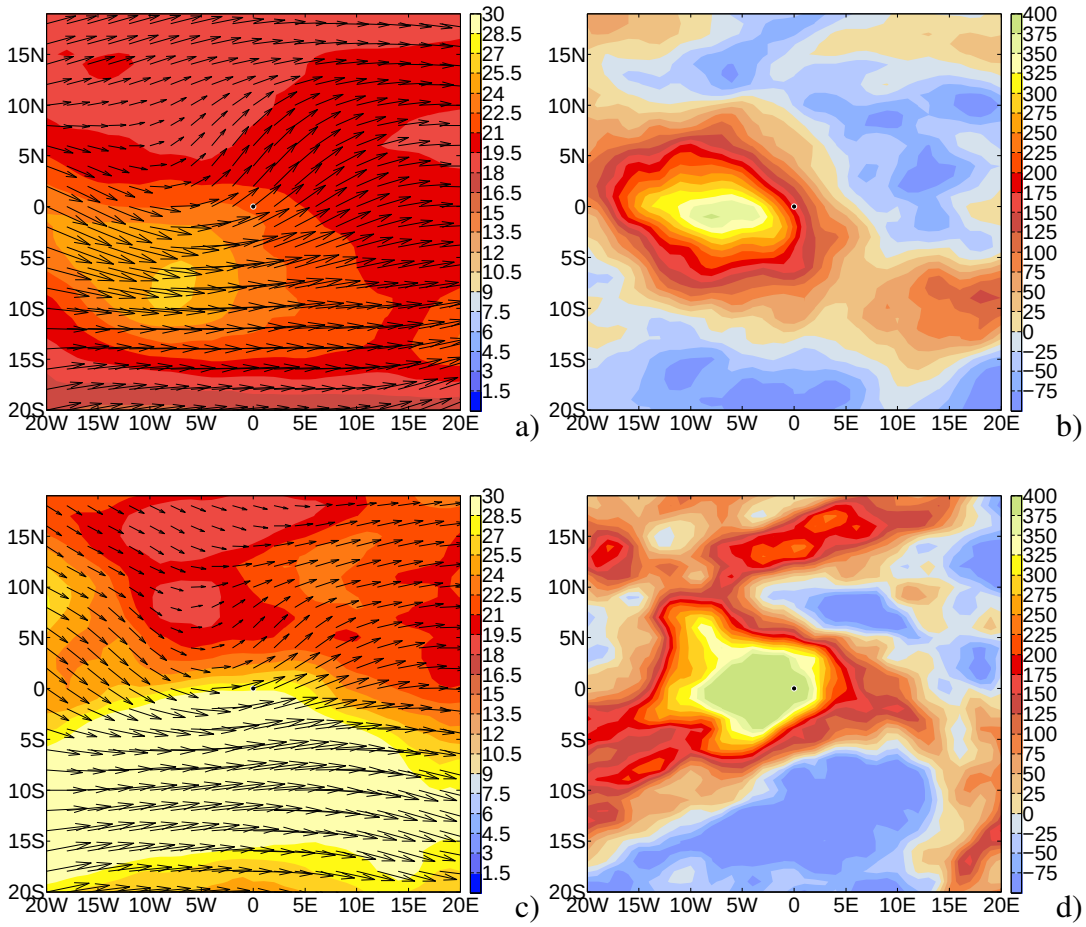

Figure 4.14: Comparison between summer season type (upper row) and winter season type (lower row) for wind velocity (left side) in m s^{-1} on 250 hPa and for vorticity (right side) in 10^{-6} s^{-1} during the event. The black dots mark the position of the tornado events.

Vorticity on the 850 *hPa* level shows a maximum close to the affected area in summer. This is also the case in winter, but then the signal is larger and shows more variance. It is remarkable that in wintertime to the north of affected area vorticity is mainly cyclonic, whereas to the south of the point vorticity is mostly negative, especially in an area located between 10°S and 20°S.

In both cases a strong vorticity signal is present on the 250 *hPa* pressure level in both type classes, but better placed over the affected area in winter (see figure 4.14b and d). The maximal values of the vorticity feature are somewhat higher in winter. Also here an area with negative vorticity values is visible in area between 10°S and 20°S, especially during winter time. It can be assumed that vorticity is the better predictor for tornadoes during winter. It is also possible, that strong synoptic systems are more common in winter whereas in summer also mesoscale convective systems, which are not necessarily detected by ECMWF, are a factor in the evolution of tornadic storms.

Potential vorticity on 320 *K* and 330 *K* isentropic levels are higher in winter which is consistent with the climatological mean. However, the PV trough seems to be better developed in summer. In both cases, a high PV gradient can be observed to the south on the 330 *K* level in summer and on the 320 *K* and the 330 *K* level in winter. In the N-S vertical cross section through PV during winter time a tropopause fold is visible, whereas in summer only a high gradient is visible in the south of the struck area (see figure 4.15a and c). Both types show a distinct vorticity maximum, but much higher values can be observed in winter, especially on jet stream level. In the W-S cross section, it is also indicated that the vorticity maximum is better placed over the tornado region than in summer.

Moisture flux on 850 *hPa* shows in both cases a maximum over the tornado area. Moisture fluxes are a slightly higher during winter time. Lower moisture content can be compensated by higher wind speed. Interestingly, moisture flux convergence shows a significant different signal for moisture flux convergence. It shows a small north-south oriented band with high moisture flux convergence in winter. Low level forcing seems to be much more important during winter time.

Summary

CAPE and SRH seem to be more useful as predictors in winter, when they are related to the climatological mean, which is significantly lower. Also synoptic systems appear to be more important in winter for tornado genesis, which is indicated by vorticity and upper-level PV. Eventually, in winter a stronger forcing is needed to produce convective cells which are capable to develop tornadoes. Moisture flux seems to be similar in both season, which makes it a good predictor for the whole year. However, it is not clear, if moisture flux is a good discriminator between convection cells and tornadic storms. (for more details see also figures in section B.2.2)

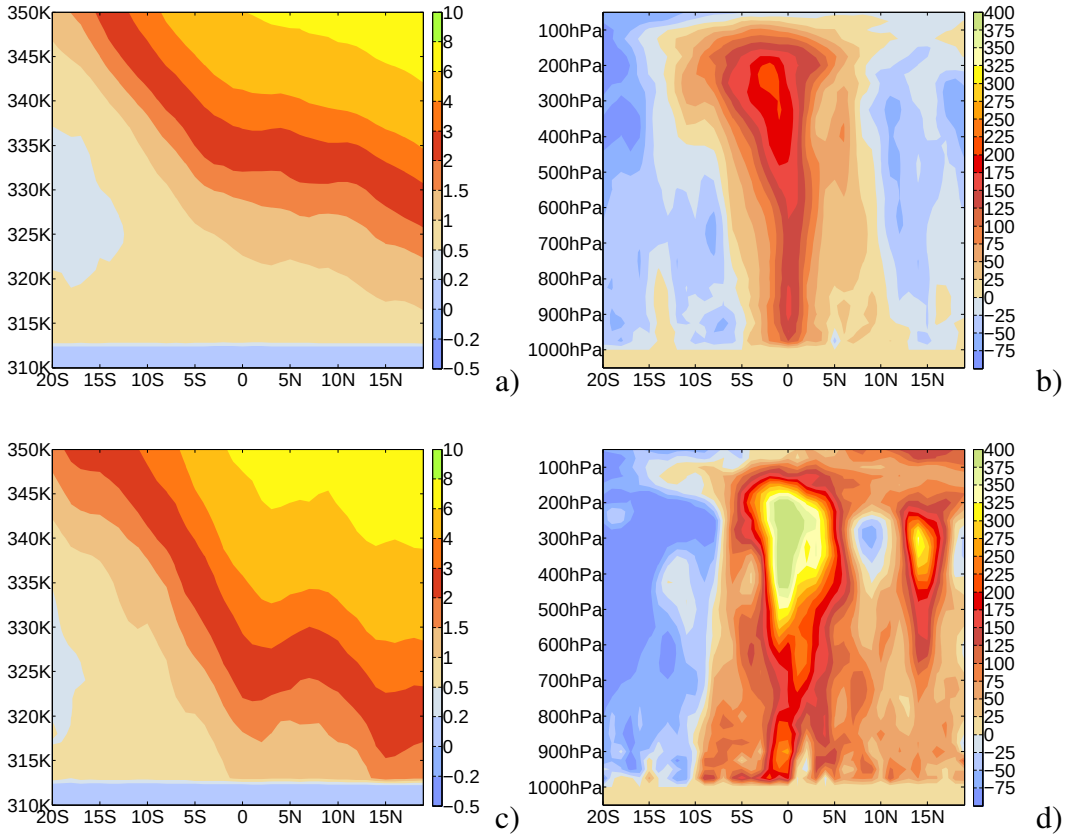

Figure 4.15: Comparison between summer season type (upper row) and winter season type (lower row) for a north-south PV [PVU] cross section (left side) and a north-south vorticity [10^{-6} s^{-1}] cross section (right side) during the event.

4.2.3 Weak and damaging

In this section a comparison between weak F0 tornadoes and damaging F1+ tornadoes was made. Only land tornadoes were compared with each other. For the composites of F0 tornadoes, 418 events were averaged including funnel clouds, whereas the number of F1+ tornadoes amounts to 279 cases.

CAPE values show in both cases a maximum south of the tornado events (see figure 4.16a and c). But the values are significantly higher for the damaging type, which is consistent with observations in the United States, where significant tornadoes (F2+) are associated with higher mean CAPE values (see figure 1.10a). Mean values amount to 500 $J\ kg^{-1}$ for damaging tornadoes and 350 $J\ kg^{-1}$ for F0 tornadoes in Europe. However, the absolute CAPE values are much lower in Europe compared to the US.

SRH values show only a weak maximum for F0 cases, whereas for damaging tornadoes there is a distinct maximum present in the south of the affected area (see figure 4.16b and d). The values reach 50 $J\ kg^{-1}$ for weak tornadoes and 70 to 80 $J\ kg^{-1}$ for cases with damaging tornadoes. This indicates that stronger tornadoes are possibly partly accompanied by supercells, although the threshold value of 100 $J\ kg^{-1}$ is not reached. As for CAPE values, the absolute SRH values are rather low compared to the US (see figure 1.10b).

The comparison is indicating that CAPE and SRH values correlate with the strength of tornadoes. However, SRH seems to be the better discriminator because of the more distinct SRH signal. Probably, this is due to the fact that stronger tornadoes are normally associated by supercells. Further, the low SRH values compared to the US indicates eventually that many tornadoes in Europe are non-supercellular. (for more details see also figures in section B.2.3)

The **wind velocity** field on 700 *hPa* shows significantly higher values for damaging tornadoes. In the wind field of damaging tornadoes a low level jet is visible with wind speed values around 13 $m\ s^{-1}$. For weak cases no clear maximum can be observed. The values amounts only to 10 $m\ s^{-1}$ which lies not clearly over the climatological mean. This indicates that wind speed eventually can be used as predictor for stronger tornadoes. A correlation analysis was indicating that correlation of wind speed with tornado strength was largest compared to other parameters.
On the 250 *hPa* pressure level the wind speed is also higher for damaging tornadoes (see figure 4.17a and c). The area of damage is placed under the left-exit region of a jet streak with wind speed around 26 $m\ s^{-1}$. For weak tornadoes also a jet streak is visible, but with weaker appearance and shifted more to the south. The wind speeds over the affected area reaches values amounting to 22 $m\ s^{-1}$. This is indicating that a stronger jet streak can be important for tornado genesis. Especially the left-exit region seems to be conducive for tornado development which was also observed in the United States. Eventually, severe convection in this region was forced by strong lifting due to a differential vorticity advection.

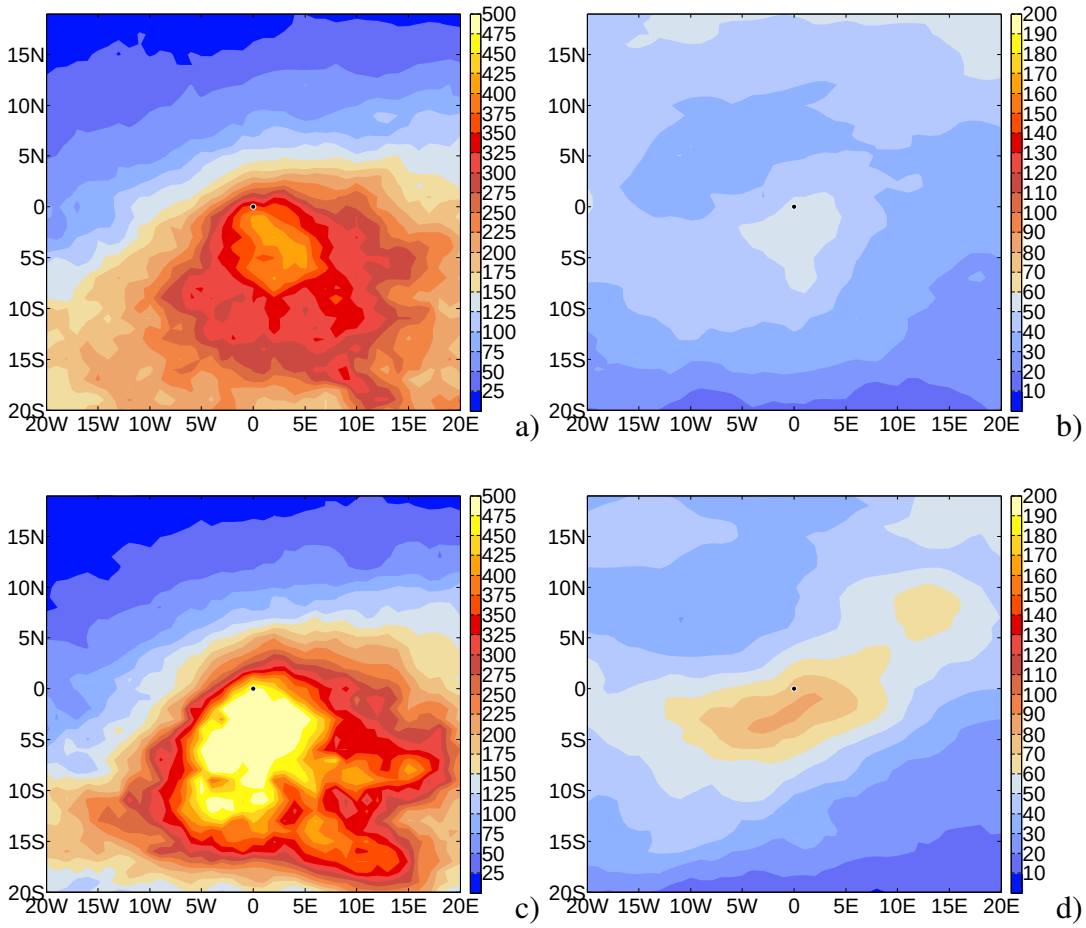

Figure 4.16: Comparison between weak (F0) type (upper row) and damaging (F1+) type (lower row) for CAPE (left side) and SRH (right side) during the event. The black dots mark the position of the tornado events.

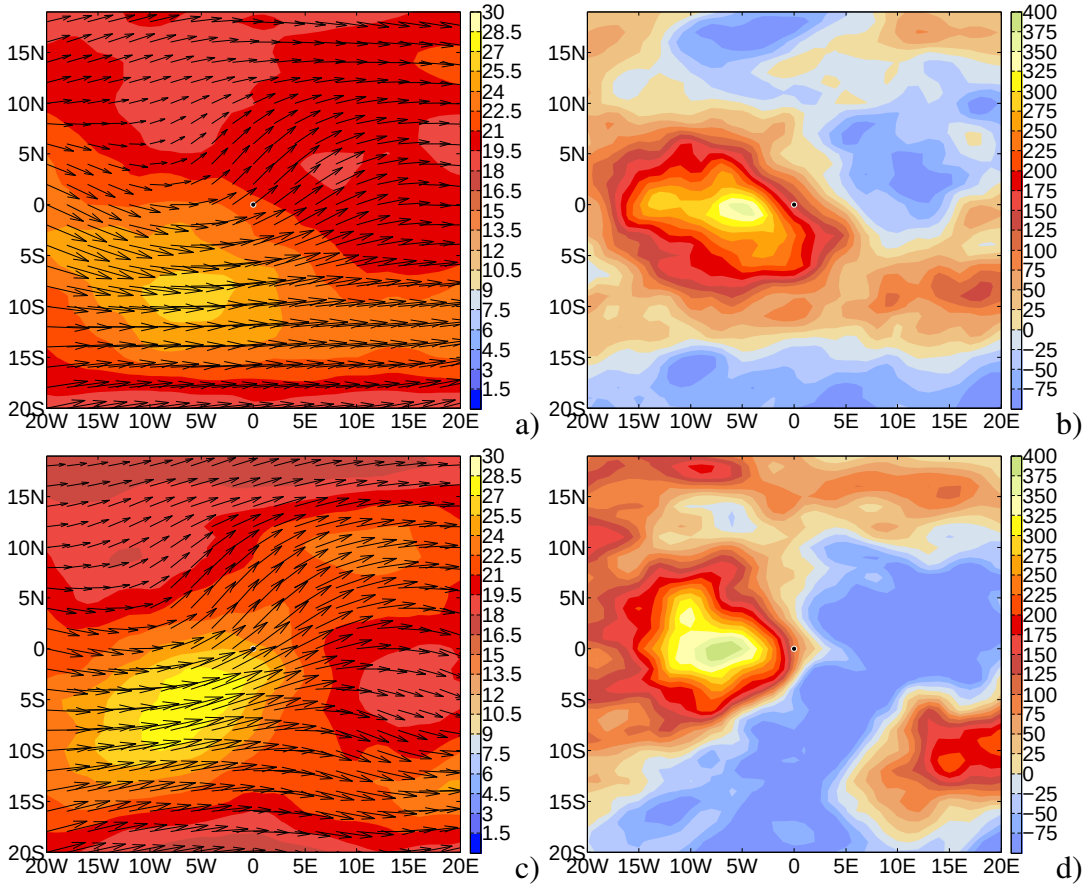

Figure 4.17: Comparison between weak (F0) type (upper row) and damaging (F1+) type (lower row) for wind velocity (left side) in m s^{-1} on 250 hPa and vorticity (right side) in 10^{-6} s^{-1} on 250 hPa during the event. The black dots mark the position of the tornado events.

Vorticity on 850 the *hPa* pressure level shows similar values for both cases. The spatial distribution is also similar. The vorticity values on the 250 *hPa* level are similar (see figure 4.17b and d). The maximum values were reached at around 5°W of the affected area. Differences can be seen in the vorticity gradients. In weak cases, the vorticity gradient is lower and shows an increase from NE to SW. In damaging cases, the vorticity gradient is higher and shows an increase from E to W. There, negative values are visible to the east and south of the tornado region. It can be speculated that the high gradient zone is conductive for the development of mesoscale convective systems or supercells produced by mesoscale lifting zones. However, vorticity seems to be an important parameter for both types, but it seems to be not very useful as discriminator between weak and strong tornadoes. Eventually, vorticity gradients or differential vorticity advection is more suitable for this use.

PV values are similar for both cases, but the gradients also show significantly higher values for damaging tornadoes. This also can be seen in the N-S cross section of PV (see figure 4.18a and c). Damaging tornadoes show an indicated tropopause fold whereas weak tornadoes only point out a continuous decrease of the dynamical tropopause from south to the point of the tornado location. In the N-S cross section of vorticity higher values can be observed for weak tornadoes at the jet stream level (see figure 4.18b and d). In the lower troposphere, vorticity values are higher for damaging cases. The vorticity gradients are higher for damaging cases and to the south negative values are present.

In the W-E cross section the maximum vorticity is present in both cases at about 7°W and on 300 *hPa* pressure level (see figure 4.19). For damaging cases higher vorticity values can be observed which is indicating that a stronger upper-level trough is situated west of the affected area. Also here a higher gradient is visible for damaging tornadoes and vorticity values are negative to the east.

The PV fold seems to be an important feature associated with stronger tornadoes. However, the physical connection is not clear. Possibly, the tropopause fold leads to high vorticity values below it. This can cause strong differential vorticity advection in combination with the jet streak, which leads to a strong upward motion acting as a trigger of convection. Eventually, a strong destabilization caused by cooling of the upper troposphere enhances severe convection. However, strong convection is not necessarily associated with tropopause folds. So, further investigations of this PV feature and its connection with tornadoes are needed.

Moisture fluxes show significant differences between the two types (see figure 4.20a and b). The values are clearly higher in case of damaging tornadoes. The values amount to about $55 \cdot 10^{-3}$ $kg\ m\ s^{-1}$ in case of damaging tornadoes and to about $75 \cdot 10^{-3}$ $kg\ m\ s^{-1}$ in case of weak tornadoes. Maximum values are placed quite exactly over the tornado location. This indicates that moisture flux is eventually a good discriminator between weak and damaging tornadoes.

Moisture flux convergence also shows a maximum over the affected area for both types. The values are also significantly higher in case of damaging tornadoes with values around $400 \cdot 10^{-3}$ $kg\ m\ s^{-1}$, whereas the mean moisture flux convergence amounts to $200 \cdot 10^{-3}$ $kg\ m\ s^{-1}$ nearby weak tornadoes. Also this parameter is eventually a good discriminator between weak and strong tornadoes. However, it should be kept in mind that mean CAPE values are higher in case of damaging tornadoes. This leads probably to stronger upward motion by convection in the ECMWF analysis data and causes stronger convergence in the lower troposphere. This relativizes slightly the differences between weak and strong tornadoes.

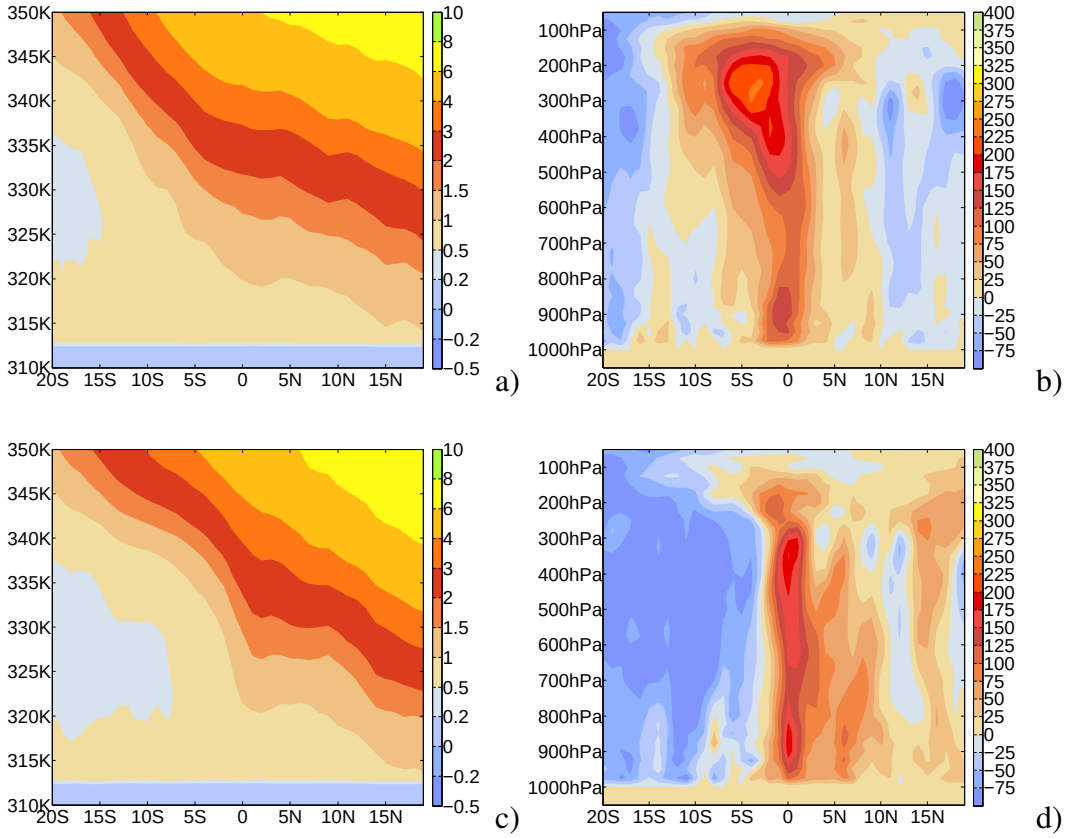

Figure 4.18: Comparison between weak (F0) type (upper row) and damaging (F1+) type (lower row) for a north-south PV [PVU] cross section (left side) and a north-south vorticity [10^{-6} s^{-1}] cross section (right side) during the event.

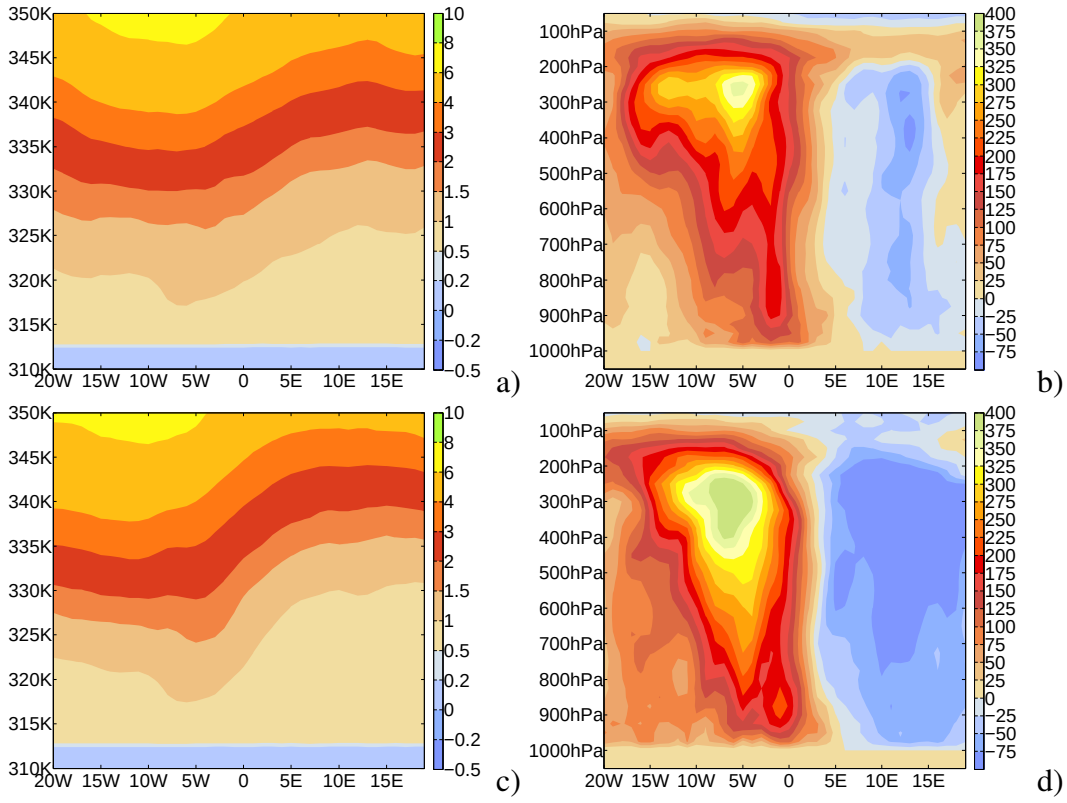

Figure 4.19: Comparison between weak (F0) type (upper row) and damaging (F1+) type (lower row) for a west-east PV [PVU] cross section (left side) and a west-east vorticity [10^{-6} s^{-1}] cross section (right side) during the event.

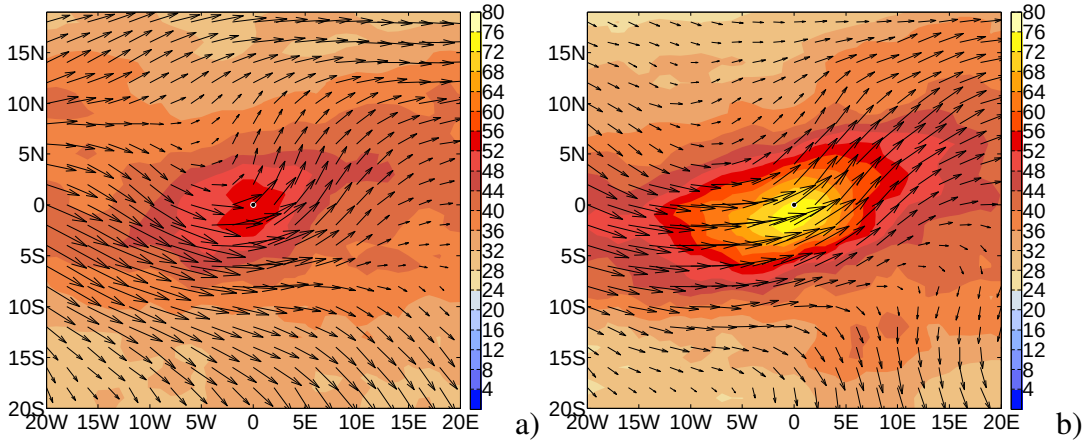

Figure 4.20: Comparison between weak (F0) type (figure a) and damaging (F1+) type (figure b) for moisture flux in 10^{-3} kg m s^{-1} on 850 hPa during the event. The black dots mark the position of the tornado events.

Summary

The parameters CAPE and SRH show significant differences between weak and damaging (F1+) tornadoes. Especially SRH show a much more distinct signal in case of damaging tornadoes. This leads to the assumption that SRH is the better discriminator between weak and strong storms, probably because SRH is also a predictor for supercells which are normally a requirement for strong tornadoes. Absolute values of vorticity are a rather bad discriminator, but vorticity gradients are significantly larger in case of F1+ tornadoes. The most prominent feature, which discriminates between weak and damaging storms, is a indicated PV or tropopause fold. The physical meaning of this structure it not clear. Moisture fluxes are eventually a useful forecast parameter to distinguish between weak and strong tornadoes. (for more details see also figures in section B.2.3)

4.3 Synthesis

Also in Europe, classic tornado forecast parameters like CAPE and SRH seem to be useful predictors for tornadoes. CAPE fits better in winter, whereas SRH operates well all over the year. Furthermore, SRH produces a more distinct signal than CAPE. This indicates that SRH is better qualified for a local exact forecast. Moreover, SRH indicates to be a good discriminator between strong and weak storms.

Vorticity seems to be a good predictor in Europe as well, but it is not a good discriminator between weak and strong tornadoes. Eventually, vorticity gradients or vorticity advection are better applicable for discriminating between these two types. More useful for the differentiation seem to be PV structures like PV folds. This also indicates that synoptic systems are quite strongly related to tornadoes. This can be said for all types of tornadoes, even for weak storms and waterspouts.

Moisture flux and moisture flux convergence also show clear signals in the composites in case of land tornadoes. However, it is not clear if this parameters are useful for distinguishing between tornadoes and convection. Also wind velocity on the 700 hPa level is indicated to be a good discriminator between weak and strong tornadoes. However, statistical analysis will be needed to check these assumptions.

A further interesting feature visible in the composites is an ageostrophic circulation which seems to be quite strongly related with tornadoes. However, its meaning is not yet clear.

Chapter 5

Case studies

5.1 Cut-off case

This tornado event developed on 22th July 2005 at 1351 UTC in the northerneastern corner of Poland. It occurred over flat terrain. The tornado reached F3 strength on the Fujita scale and had a duration of 14 minutes and an average path width of 250 m. It was the only tornado detected in the environmental area. Considering the strength and duration, the tornado was likely associated by a supercell.

Most unstable CAPE reached values between 450 and 600 $J\ kg^{-1}$ during the tornado event nearby the affected area. This values are not very high compared to other events in this region. It can be noticed that the region with maximum CAPE-values is quiet small, because of a convergence zone. However, it is possible that locally higher values were present.

SRH maps show a west-east oriented band with relatively high values (see figure 5.1). Maximum values were reached to the south of the affected area which is consistent with the composite shown in chapter 4 (see e.g. figure 4.5). The SRH values are lowering slightly with time. In the tornado area, measurements reached values around 80 $J\ kg^{-1}$ which is also low for the generation of supercells. Normally, they occur with values higher then 100 $J\ kg^{-1}$. However, it cannot be ruled out that locally higher SRH values were present. Further, it needs to be mentioned that values around 100 $J\ kg^{-1}$ are rare in this region during summer.

Like in the composites, the maximum SRH values are positioned south of the affected area in the region of the LLJ maximum. This indicates that the use of SRH as a forecast parameter can be problematic. (for more details see also figures in section B.3.1)

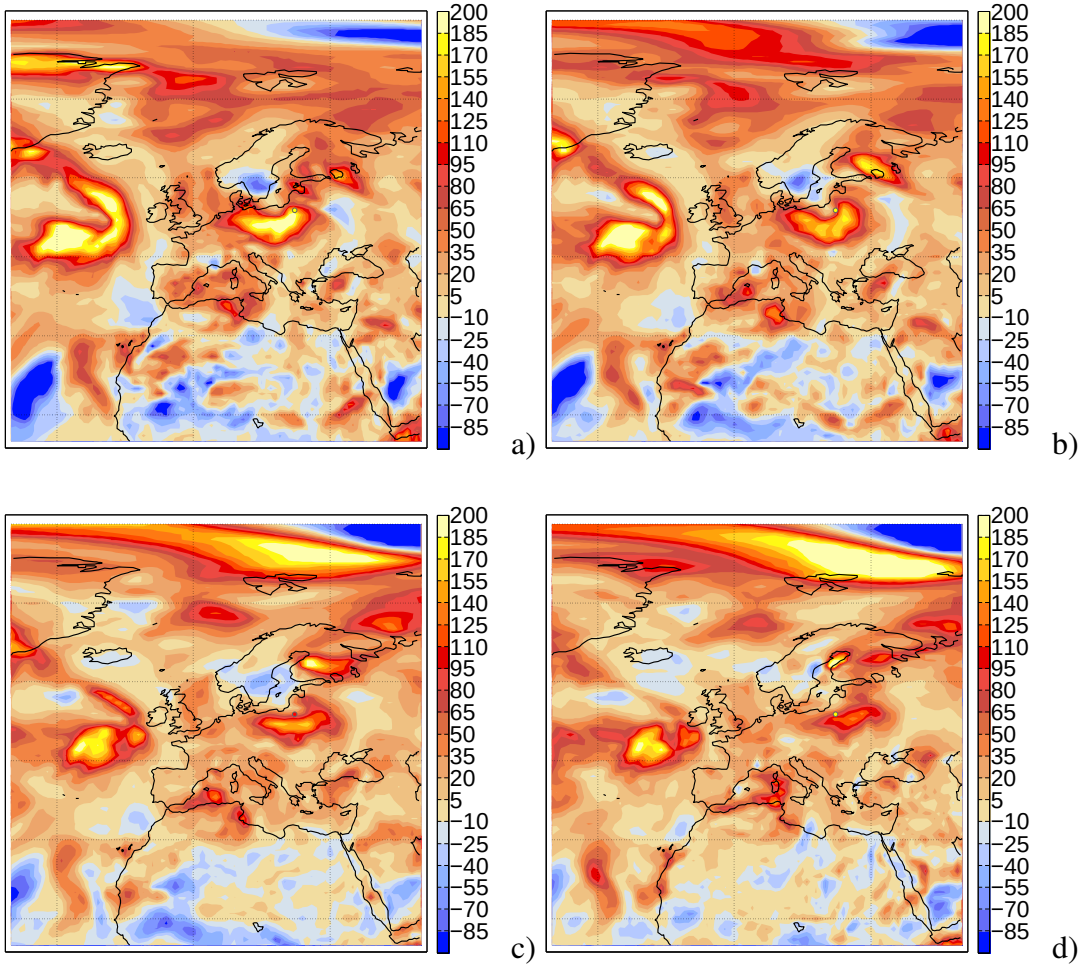

Figure 5.1: Temporal evolution of storm-relative helicity (SRH) in [J kg^{-1}] a) 12 h before, b) 6 h before, c) during and d) 6 h after the tornado event. The yellow respectively red point (during the tornado event) mark the position of the tornado.

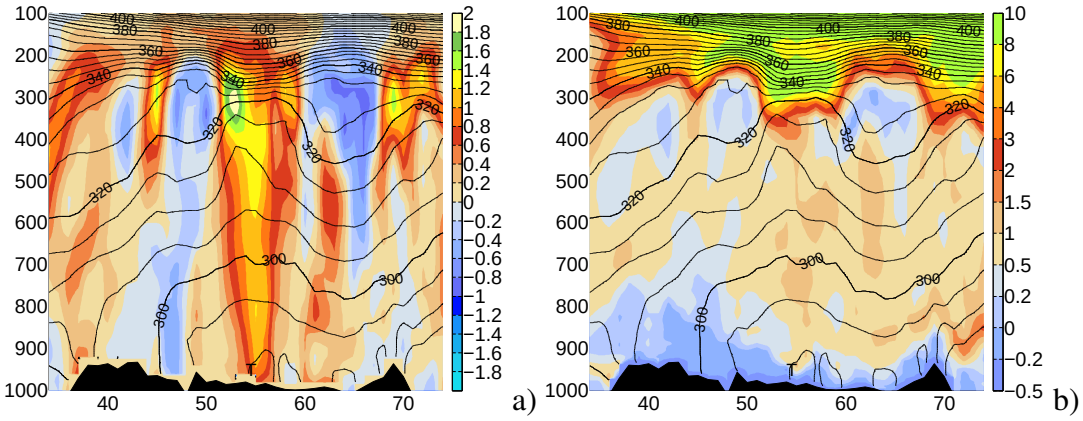

Figure 5.2: Vertical cross section of vorticity (figure a) in [10^{-4} s^{-1}] and PV (figure b) in [PVU] plotted in north-south direction during the tornado event.

PV plots show that the affected area is lying on the southern border of a PV cut-off (see figure 5.3). A zone with higher PV values (6 to 10 PVU) is moving towards the tornado position. Possibly, this PV anomaly leads to destabilization and so promote the development of convection. In the vertical cross section, it can also be recognized that a PV anomaly can produce vorticity penetrating deep into the troposphere (see figure 5.2). Furthermore, under the PV anomaly, isentropic surfaces were pulled up, which leads to destabilization, especially in the upper troposphere. Eventually, this enhances severe convection.

Vorticity plots show a narrow band with high values wrapping around the PV cut-off. A zone with higher vorticity values is moving towards the tornado point reaching it during the event takes place. Positive vorticity advection can lead to upward motion and thus, also enhance convection. In the vertical cross section, a deep tropospheric vorticity signal is visible situated above the location of the tornado (see figure 5.2).

The vorticity and PV structures are consistent with those seen in the composites. This indicates the relevance of this signal and again suggests that these parameters are probably usefull predictors for tornadoes. But for a confirmation of this assumption further investigations are needed. (for more details see also figures in section B.3.1)

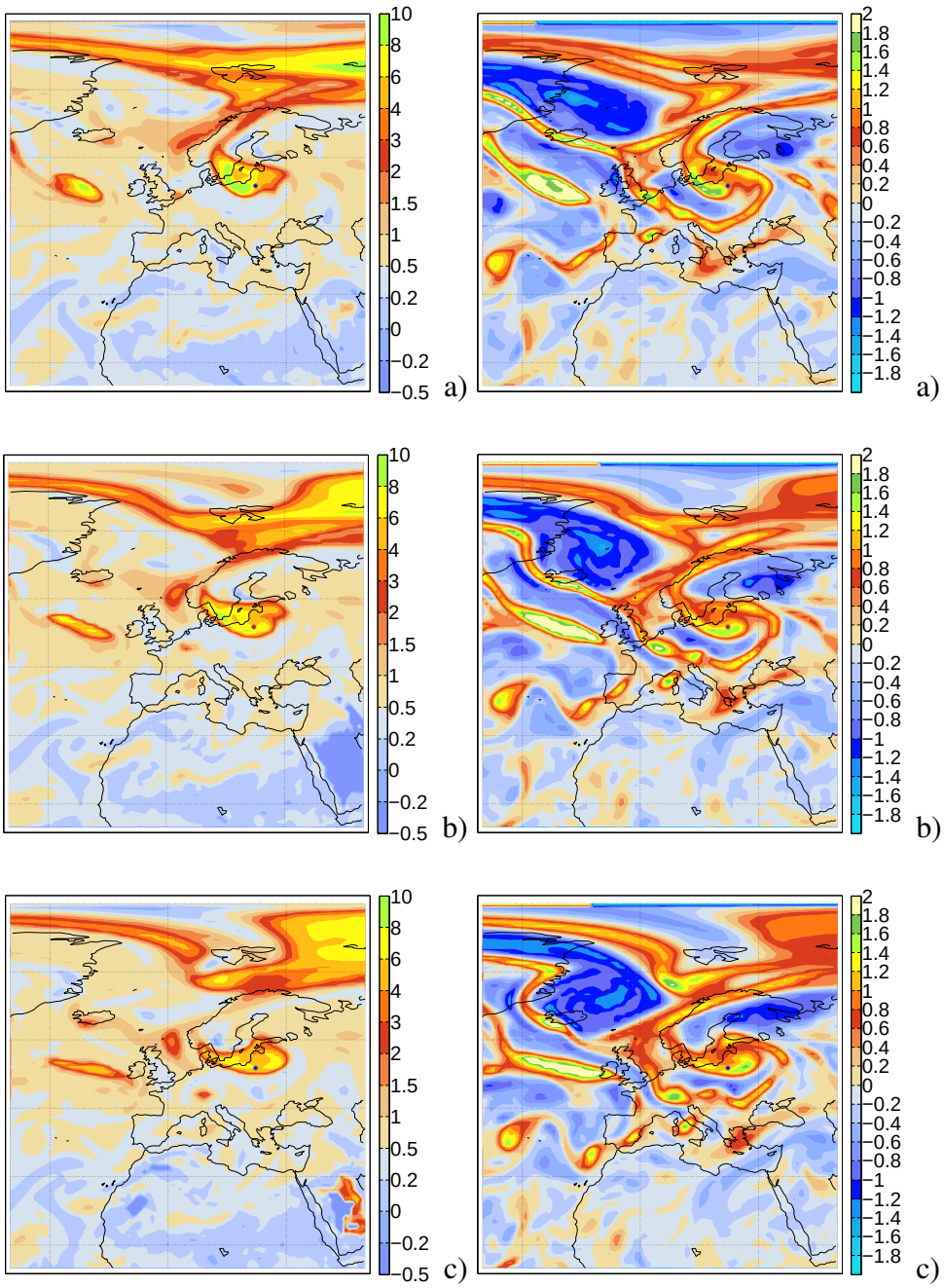

Figure 5.3: Temporal evolution of potential vorticity (PV) (left side)on 320 K in [PVU] and vorticity (right side) in vorticity in [10^{-4} s^{-1}] a) 6 h before, b) during and c) 6 h after the tornado event. The blue respectively red point mark the position of the tornado.

5.2 PV streamer case

On the 4th August 2006 multiple waterspouts were observed over the Lake of Constance around 8 UTC. The waterspouts were quiet long-living events with a life time about an hour. Water surface temperature was relatively high with $22°C$ to $23°C$ because of an exceptionally warm July[1]. The 2m air temperature was lying between $15°C$ and $16°C$ and thus about $8°C$ colder then the water surface temperature.

CAPE plots show low CAPE values after the waterspout event with around 150 $J\ kg^{-1}$. This is consistent with the composite shown in chapter 4 (see e.g. figure 4.8) indicating that waterspouts occur with lower CAPE values. However, it is very likely that over the Lake of Constance higher CAPE values were present due to the high SST in combination with weak winds which allows the warming of the boundary layer. Such small-scale processes cannot be resolved by ECMWF.

SRH plots also show low values over the Lake of Constance with values about 10 $J\ kg^{-1}$. This is consistent with the composite shown in chapter 4 (see e.g. figure 4.8) indicating that waterspouts occur with lower SRH values.

Also in this case SRH is not useful as a predictor. Eventually this is because SRH is a predictor for supercells and waterspouts are normally non-supercellular. A further problem which is clarified in this case is the course resolution of 1°x 1° of ECMWF analysis data which cannot capture the small-scale CAPE anomaly present over the lake. However, this is a general problem in global and also partly in mesoscale models which cannot capture distinct small-scale features. There is already a difficulty to assimilate them into initial model data.

PV values on 320 K shows a PV streamer moving over the affected area from west to east (see figure 5.5). It was lying exactly over the Lake of Constance during the waterspouts occurred (see also figure 5.4). The PV signal weakened slightly with time. The streamer wasn't associated with a front. Further, it is visible that the PV leads to a cooling of the upper troposphere which is an additional enhancement for deep convection.

In the **Vorticity** plots on 250 hPa multiple narrow bands with high vorticity values are visible (see figure 5.5). These features are associated with PV streamers (see figure 5.4). Contrary to the first case (see section 5.1) where a deep tropospheric vorticity signal was visible, in this case high vorticity values were only present in the upper troposphere.

[1] In July 2006 highest monthly mean since the beginning of meteorological measurements were observed in the environmental region.

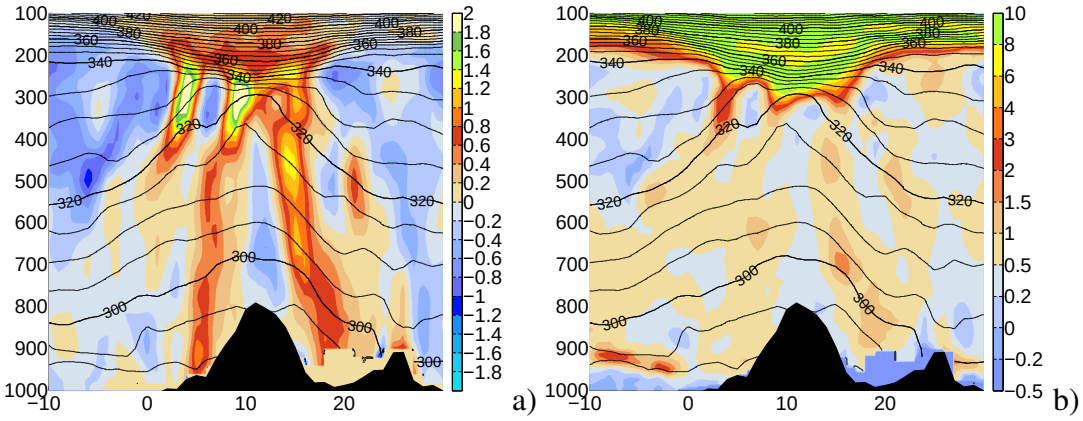

Figure 5.4: Vertical cross section of vorticity (figure a) in [10^{-4} s^{-1}] and PV (figure b) in [PVU] in west-east direction during the tornado event.

The PV anomaly seems to play an important role in the generation of waterspouts in this case. This is consistent with the composites for waterspouts which are showing a distinct PV anomaly over the affected area (see figure 4.11c). Also the high vorticity maximum in the upper troposphere is also indicated in the composites (see figure 4.11d). This indicates that PV-streamer or cut-offs are generally important for the evolution of waterspouts.

For waterspouts PV and vorticity seem to be the best predictors whereas SRH is not useful. However, further investigations are needed to quantify their skill score. (for further details see also figures in section B.3.2)

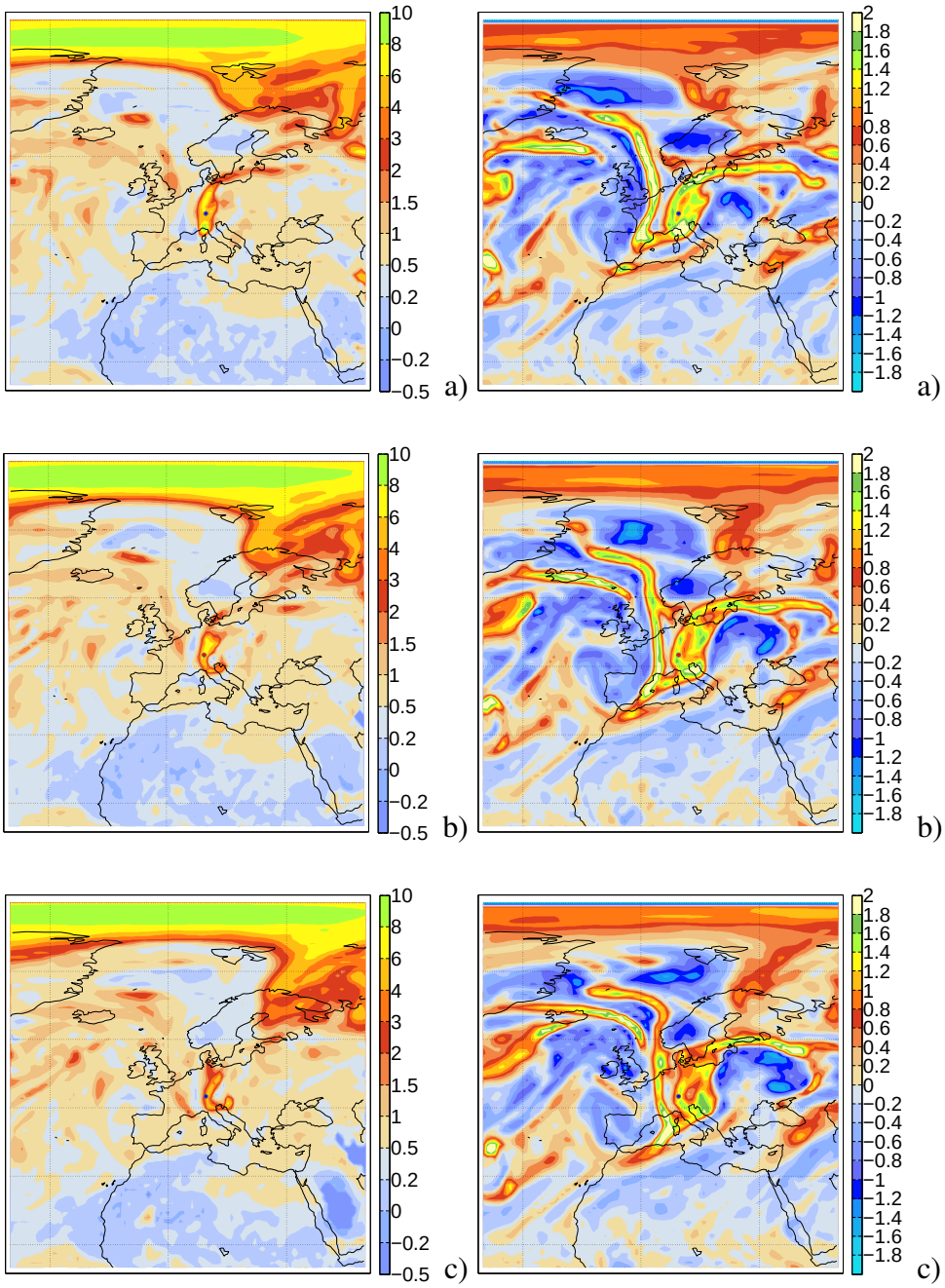

Figure 5.5: Temporal evolution of potential vorticity (PV) (left side) on 320 K in [PVU] and of vorticity (right side) on 250 hPa in [10^{-4} s^{-1}] a) 6 h before, b) during and c) 6 h after the tornado event. The blue respectively red point (during the tornado event) marks the position of the tornado.

5.3 MCS case

In the late evening of 29th July 2005, several tornadoes occurred in the Erzgebirge, which is situated in Germany. The strongest tornado developed at 2115 UTC and reached F2/T5 intensity on the Fujita/Torro scale. He had a life duration of 15 minutes and the path length amounted to 10 km. Most of the tornadoes moved from SSW to NNE.

The tornadoes were occurring after a hot day with temperatures reaching values up to $34°C$. In the afternoon, already some supercells took place producing large hail (up to 10 cm diameter), but no tornadoes were observed in the environmental region. In the evening, a large mesoscale convective system (MCS) developed west of the Erzgebirge. It was associated with a distinctive squall line which produces the tornadoes and also strong straight-line winds in the following hours.

Most unstable CAPE plots show high values prior to the tornado event (see figure 5.6). 6 hours before the CAPE reached values around 2000 $J\ kg^{-1}$. Such high values were rather rare and reached on average once per year. During the tornado event a large decrease can be observed, because a cold front passing by. Obviously, CAPE is a good predictor for severe convection. But high CAPE values are not necessary connected with tornadoes.

SRH values were also exceptionally high with values around 150 $J\ kg^{-1}$ 6 hours before the tornadoes occurred (see figure 5.7). During this time several supercells were observed producing large hail. This indicates that SRH in combination with CAPE is also in Europe a good predictor for supercells. A strong decrease of SRH is visible during the tornadoes occurred. But it cannot be ruled out that the MCS, respectively the squall line produces high storm-relative helicity by itself. However, regarding this case the usefulness of SRH as a predictor for tornadoes is doubtful.

In this case a **PV** anomaly is situated over the UK and western France on 325 K (see figure 5.8). A tongue of high PV air is moving towards NE reaching northern Germany in the night. During the tornado event, a small PV anomaly is visible just to the north of the affected area. In the north-south cross section it is also visible that this anomaly is located in the mid-troposphere (see figure 5.9). Possibly, it is produced by diabatic heating trough the MCS. A further possibility is a sinking of the high PV surface on the rear of the MCS, which was eventually supported by the following strong cold front. (for further details see also figures in section B.3.3)

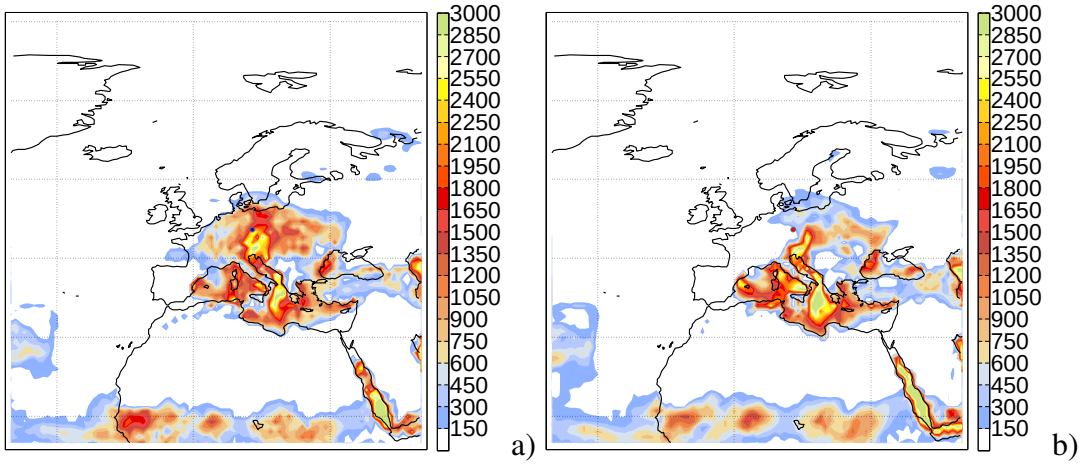

Figure 5.6: Temporal evolution of most unstable CAPE in [J kg^{-1}] a) 6 h before and b) during the tornado event. The blue respectively red point (during the tornado event) marks the position of the tornado.

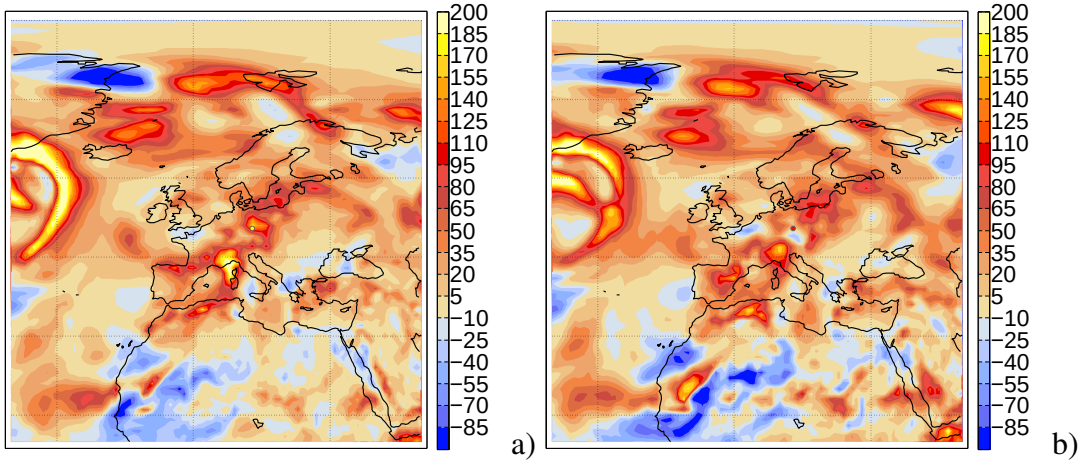

Figure 5.7: Temporal evolution of storm-relative helicity (SRH) in [J kg^{-1}] a) 6 h before, b) and during the tornado event. The yellow respectively red point (during the tornado event) marks the position of the tornado.

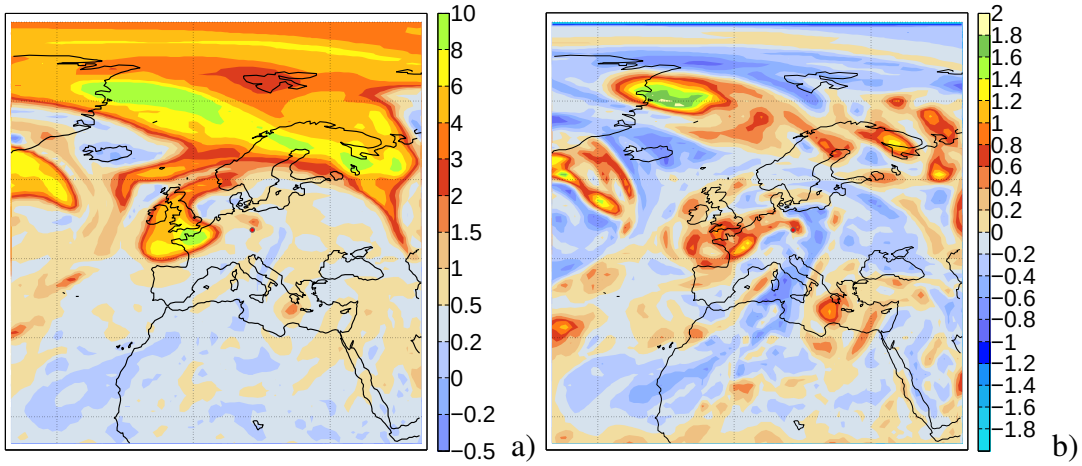

Figure 5.8: Potential vorticity (PV) (figure a) on 325 K in [PVU] and vorticity (figure b) in [10^{-4} s^{-1}] on 500 hPa during the tornado event.

The **vorticity** maps are also showing a maximum on 500 hPa pressure level which develops during the tornado case and then is moving towards NE (see figure 5.8). It is also visible 6 hours after the event whereas the PV signal disappears. In the north-south cross section there is again visible that the PV and vorticity signal are connected with each other. The vorticity cross section shows a signal with high vorticity up to 350 hPa. Above that level negative vorticity values can be observed. That is not in agree with the cut-off case (shown in section 5.1) where the vorticity signal is extending through the whole troposphere. It can be guessed that the vorticity in this case is not produced by a synoptic system, but rather by the MCS itself or the following cold front.

5.4 Synthesis

Regarding all cases, it seems to be reasonable to have a look at parameters like vorticity or PV. Also in other case studies (not shown in this work) vorticity signals were always visible (even in weak cases) and PV features were always visible in case of stronger tornadoes. This emphasizes the importance of these parameters and is a strong motivation for further research about such features.

CAPE and SRH, however, seem to be not very useful as predictors for tornadoes in Europe in general. Eventually, this is due to the fact that only a small number of tornadoes are associated with supercells. Because no data about supercells in Europe were available, this assumption cannot be proved at this time. But in a case study of a supercell tornado in Germany (not shown in this work) relatively high CAPE and SRH values were visible which is speaking for that hypothesis. Because this kind of storms is most destructive further investigations on supercell tornadoes in Europe are necessary.

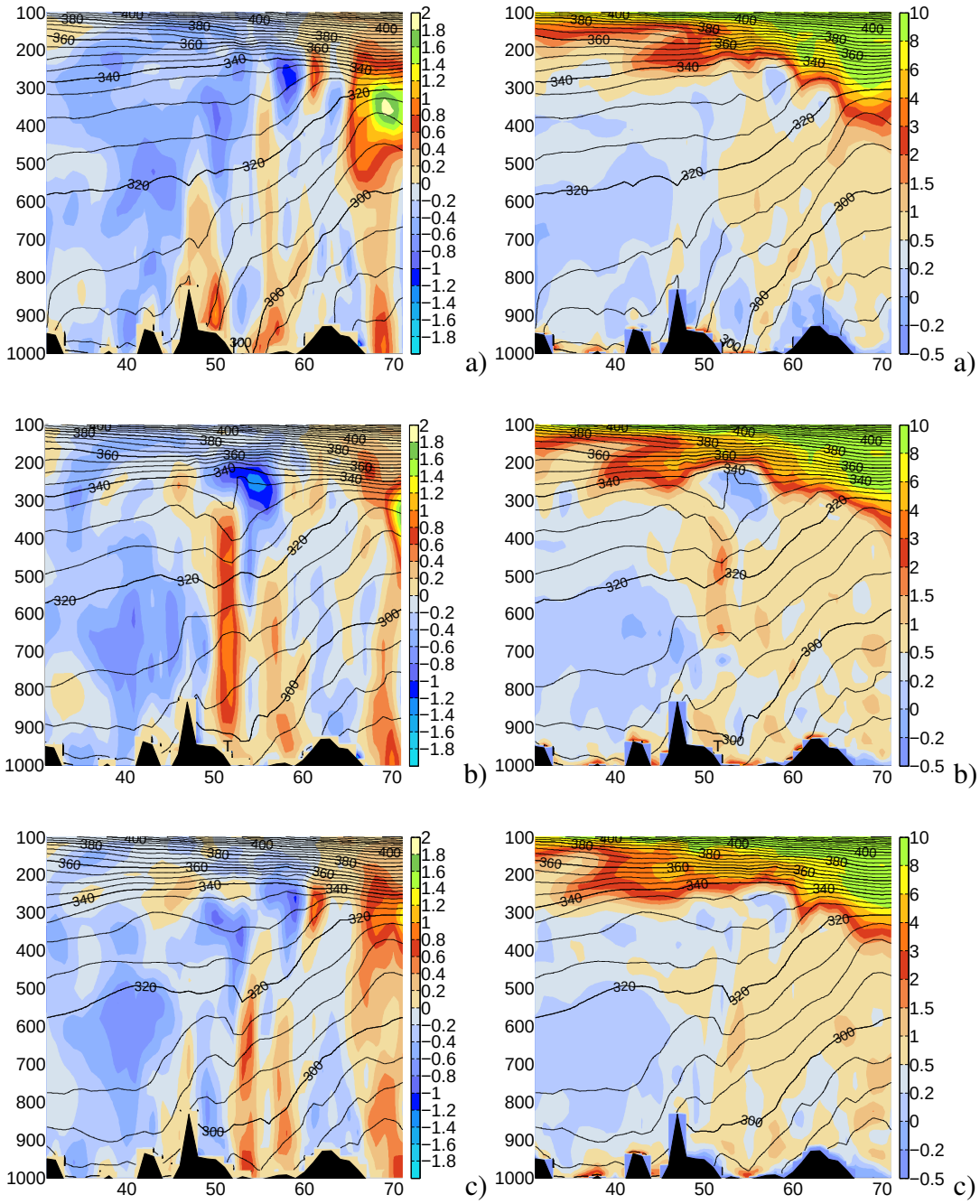

Figure 5.9: Vertical cross section of vorticity (left side) in [10^{-4} s^{-1}] and PV (right side) in [PVU] in north-south direction a) 6 h before, b) during and c) 6 h after the tornado event.

Chapter 6

Conclusions/Discussion

The results suggest that tornadoes in Europe are strongly related with synoptic and larger mesoscale systems. It seems that the synoptic situation is important for the genesis of tornadoes and waterspouts. Considering the large differences in size (factor 10^3 to 10^4) this is astonishing. Most probably, the synoptic system produces the basic conditions for tornado genesis.

CAPE and SRH seem to be usable as predictors, but their spatial and temporal distribution in the composites and the case studies indicate, that these parameters are of rather limited use in Europe. Eventually, this is because the occurrence of supercell tornadoes in Europe is low compared to the United States. However, several case studies with verified supercells in Europe are indicating that CAPE and SRH in combination are a good forecast parameter as well. Furthermore, SRH seems to be slightly better, especially in case of stronger tornadoes. So, it can eventually be used as discriminator between weak and strong tornadoes.

The absolute values of CAPE and SRH are relatively low compared with the US. This is a further sign that tornadic supercells are rather rare in Europe and explains partly the low skill of these parameters in Europe.

If velocity on 700 hPa level is compared with SRH, a strong correlation is visible. However, the maximum of velocity is placed exactly over the affected area in case of stronger tornadoes, whereas the SRH maximum is located more southerly. Therefore the question arises whether the 700 hPa wind field in ECMWF is more useful for predicting tornadoes than SRH.

Vorticity and PV are clearly better qualified as tornado forecast parameters, which is indicated by the composites and the case studies as well. However, their physical meaning for tornadoes is not clear yet. Eventually, vorticity advection is leading to strong upward motion which can act as a trigger for convection. The PV anomaly is associated with vorticity below it and leads to a cooling of the upper troposphere. Possibly, these factors enhance the probability for severe convection. However, vorticity and PV are not necessary for large instability and lifting. Moreover, the PV structure seems

to be a promising discriminator between weak and strong tornadoes. In case of strong tornadoes a PV fold is indicated in the composites.

In case of land tornadoes, a fast moving vorticity maximum is visible, whereas in case of waterspouts this feature is rather stationary. This indicates that vorticity advection is not the only reason for the generation of tornadoes. Also the structure of the PV anomalies varies for different types. PV streamer and PV cut-offs are often associated with waterspouts, whereas stronger land tornadoes are usually accompanied by narrower PV features like PV folds. This points to the high importance of these structures and strongly motivates further research about the connection between upper-level PV and tornadoes.

Moisture flux and moisture flux convergence will probably serve as good forecast parameters for tornadoes over land. However, it is not clear whether they are a good discriminators between tornadoes and non-tornadic thunderstorms. In case of waterspouts, moisture fluxes seem to be less important. This is probably caused by evaporation of water which can compensate for lower moisture advection.

Chapter 7

Acknowledgments

I thank Michael, my supervisor, for granting me the opportunity to work on this specific topic. He was always willing to support me, I especially appreciated his assistance in solving programming problems. I also thank Rich for his efforts and ideas during this thesis. Thanks to Olivia for inspiring me to write about this subject. I also thank all dynamo group members for always giving me advice when needed.

I especially thank Nikolai for providing the ESWD data which were absolutely fundamental for the success of this thesis. I also thank all staff members who worked voluntarily to establish the data base. I thank Bernhard for providing the lightning data which will be very useful when doing further research.

I thank Yvonne for proof-reading my thesis and for her encouragement. I thank Karel Holvoet for providing his amazing picture of an European tornado. Finally, I would like to thank my family for their interest and their support during my studies.

At all other people who have supported me and my thesis: **Thank you very much!**

Bibliography

Barnes, S. L. 1970. Some aspects of a severe, right-moving thunderstorm deduced from mesonetwork rawinsonde observations. *J. Atmos. Sci.* **27**, 634–648.

Barnes, S. L. 1978. Oklahoma Thunderstorms on 29-30 april 1970. part 1: Morphology of a tornadic thunderstorm. *Mon. Wea. Rev.* **106**, 673–684.

Bolton, N., D. M. Elsom, and G. T. Meaden. 2003. Forecasting tornadoes in the United Kingdom. *Atmos. Res.* **67–68**, 53–72.

Brooks, H. E., and C. A. Doswell III. 2000. Normalized Damage from Major Tornadoes in the United States: 1890–1999. *Wea. Forecasting* **16**, 168–176.

Brown, R. A., L. R. Lemon, and D. W. Burgess. 1978. Tornado detection by pulsed Doppler radar. *Mon. Wea. Rev.* **106**, 29–38.

Burgess, D. W., and R. J. Donaldson. 1979. 11th Conf. on Severe Local Storms. *Contrasting tornadic storm types*. Pp. 189–192.

Burgess, D. W., R. A. Brown, L. R. Lemon, and C. R. Safford. 1977. 10th Conf. on Severe Local Storms. *Evolution of a tornadic thunderstorm*. Amer. Meteor. Soc.. Omaha, NE. Pp. 84–89.

Cooley, J. 1978. Cold air funnel clouds. *Mon. Wea. Rev.* **106**, 1368–1372.

Davies-Jones, R. P. 1985. Tornado dynamics. Pp. 197–236. *Thunderstorm Morphology and Dynamics*. University of Oklahoma Press.

Davies-Jones, R. P., D. Burgess, and M. Foster. 1990. 16th Conf. on Severe Local Storms. *Test of helicity as a tornado forecast parameter*. Kananaskis Park, AB, Canada. Pp. 588–592.

Dessens, J., and J. T. Snow. 1993. *Comparative description of tornadoes in France and the United States*. Vol. 79. Geophys. Monogr.

Doswell III, C. A., H. E. Brooks, and N. Dotzek. 2007. On the implementation of the Enhanced Fujita scale in the USA. *Atmos. Res.*

Dotzek, N. 2000. Tornadoes in Germany. *Atmos. Res.* **56**, 233–251.

Dowell, D. C., and H. B. Bluestein. 1997. The Arcadia, Oklahoma, Storm of 17 may 1981: Analysis of a supercell during tornadogenesis. *Mon. Wea. Rev.* **125**, 2562–2582.

Emanuel, K. 1995. *Atmospheric Convection*. Oxford University Press.

Ertel, H. 1942. Ein neuer hydrodynamischer Wirbelsatz. *Meteor. Z.* **59**, 277–281.

Fawbush, W. J., and R. C. Miller. 1952. A mean sounding representative of the tornadic airmass environment. *Bull. Amer. Meteor. Soc.* **33**, 303–307.

Finke, U., and T. Hauf. 1996. The characteristics of lightning occurrence in southern Germany. *Contrib. Atmos. Physics* **69**, 361–374.

Fujita, T. T. 1975. 9th Conf. on Severe Local Storms. *New evidence from the April 3–4, 1974 tornadoes*. Amer. Meteor. Soc.. Norman, OK. Pp. 248–255.

Fujita, T. T. 1992. The mystery of severe storms. *WRL Res. Pap. 239*.

Fujita, T. T., and A. D. Pearson. 1973. Preprints 8th Conf. on Severe Local Storms. *Results of FPP classification of 1971 and 1972 tornadoes*. Denver. Pp. 142–145.

Gayà, M., V. Homar, R. Romero, and C. Ramis. 2000. Tornadoes and waterspouts in the Balearic Islands: phenomena and environment characterization. *Atmos. Res.* **56**, 253–267.

Giaiottia, D. B., M. Giovannoni, A. Pucillo, and F. Stel. 2005. The climatology of tornadoes and waterspouts in Italy. *Atmos. Res.* **83**, 534–541.

Groenemeijer, P. 2005. *Sounding-derived parameters associated with severe convective storms in the Netherlands*. Master's thesis. Institute of Marine and Atmospheric research Utrecht (IMAU).

Grzych, M. L., B. D. Lee, and C. A. Finley. 2006. Thermodynamic Analysis of Supercell Rear-Flank Downdrafts from Project ANSWERS. *Mon. Wea. Rev.* **135**, 240–246.

Hagen, M., B. Bartenschlager, and U. Finke. 1999. Motion characteristics of thunderstorms in southern Germany. *Meteor. Appl.* **6**, 227–239.

Holzer, A. M. 2000. Tornado Climatology of Austria. *Atmos. Res.* **56**, 203–212.

Hoskins, B. 1990. *Dynamics of mid-latitude cyclones*. Amer. Meteor. Soc.

Hoskins, B., M. McIntyre, and A. Robertson. 1985. On the use and significance of isentropic potential vorticity maps. *Q. J. R. Meteorol. Soc.* **111**, 877–946.

Hubrig, M. 2004. Analysis of Tornado and Downburst Wind Damage to Trees. *Forst und Holz* **59**, 78–84.

Jenkner, J. 2008. *Stratified verifications of quantitative precipitation forecasts over Switzerland*. PhD thesis. Swiss Federal Institute of Technology Zurich (ETH).

Kaltenböck, R., G. Diendorfer, and N. Dotzek. 2007. An Evaluation of ECMWF Analyses Sounding Parameters in Thunderstorm and Severe Local Storm Forecasting for Europe, obtained from Comparison between ESWD - European Severe Weather Database and EUCLID - Lightning Data. *submitted to Atmos. Res.*

Lemon, L., A. Stan-Sion, C. Soci, and E. Cordoneanu. 2003. A strong, long-track, Romanian tornado. *Atmos. Res.* **67–68**, 391–416.

Lemon, L. R., and C. A. Doswell III. 1979. Severe thunderstorm evolution and mesocyclone structure as related to tornadogenesis. *Mon. Wea. Rev.* **107**, 1184–1197.

Lewellen, W. S. 1993. Tornado vortex theory. *The Tornado: Its Structure, Dynamics, Prediction and Hazards, Geophys. Monogr.* **79**, 19–39.

Ludlam, F. H. 1963. Severe local storms: a review. *Meteor. Monogr.* **5**, 1–30.

Markowski, P. M. 2001. Hook Echoes and Rear-Flank Downdrafts: A Review. *Mon. Wea. Rev.* **130**, 852–876.

McDonald, J. R. 2002. Preprints of 21st Conf. on Severe Local Storms. *Development of an enhanced Fujita scale for estimating tornado intensity*. Austin, TX. Pp. 174–177.

Meaden, G. T. 1976. Tornadoes in Britain: their intensities and distribution in space and time. *J. Meteor.* **1**, 242–251.

Paul, F. 2000. A developing inventory of tornadoes in France. *Atmos. Res.* **56**, 269–280.

Rasmussen, E. N., and D. O. Blanchard. 1998. A Baseline Climatology of Sounding-Derived Supercell and Tornado Forecast Parameters. *Wea. Forecasting* **13**, 1148–1164.

Rasmussen, E. N., J. M. Straka, R. P. Davies-Jones, C. A. Doswell III, F. H. Carr, M. D. Eilts, and D. R. MacGorman. 1994. The Verifications of the Origins of Rotation in Tornadoes Experiment: Vortex. *Bull. Amer. Meteor. Soc.* **75**, 997–1006.

Ray, P. S., C. E. Hane, R. P. Davies-Jones, and R. L. Alberty. 1976. Tornado-parent storm relationship deduced from a dual-doppler radar analysis. *Geophys. Res. Lett.* **3**, 721–723.

Reynolds, D. J. 1999. European tornado climatology 1960-1989. *J. Meteor.* **24**, 376–403.

Romero, R., M. Gayà, and C. A. Doswell III. 2007. European climatology of severe convective storm environmental parameters: A test for significant tornado events. *Atmos. Res.* **83**, 389–404.

Rotunno, R. 1986. Tornadoes and tornadogenesis. *Mesoscale Meteorology and Forecasting* Pp. 414–436.

Rotunno, R., and J. B. Klemp. 1985. On the rotation and propagation of simulated supercell thunderstorms. *J. Atmos. Sci.* **42**, 271–292.

Schaefer, J. T., D. L. Kelly, C. A. Doswell III, J. G. Galway, R. J. Williams, R. P. McNulty, L. R. Lemon, and B. D. Lambert. 1980. Tornadoes: When, where, how often. *Weatherwise* **33**, 52–59.

Schlemmer, L. 2007. *Disentangling the forcing mechanisms of extreme precipitation events along the Alpine south-side by using potential vorticity inversion*. Master's thesis. Swiss Federal Institute of Technology Zurich (ETH).

Sioutas, M. V. 2003. Tornadoes and waterspouts in Greece. *Atmospheric Research* **67–68**, 645–656.

Stohl, A. 1998. Computation, accuracy and applications of trajectories - a review and bibliography. *Atmospheric Environment* **32**, 947–966.

Tyrell, J. 2005. Winter tornadoes in Ireland: The case of the Athlone tornado of 12 January 2004. *Atmos. Res.* **83**, 242–253.

Wakimoto, R. M., and J. M. Wilson. 1989. Non-supercell tornadoes. *Mon. Wea. Rev.* **117**, 1113–1140.

Walko, R. L. 1993. Tornado spin-up beneath a convective cell: Required basic structure of the near-field boundary layer winds. *The Tornado: Its Structure, Dynamics, Prediction and Hazards, Geophys. Monogr.* **79**, 89–95.

Ward, N. B. 1972. The explanations of certain features of tornado dynamics using a laboratory model. *J. Atmos. Sci.* **49**, 1194–1204.

Wegener, A. L. 1917. *Wind- und Wasserhosen in Europa*. Vieweg.

Wernli, H., and H. C. Davies. 1997. A Lagrangian-based analysis of extratropical cyclones. i: the method and some applications. *Quart. J. Roy. Meteor. Soc.* **123**, 467–489.

Wernli, H., and M. Sprenger. 2005. Identification and ERA-15 Climatology of Potential Vorticity Streamers and Cutoffs near the Extratropical Tropopause. *J. Atmos. Sci.* **64**, 1569–1589.

Wilson, J. W. 1986. Tornadogenesis by nonprecipitation-induced wind shear lines. *Mon. Wea. Rev.* **114**, 270–284.

Appendix A

Glossary

CAPE = convective available potential energy: The maximum energy available to an ascending parcel, according to parcel theory[1].

Critical values of CAPE adapted to Europe:

- $< 300\ J\ kg^{-1}$ = showers, no thunderstorm activity
- 300 - 1000 $J\ kg^{-1}$ = weak instability, thunderstorms can occur
- 1000 - 2000 $J\ kg^{-1}$ = moderate instability, severe convection is possible
- $> 2000\ J\ kg^{-1}$ = strong instability, risk for severe convection is enhanced

CIN = convective inhibition: CIN is a numerical measure in meteorology that indicates the amount of energy that will prevent an air parcel from rising from the surface to the level of free convection[1].

ECSS = European conference on severe storms

ECMWF = European center for medium-range weather forecasts

EHI = energy helicity index: EHI is a combination of CAPE and SRH. This incorporates not only the helicity but the energy of the air parcel and thus tries to eliminate weak potential for thunderstorms even in strong SRH regions[2].

The critical values of EHI:

- EHI = 1: possible tornadoes
- EHI = 1-2: moderate to strong tornadoes
- EHI > 2: strong tornadoes

[1] from http://amsglossary.allenpress.com/glossary
[2] from http://en.wikipedia.org

EL = equilibrium level: The EL is the height at which a rising parcel of air is at a temperature of equal warmth to it. This means that unstable air is now stable when it reaches the equilibrium level and convection stops[1].

ESSL = European severe storms laboratory

ESWD = European severe weather database

HSS = Heidke skill score: Measures the fraction of correct forecasts after eliminating those forecasts which would be correct due purely to random chance. This is a form of the generalized skill score, where the score in the numerator is the number of correct forecasts, and the reference forecast in this case is random chance. In meteorology, at least, random chance is usually not the best forecast to compare to - it may be better to use climatology (long-term average value) or persistence (forecast = most recent observation, i.e., no change) or some other standard[3].

LCL = lifting condensation level: The level at which a parcel of moist air lifted dry-adiabatically would become saturated[2].

LFC = level of free convection: The level at which a parcel of air lifted dry-adiabatically until saturated and saturation-adiabatically thereafter would first become warmer than its surroundings in a conditionally unstable atmosphere[2].

MCS = mesoscale convective system: A cloud system that occurs in connection with an ensemble of thunderstorms and produces a contiguous precipitation area on the order of 100 km or more in horizontal scale in at least one direction[2].

MLCAPE = mixed-layer CAPE

MUCAPE = most unstable CAPE

NMHS = national weather services

ORD = ordinary thunderstorm (without tornadoes)

PV = potential vorticity: The specific volume times the scalar product of the absolute vorticity vector and the gradient of potential temperature[2].

QC = quality control

RFD = rear flank downdraft: The rear flank downdraft or RFD is a region of dry air wrapping around the back of a mesocyclone in a supercell thunderstorm. These areas of descending air are thought to be essential in the production of many supercellular

[3] from http://www.bom.gov.au

tornadoes. Large hail within the rear flank downdraft often shows up brightly as a hook on weather radar images, producing the characteristic hook echo, which often indicates the presence of a tornado[2].

SFUK = British spherics bulletin

SRH = storm-relative helicity: SRH is a measurement for the transfer of horizontal vorticity into the vertical. Critical values of SRH (Storm Relative Helicity) for tornadic development, as researched in North America, are[1]:

- SRH = 150-299: supercells possible with weak tornadoes according to Fujita scale
- SRH = 300-499: very favorable to supercells development and strong tornadoes
- SRH > 450: violent tornadoes

SUP = supercell without or with weak tornado (<F2)

TOR = supercell with significant tornado (>=F2)

TVS = tornadic vortexsignature: A TVS is a Doppler weather radar detected rotation algorithm that indicates a strong possibility of a tornado. In most cases, the TVS is a tornadocyclone aloft, not a tornadic circulation[2].

Appendix B

Figures

B.1 Temporal evolution

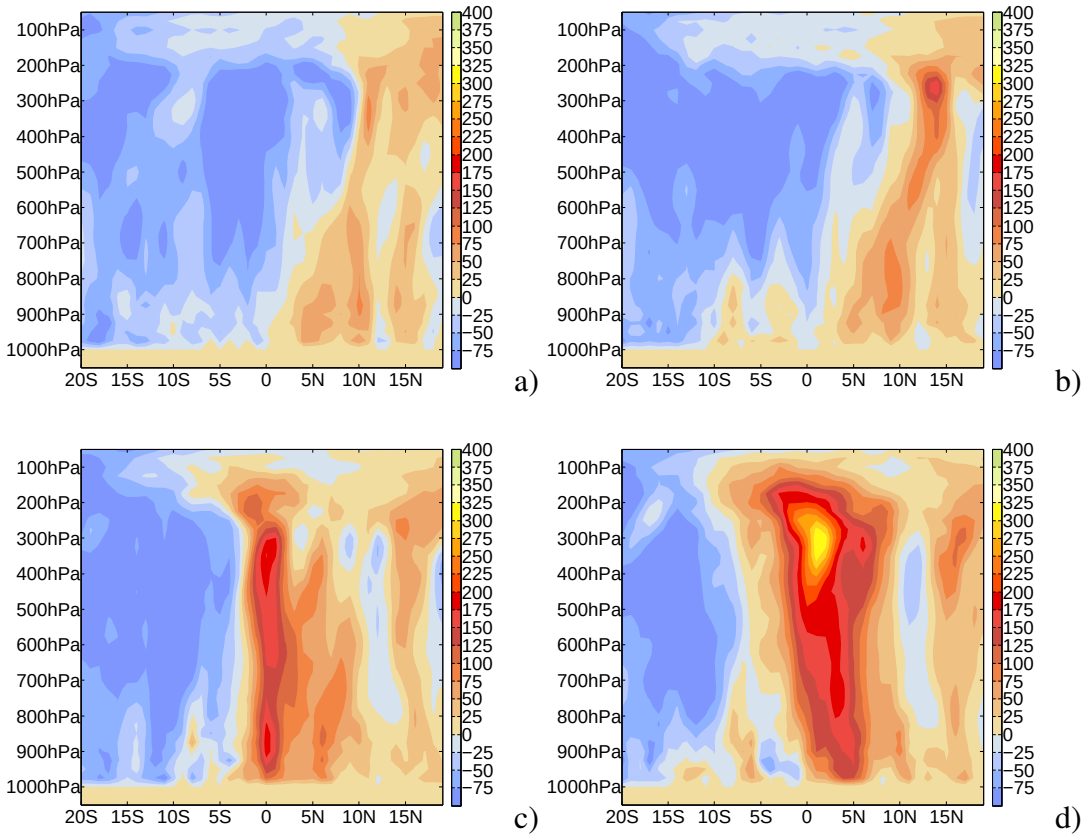

Figure B.1: Cross section in north-south direction through a composite of mean vorticity in 10^{-6} s averaged over all cases which have at least F1-strength a) 24 h before b) 12 h before c) during the tornado event and d) 12 h after the event.

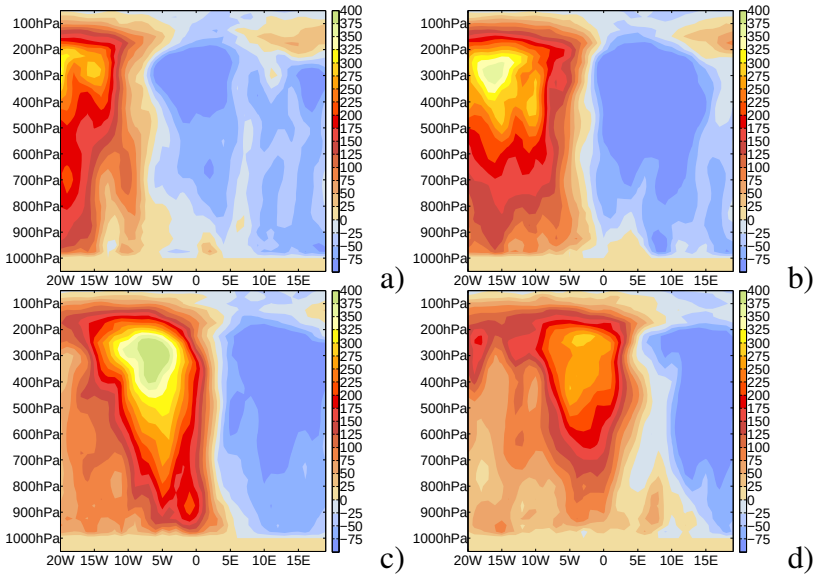

Figure B.2: Cross section in west-east direction through a composite of mean vorticity in 10^{-6}s averaged over all cases which have at least F1-strength a) 24 h before b) 12 h before c) during the tornado event and d) 12 h after the event.

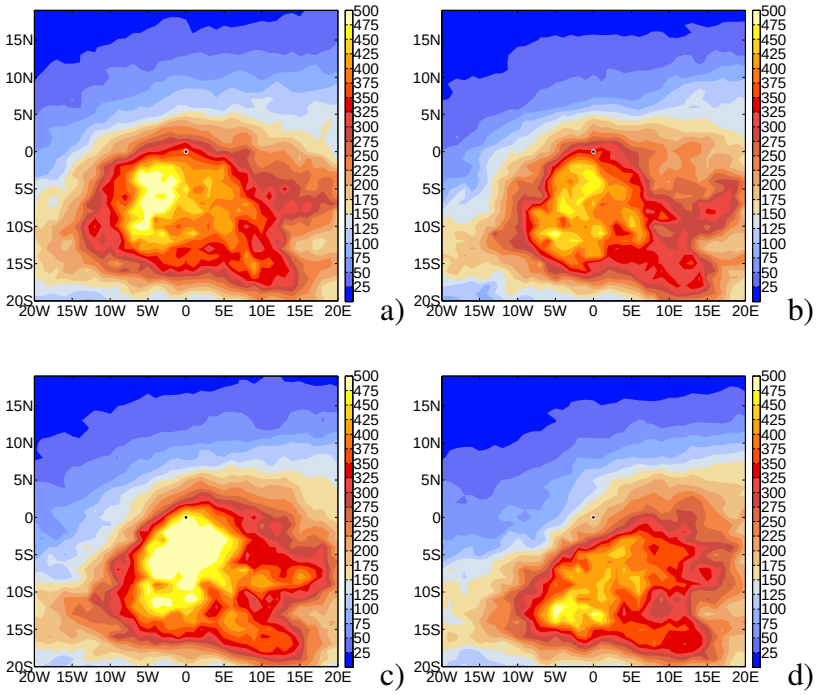

Figure B.3: Composite of mean most unstable CAPE in J kg^{-1} averaged over all cases which have at least F1-strength a) 24 h before b) 12 h before c) during the tornado event and d) 12 h after the event. The black dots mark the position of the tornado events.

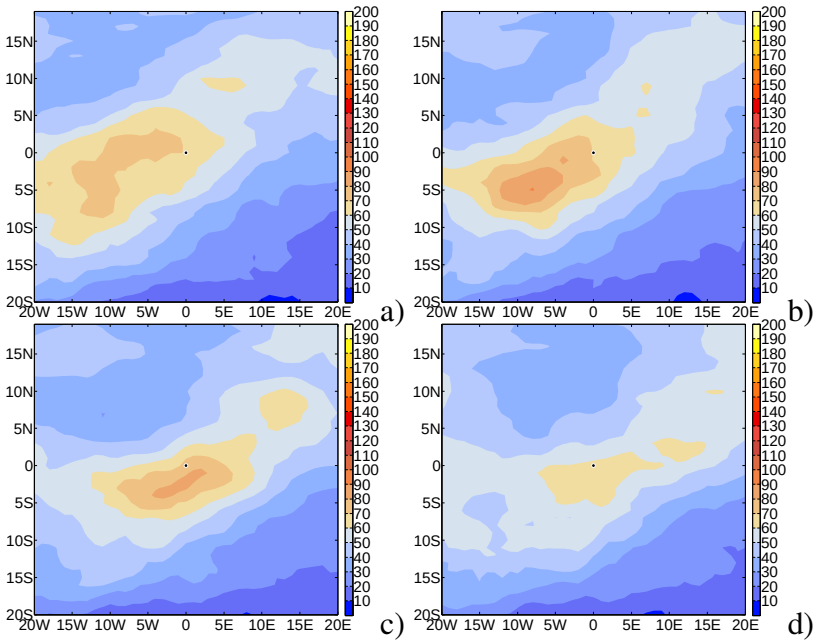

Figure B.4: Composite of mean storm-relative helicity (SRH) in J kg^{-1} averaged over all cases which have at least F1-strength a) 24 h before b) 12 h before c) during the tornado event and d) 12 h after the event. The black dots mark the position of the tornado events.

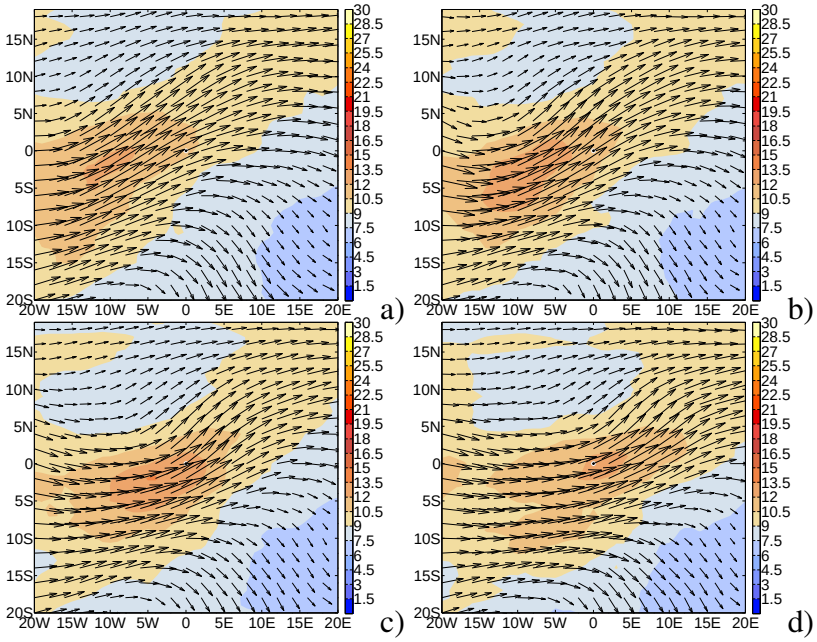

Figure B.5: Composite of mean wind velocity on 700 hPa in m s^{-1} averaged over all cases which have at least F1-strength a) 24 h before b) 12 h before c) during the tornado event and d) 12 h after the event. The black dots mark the position of the tornado events.

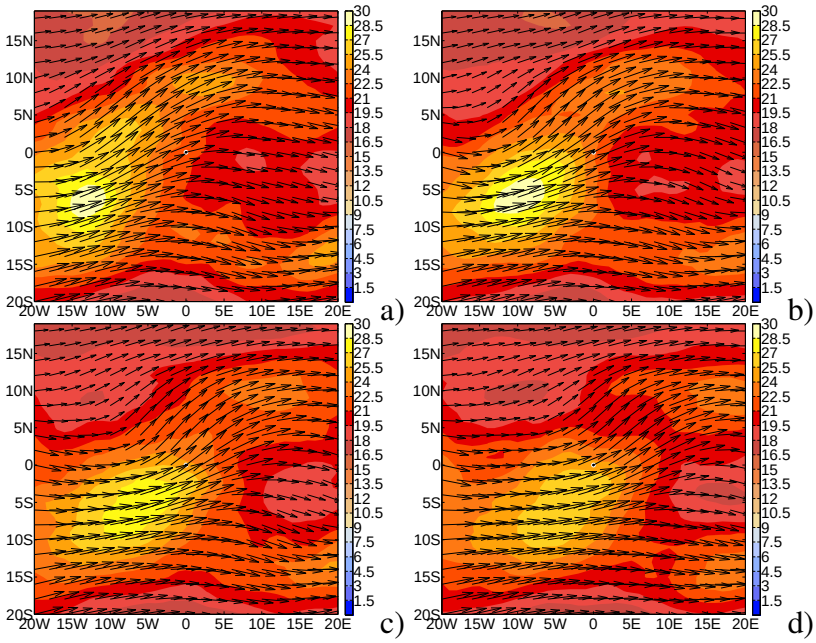

Figure B.6: Composite of mean wind velocity on 250 hPa in m s^{-1} averaged over all cases which have at least F1-strength a) 24 h before b) 12 h before c) during the tornado event and d) 12 h after the event. The black dots mark the position of the tornado events.

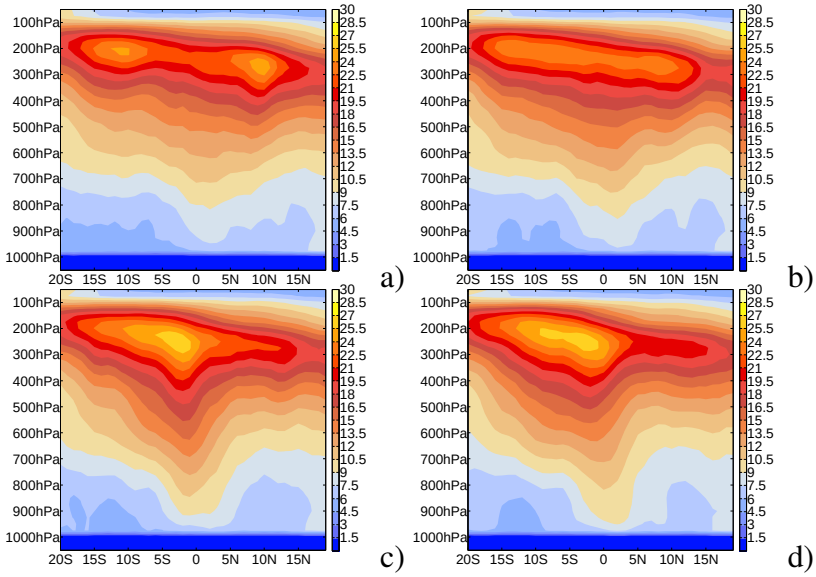

Figure B.7: Cross section in north-south direction through a composite of mean wind velocity in m s^{-1} averaged over all cases which have at least F1-strength a) 24 h before b) 12 h before c) during the tornado event and d) 12 h after the event.

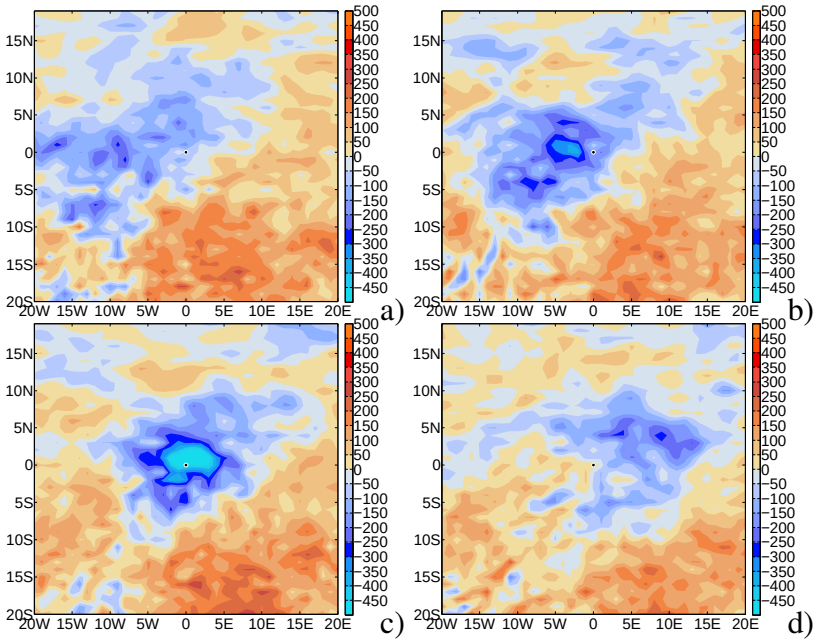

Figure B.8: Composite of mean vertical velocity on 700 hPa in hPa/h averaged over all cases which have at least F1-strength a) 24 h before b) 12 h before c) during the tornado event and d) 12 h after the event. The black dots mark the position of the tornado events.

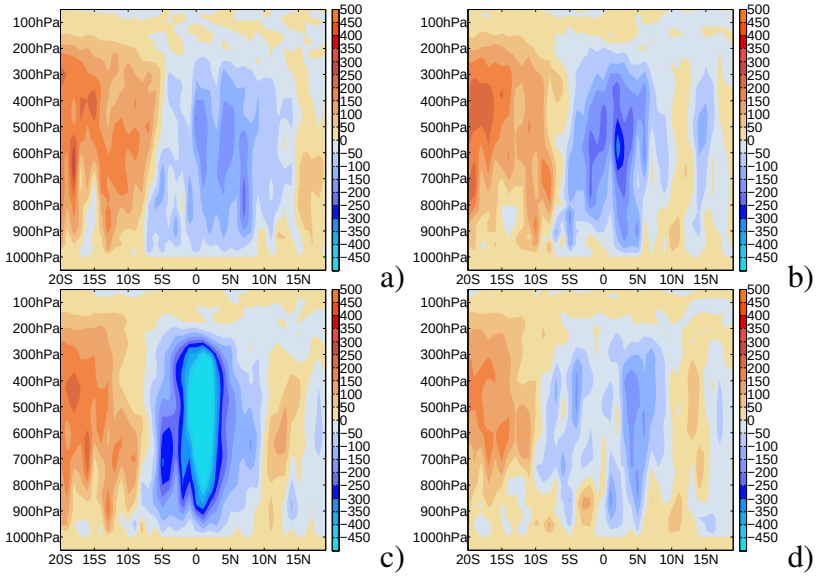

Figure B.9: Cross section in north-south direction through a composite of mean vertical velocity in hPa/h averaged over all cases which have at least F1-strength a) 24 h before b) 12 h before c) during the tornado event and d) 12 h after the event.

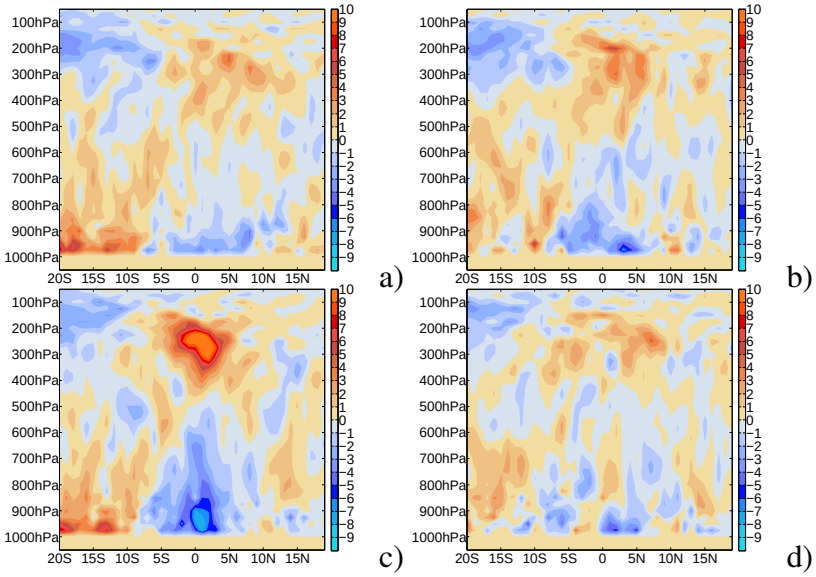

Figure B.10: Cross section in north-south direction through a composite of mean divergence in 10^{-6} averaged over all cases which have at least F1-strength a) 24 h before b) 12 h before c) during the tornado event and d) 12 h after the event.

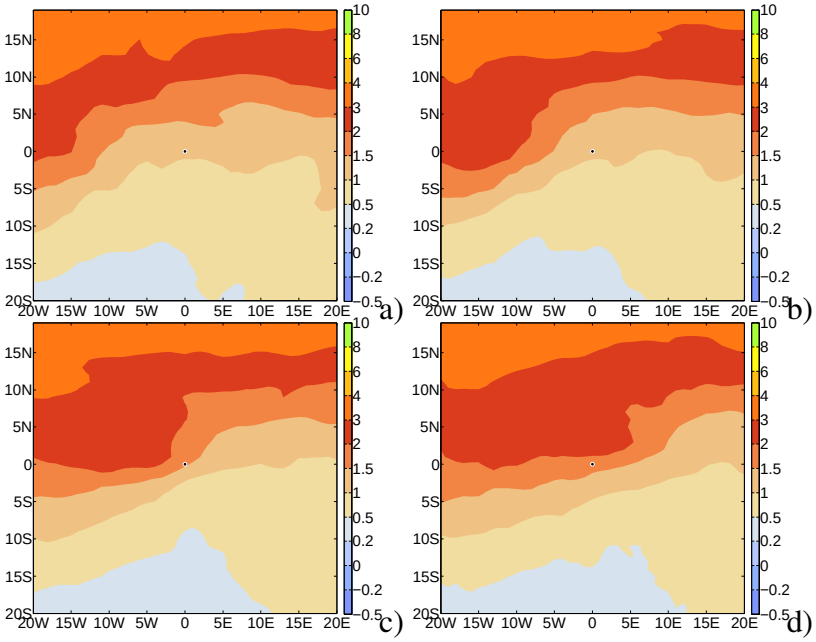

Figure B.11: Composite of mean potential vorticity on 320 K level of potential temperature in PVU averaged over all cases which have at least F1-strength a) 24 h before b) 12 h before c) during the tornado event and d) 12 h after the event. The black dots mark the position of the tornado events.

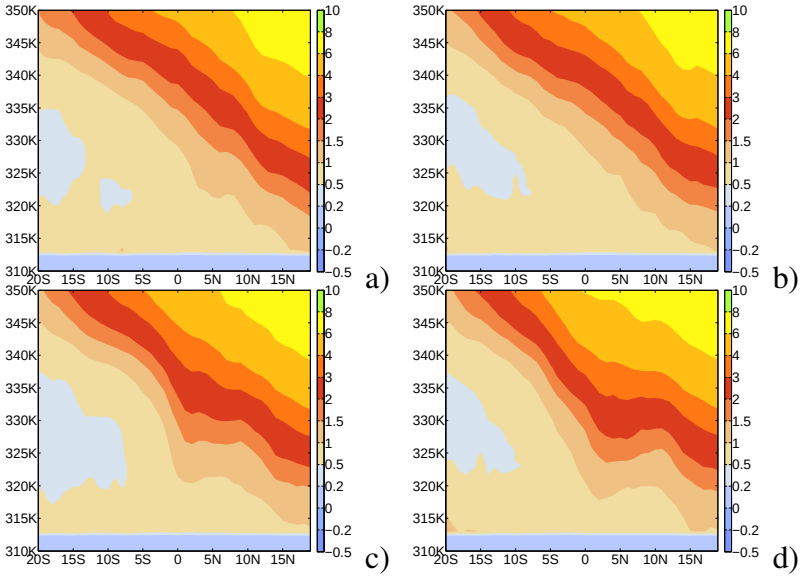

Figure B.12: Cross section in north-south direction through a composite of mean potential vorticity in PVU averaged over all cases which have at least F1-strength a) 24 h before b) 12 h before c) during the tornado event and d) 12 h after the event.

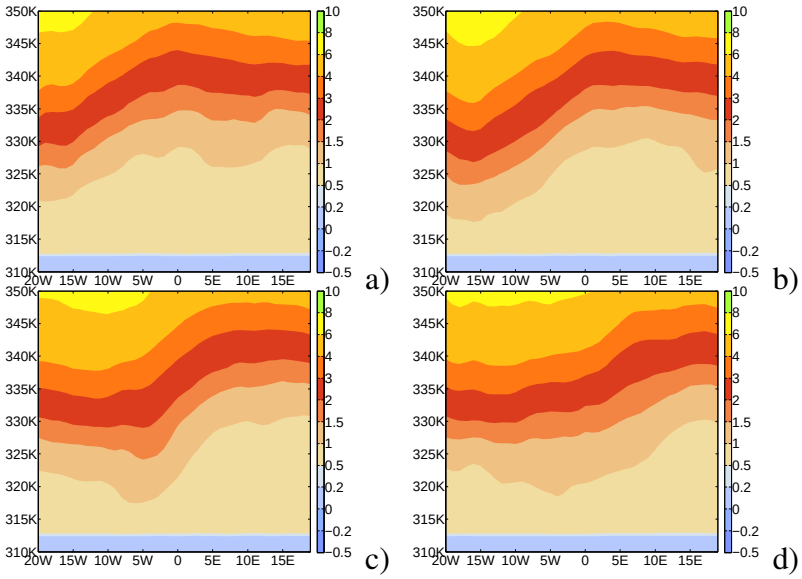

Figure B.13: Cross section in west-east direction through a composite of mean potential vorticity in PVU averaged over all cases which have at least F1-strength a) 24 h before b) 12 h before c) during the tornado event and d) 12 h after the event.

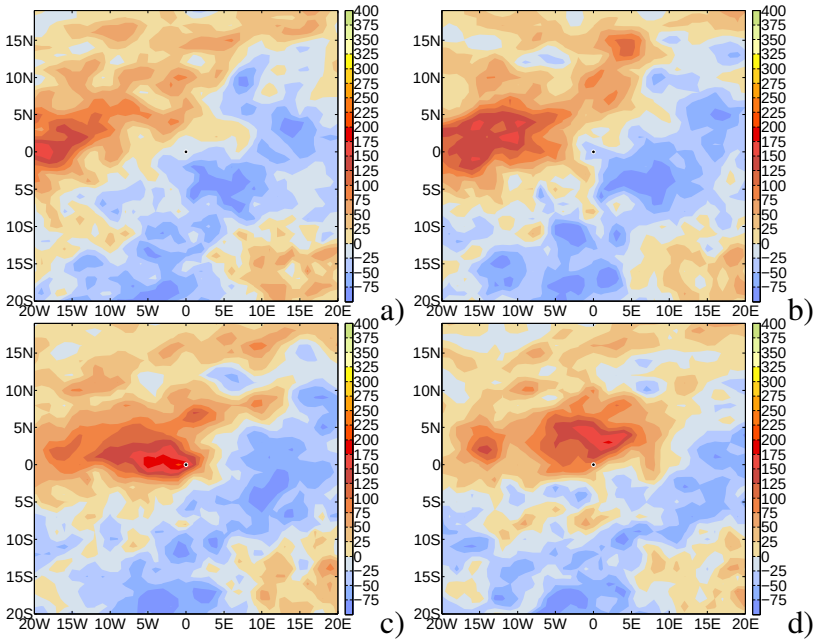

Figure B.14: Composite of mean vorticity on 850 hPa in 10^{-6} *s averaged over all cases which have at least F1-strength a) 24 h before b) 12 h before c) during the tornado event and d) 12 h after the event. The black dots mark the position of the tornado events.*

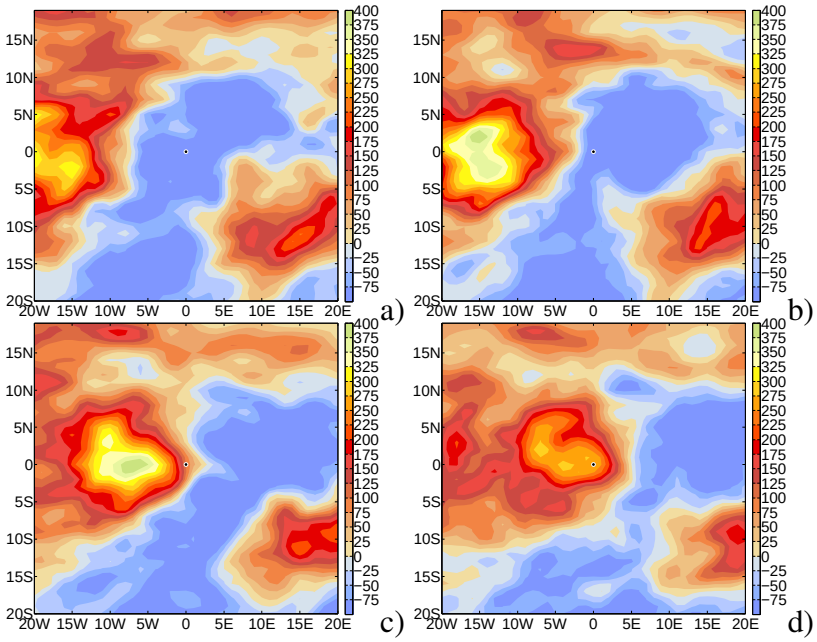

Figure B.15: Composite of mean vorticity on 250 hPa in 10^{-6} *s averaged over all cases which have at least F1-strength a) 24 h before b) 12 h before c) during the tornado event and d) 12 h after the event. The black dots mark the position of the tornado events.*

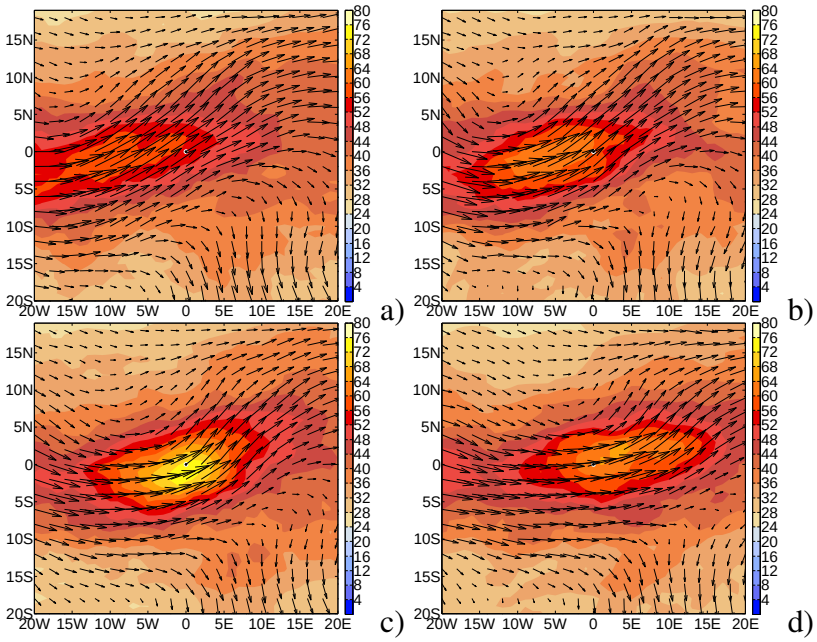

Figure B.16: Cross section in north-south direction through a composite of mean moisture flux in 10^{-3} kg m s^{-1} averaged over all cases which have at least F1-strength a) 24 h before b) 12 h before c) during the tornado event and d) 12 h after the event. The black dots mark the position of the tornado events.

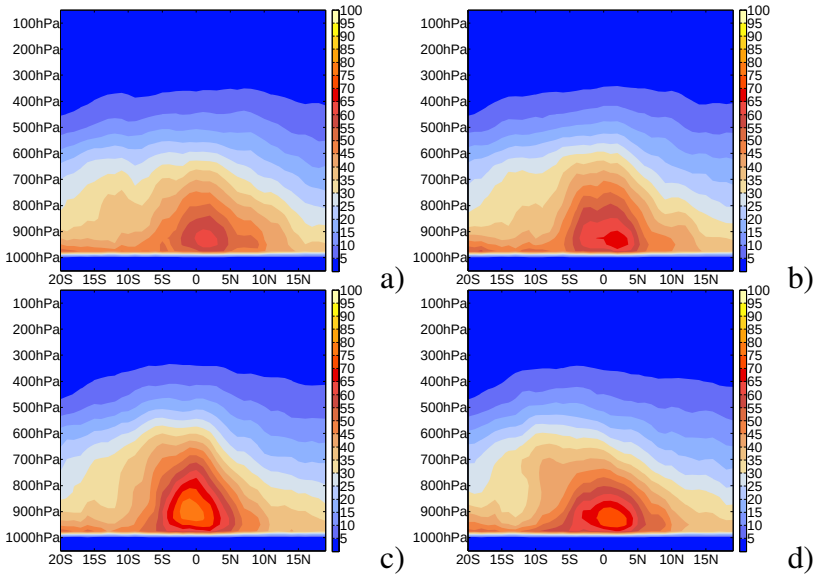

Figure B.17: Cross section in north-south direction through a composite of mean moisture flux in 10^{-3} kg m s^{-1} averaged over all cases which have at least F1-strength a) 24 h before b) 12 h before c) during the tornado event and d) 12 h after the event.

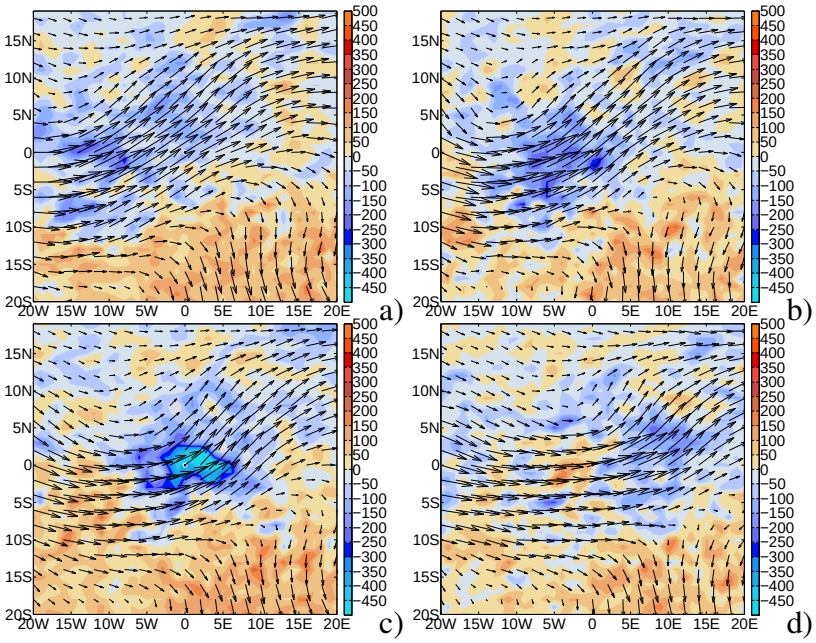

Figure B.18: Composite of mean moisture flux divergence on 850 hPa in 10^{-3} kg m s^{-1} averaged over all cases which have at least F1-strength a) 24 h before b) 12 h before c) during the tornado event and d) 12 h after the event. Negative values are standing for moisture flux convergence. The black dots mark the position of the tornado events.

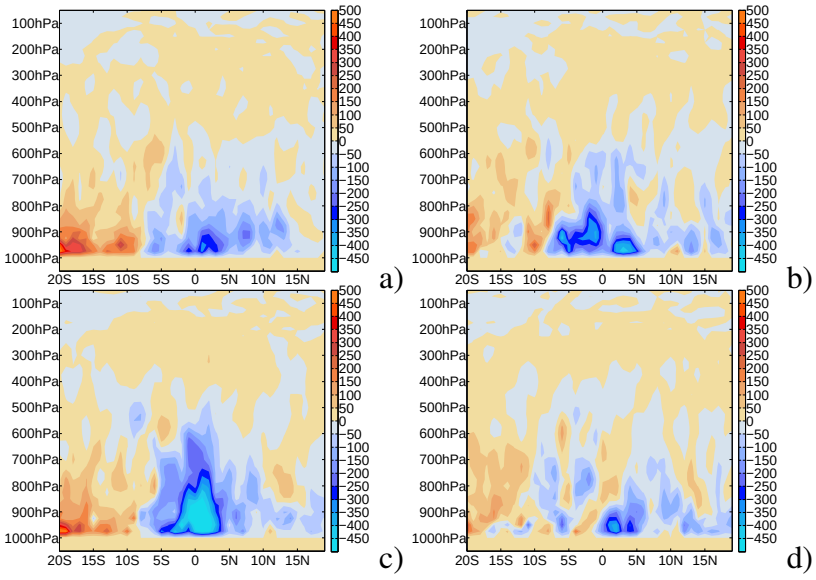

Figure B.19: Cross section in north-south direction through a composite of mean moisture flux divergence in 10^{-3} kg m s^{-1} averaged over all cases which have at least F1-strength a) 24 h before b) 12 h before c) during the tornado event and d) 12 h after the event. Negative values are standing for moisture flux convergence. The black dots mark the position of the tornado events.

B.2 Comparison of types

B.2.1 Waterspouts and land tornadoes

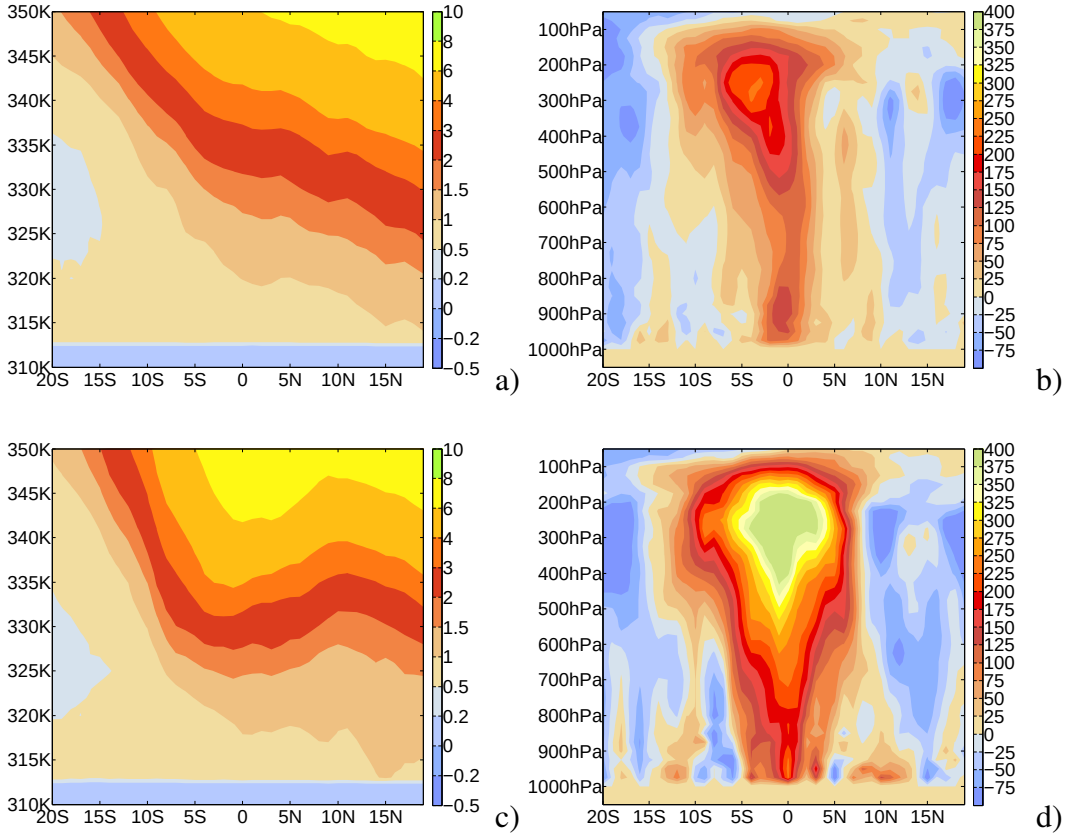

Figure B.20: Comparison between tornadoes over land (upper row) and waterspout type (lower row) for a north-south PV [PVU] cross section (left side) and a north-south vorticity [10^{-6} s^{-1}] cross section (right side) during the event.

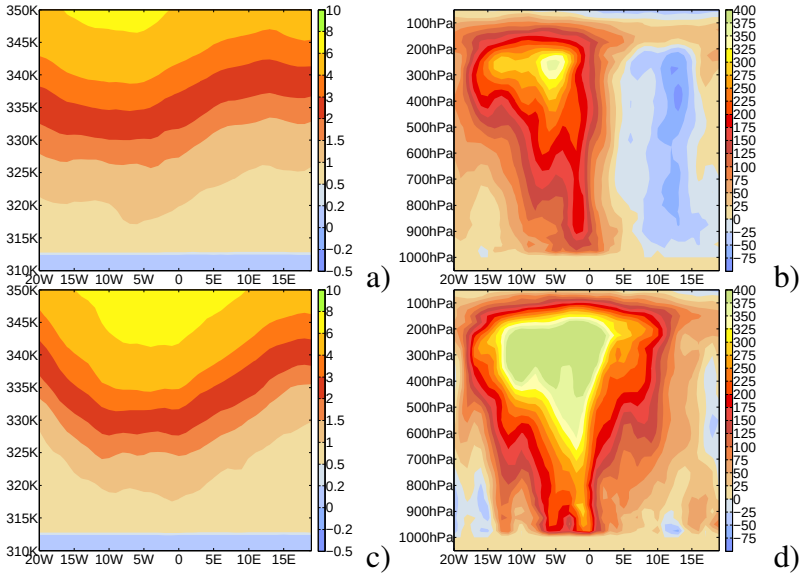

Figure B.21: Comparison between tornadoes over land (upper row) and waterspout type (lower row) for a west-east PV [PVU] cross section (left side) and a west-east vorticity [10^{-6} s^{-1}] cross section (right side) during the event.

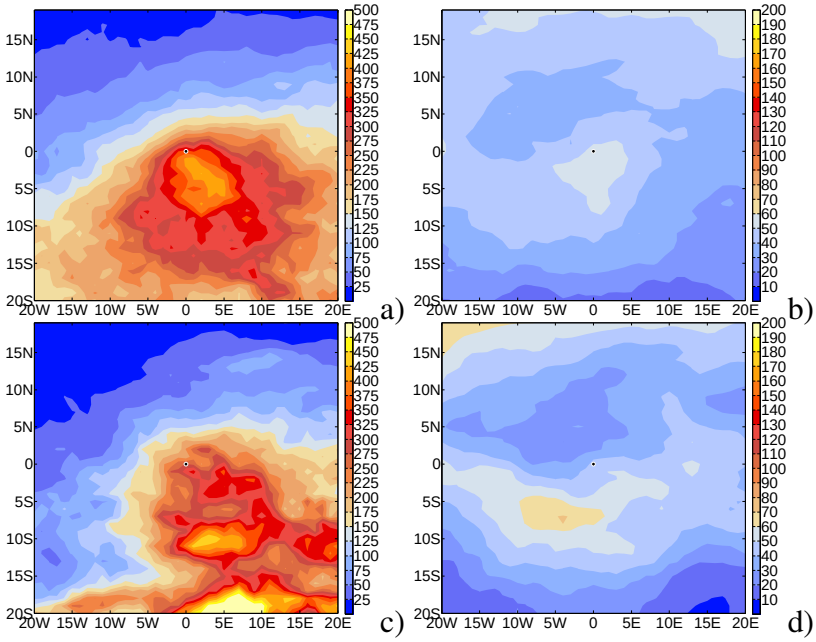

Figure B.22: Comparison between tornadoes over land (upper row) and waterspout type (lower row) for most unstable CAPE (left side) and SRH (right side) during the event. The black dots mark the position of the tornado events.

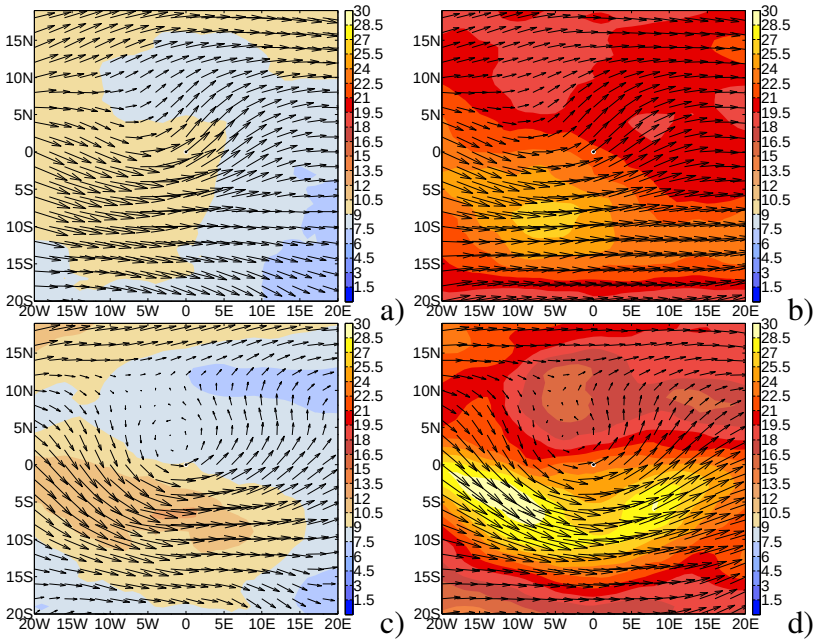

Figure B.23: Comparison between tornadoes over land (upper row) and waterspout type (lower row) for wind velocity in m s^{-1} on 700 hPa (left side) and on 250 hPa (right side) during the event. The black dots mark the position of the tornado events.

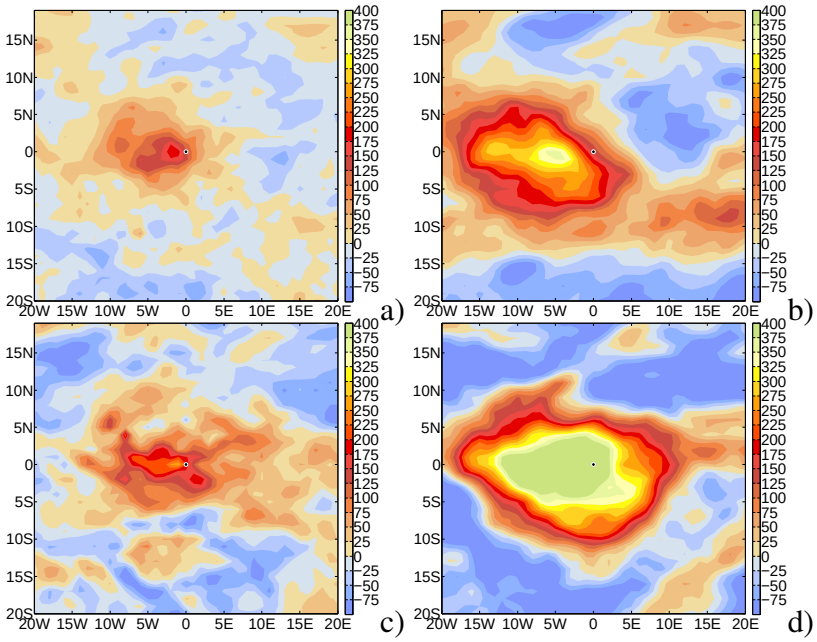

Figure B.24: Comparison between tornadoes over land (upper row) and waterspout type (lower row) for vorticity in 10^{-6} s^{-1} on 850 hPa (left side) and on 250 hPa (right side) during the event. The black dots mark the position of the tornado events.

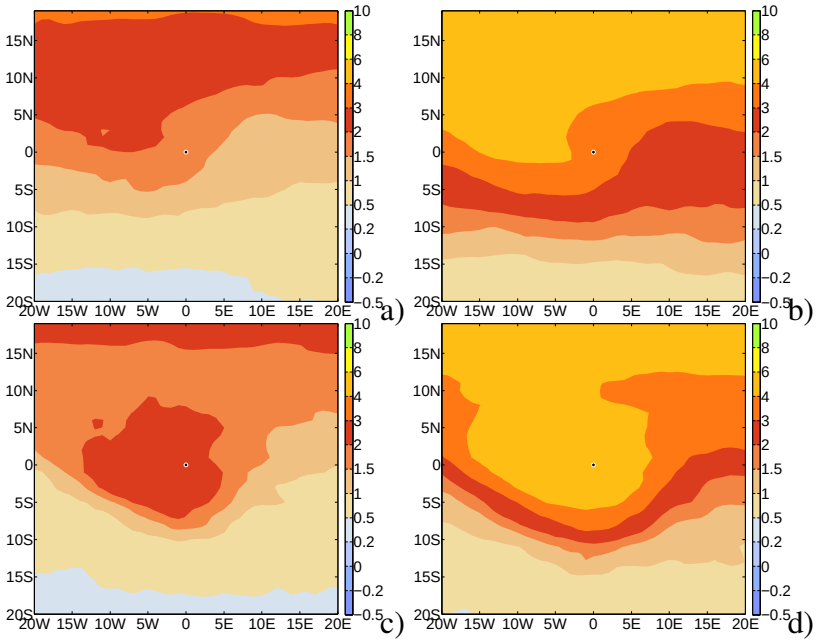

Figure B.25: Comparison between tornadoes over land (upper row) and waterspout type (lower row) for PV in PVU on the 320 K Θ-level (left side) and on the 330 K Θ-level (right side) during the event. The black dots mark the position of the tornado events.

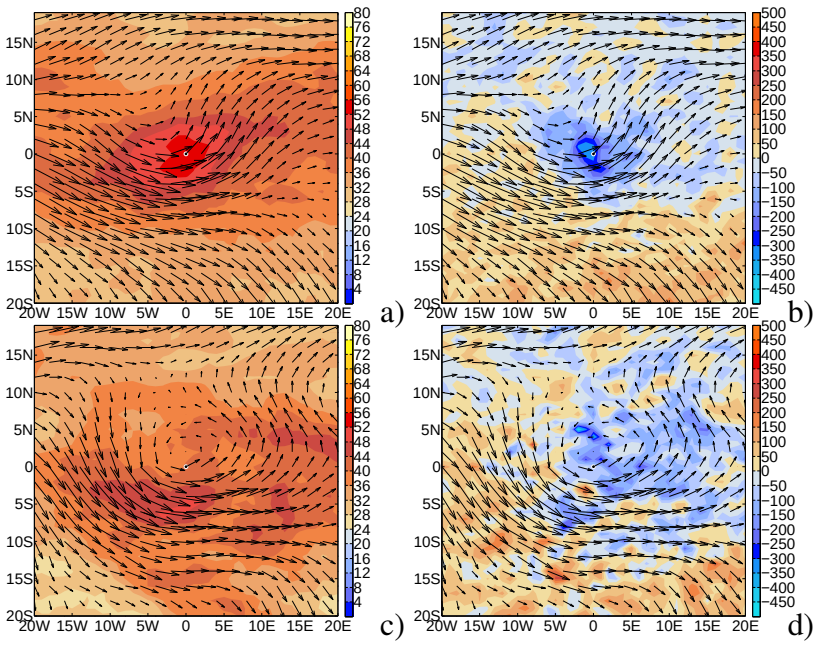

Figure B.26: Comparison between tornadoes over land (upper row) and waterspout type (lower row) for moisture flux in 10^{-3} kg m s^{-1} on 850 hPa (left side) and moisture flux convergence (negative values) in 10^{-3} kg m s^{-2} on 850 hPa (right side) during the event. The black dots mark the position of the tornado events.

B.2.2 Winter and summer

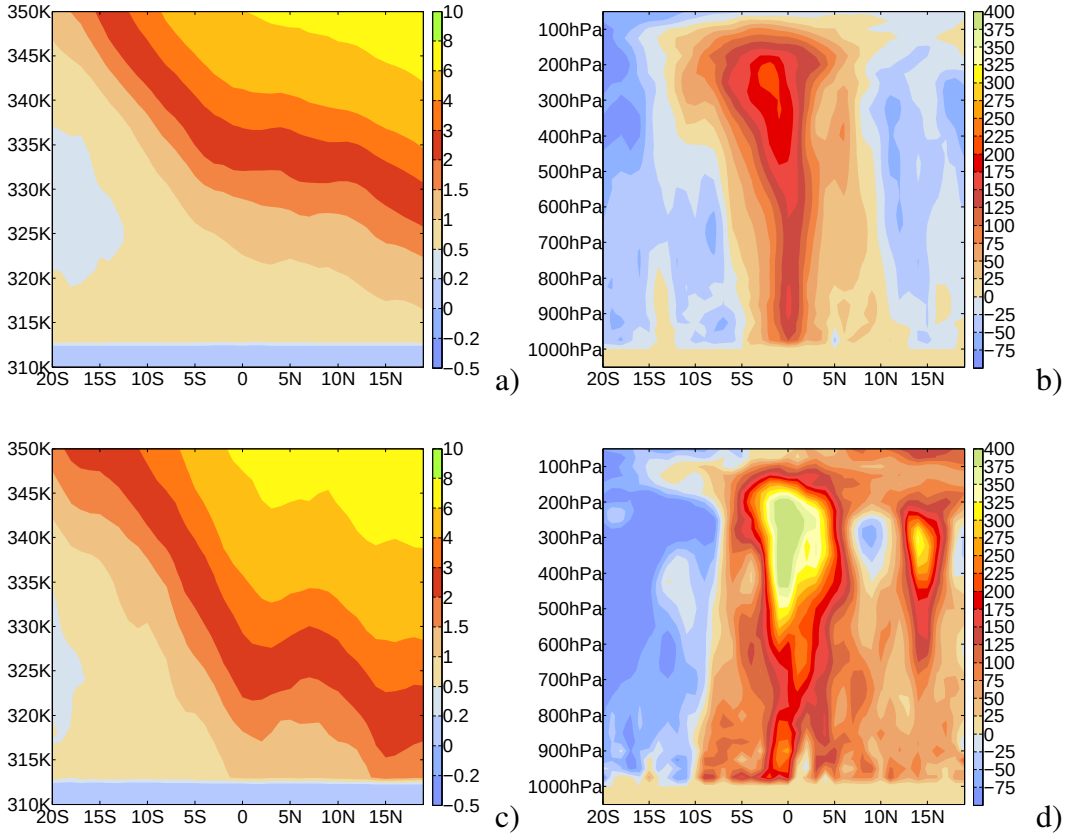

Figure B.27: Comparison between summer season type (upper row) and winter season type (lower row) for a north-south PV [PVU] cross section (left side) and a north-south vorticity [10^{-6} s^{-1}] cross section (right side) during the event.

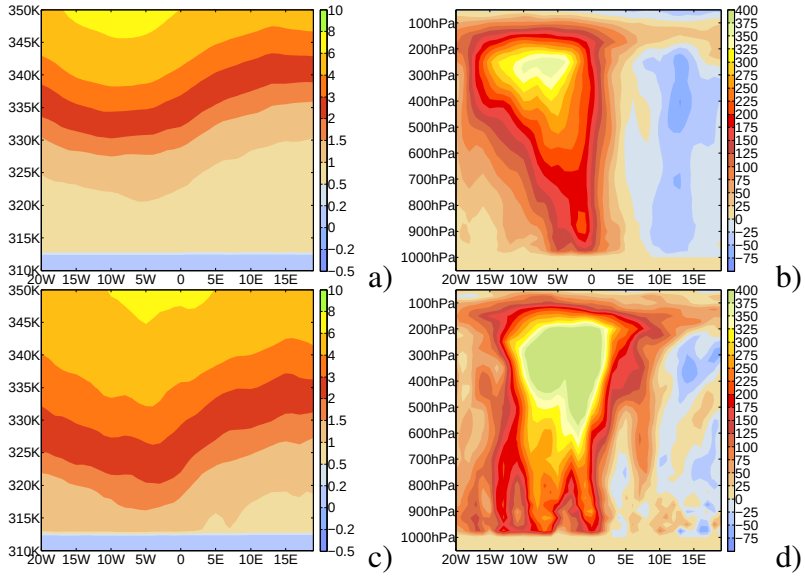

Figure B.28: Comparison between summer season type (upper row) and winter season type (lower row) for a west-east PV [PVU] cross section (left side) and a west-east vorticity [10^{-6} s^{-1}] cross section (right side) during the event.

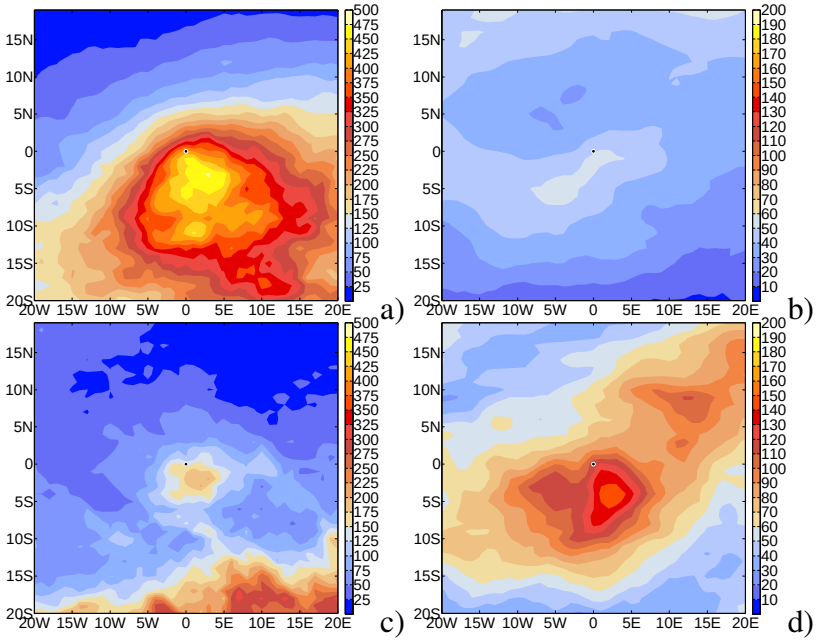

Figure B.29: Comparison between summer season type (upper row) and winter season type (lower row) for CAPE (left side) and SRH (right side) during the event. The black dots mark the position of the tornado events.

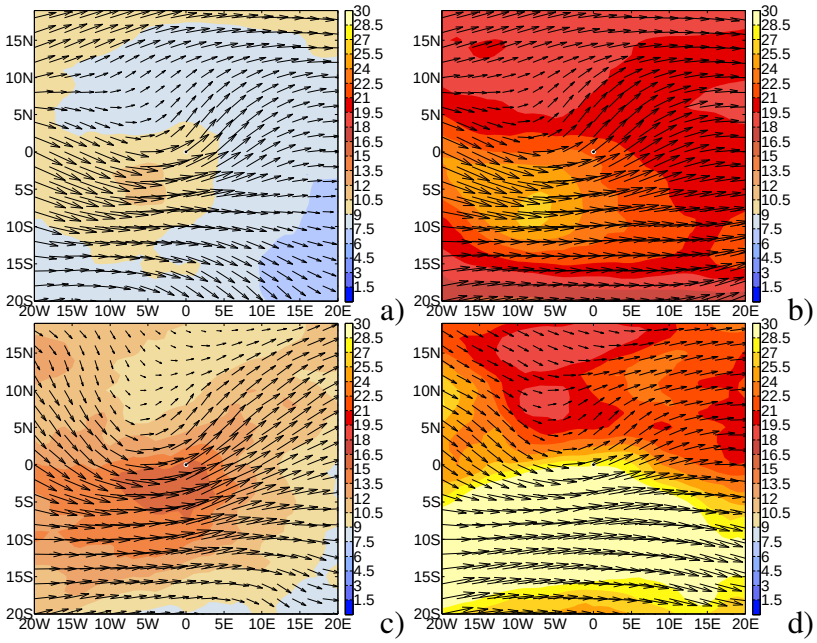

Figure B.30: Comparison between summer season type (upper row) and winter season type (lower row) for wind velocity in m s^{-1} on 700 hPa (left side) and on 250 hPa (right side) during the event. The black dots mark the position of the tornado events.

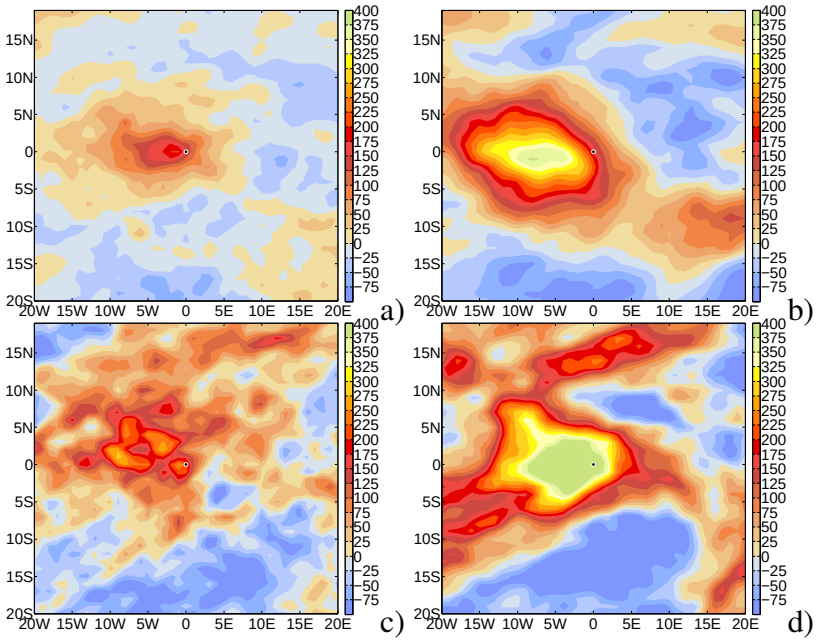

Figure B.31: Comparison between summer season type (upper row) and winter season type (lower row) for vorticity in 10^{-6} s^{-1} on 850 hPa (left side) and on 250 hPa (right side) during the event. The black dots mark the position of the tornado events.

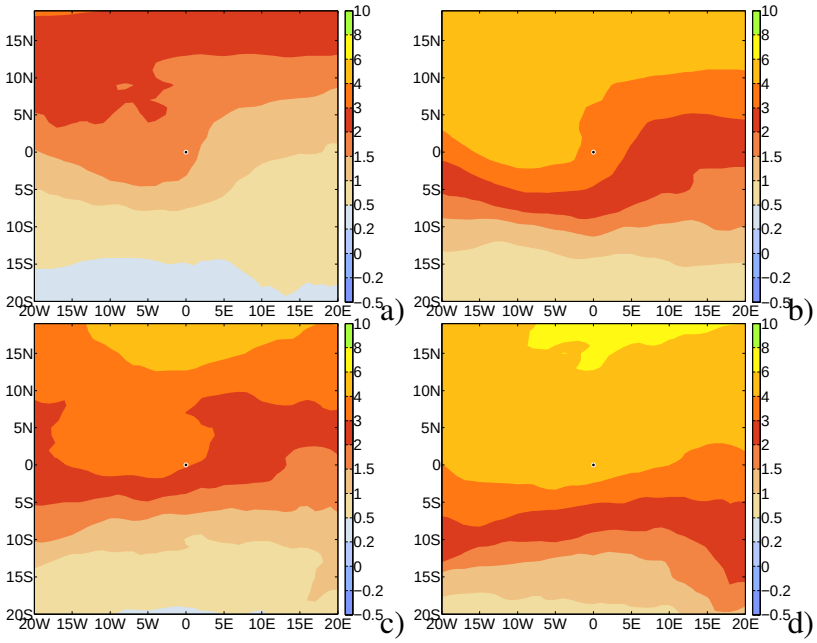

Figure B.32: Comparison between summer season type (upper row) and winter season type (lower row) for PV in PVU on the 320 K Θ-level (left side) and on the 330 K Θ-level (right side) during the event. The black dots mark the position of the tornado events.

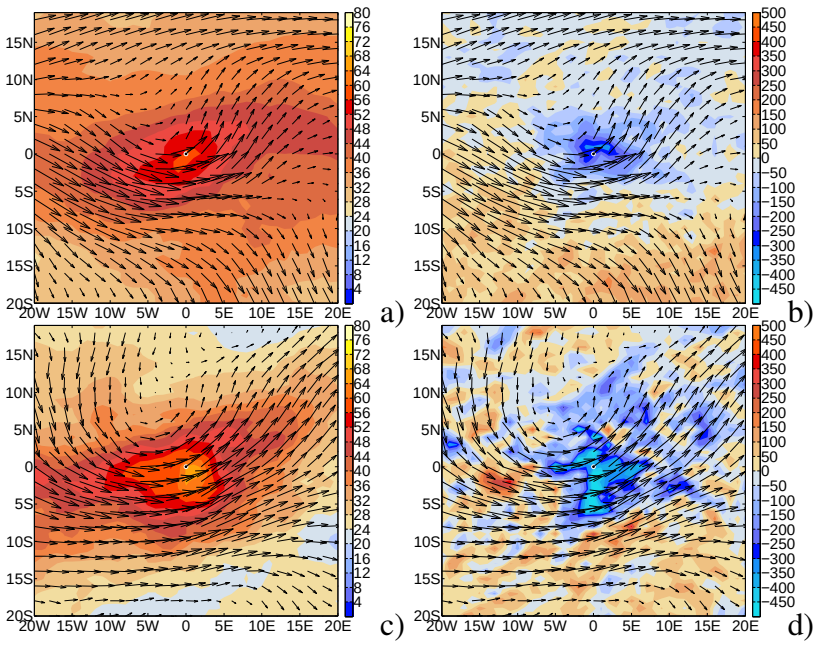

Figure B.33: Comparison between summer season type (upper row) and winter season type (lower row) for moisture flux in 10^{-3} kg m s^{-1} on 850 hPa (left side) and moisture flux convergence (negative values) in 10^{-3} kg m s^{-1} on 850 hPa (right side) during the event. The black dots mark the position of the tornado events.

B.2.3 Weak and damaging

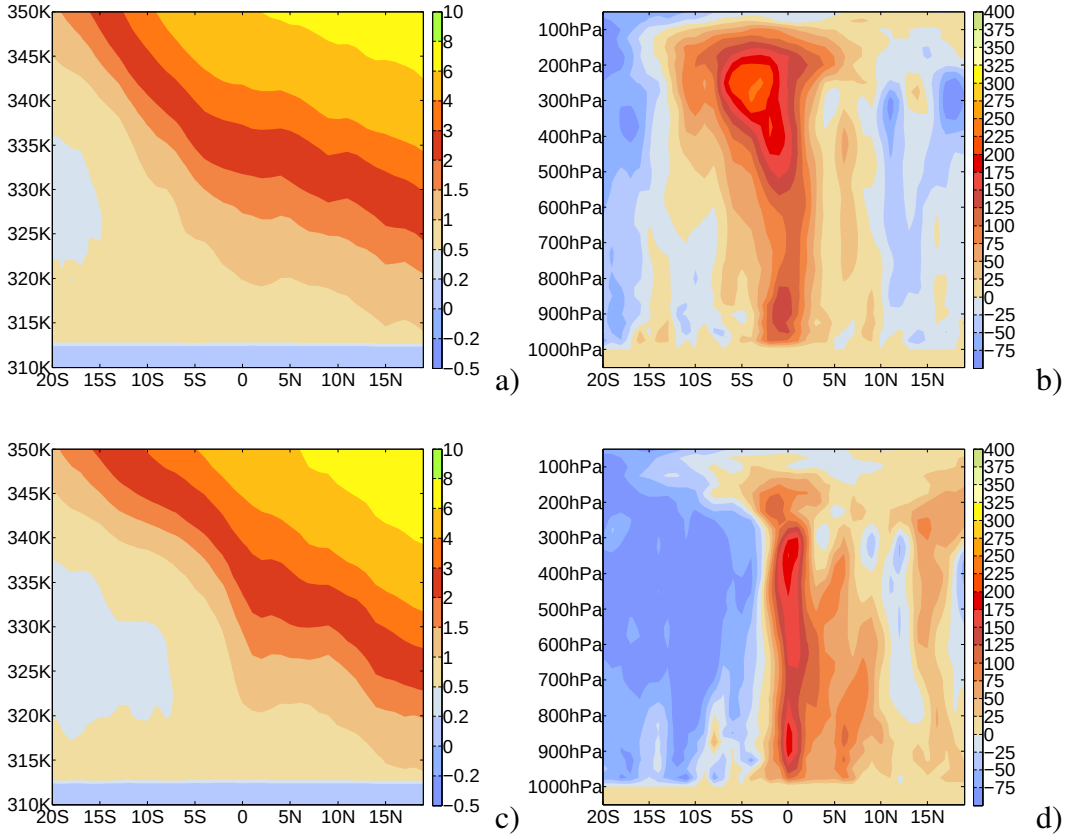

Figure B.34: Comparison between weak (F0) type (upper row) and damaging (F1+) type (lower row) for a north-south PV [PVU] cross section (left side) and a north-south vorticity [10^{-6} s^{-1}] cross section (right side) during the event.

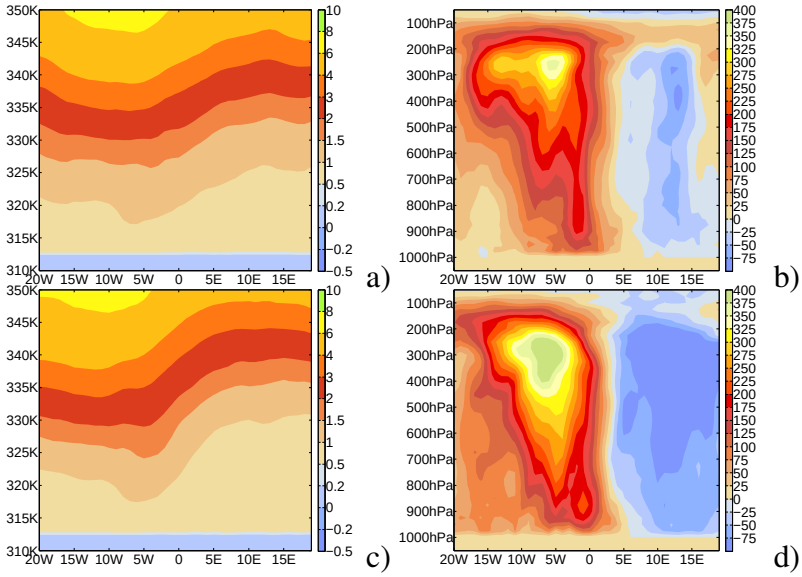

Figure B.35: Comparison between weak (F0) type (upper row) and damaging (F1+) type (lower row) for a west-east PV [PVU] cross section (left side) and a west-east vorticity [10^{-6} s^{-1}] cross section (right side) during the event.

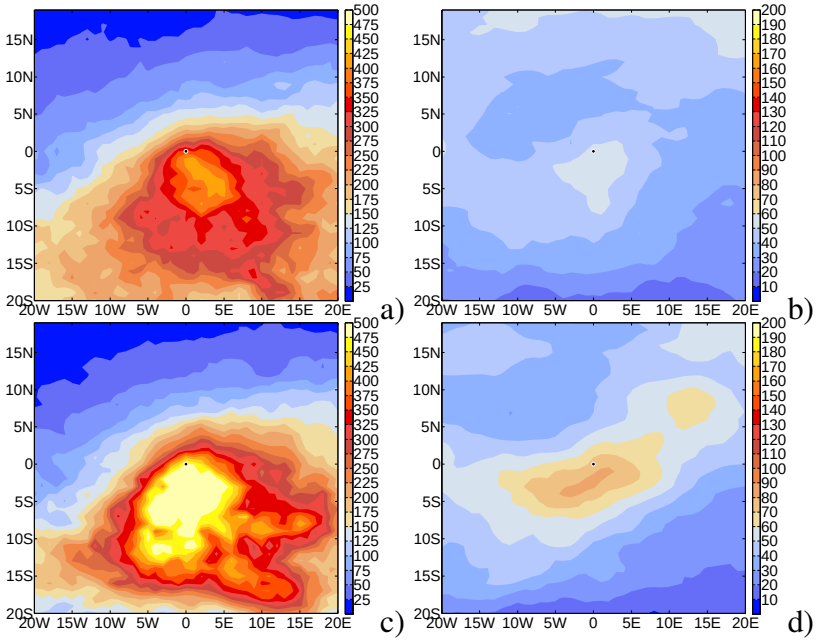

Figure B.36: Comparison between weak (F0) type (upper row) and damaging (F1+) type (lower row) for CAPE (left side) and SRH (right side) during the event. The black dots mark the position of the tornado events.

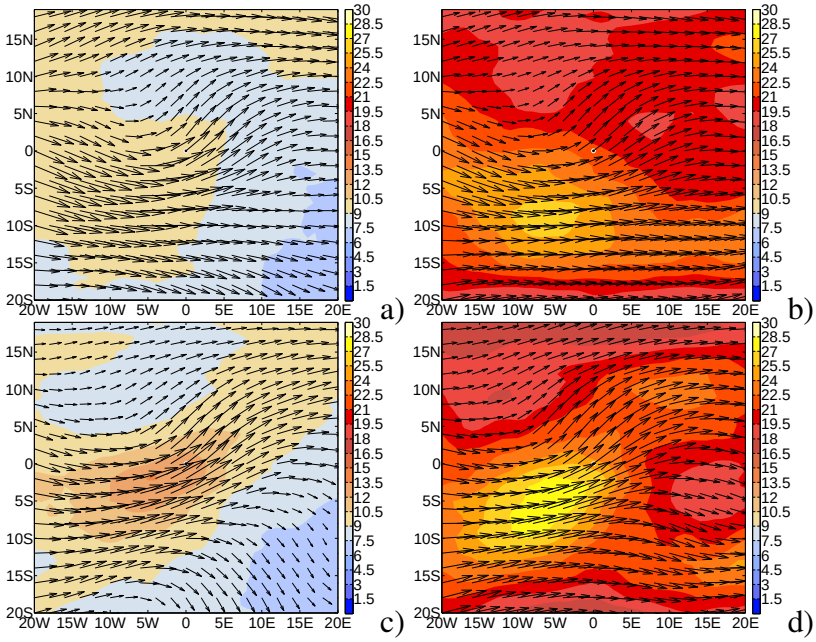

Figure B.37: Comparison between weak (F0) type (upper row) and damaging (F1+) type (lower row) for wind velocity in m s^{-1} on 700 hPa (left side) and on 250 hPa (right side) during the event. The black dots mark the position of the tornado events.

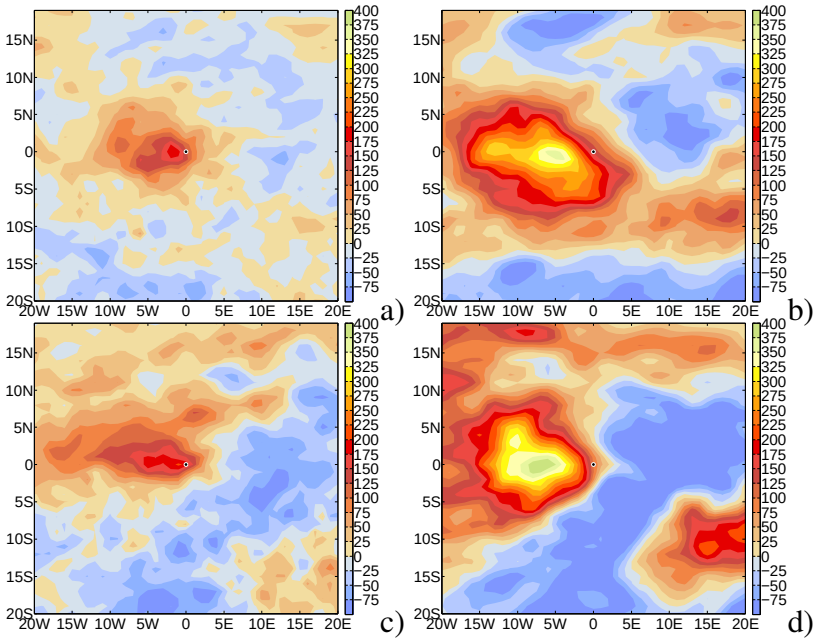

Figure B.38: Comparison between weak (F0) type (upper row) and damaging (F1+) type (lower row) for vorticity in 10^{-6} s^{-1} on 850 hPa (left side) and on 250 hPa (right side) during the event. The black dots mark the position of the tornado events.

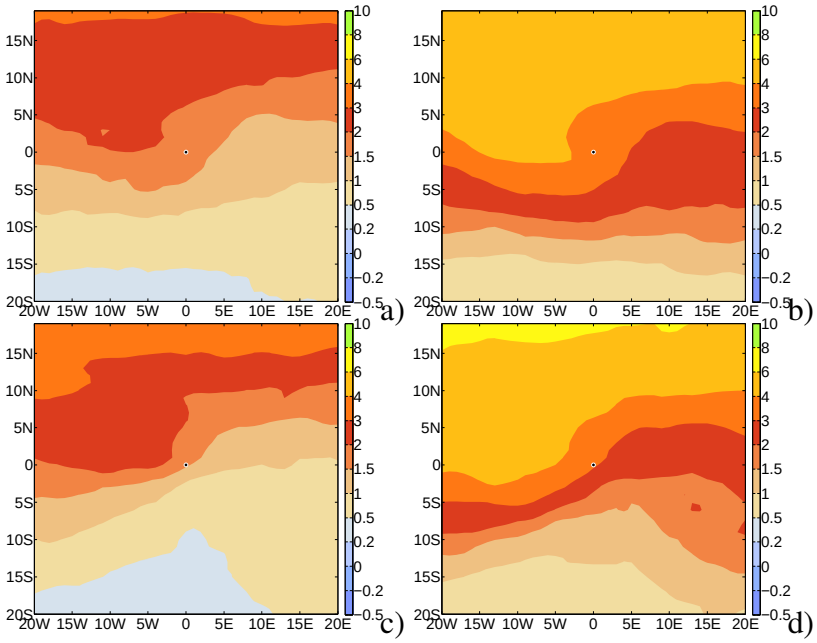

Figure B.39: Comparison between weak (F0) type (upper row) and damaging (F1+) type (lower row) for PV in PVU on the 320 K Θ-level (left side) and on the 330 K Θ-level (right side) during the event. The black dots mark the position of the tornado events.

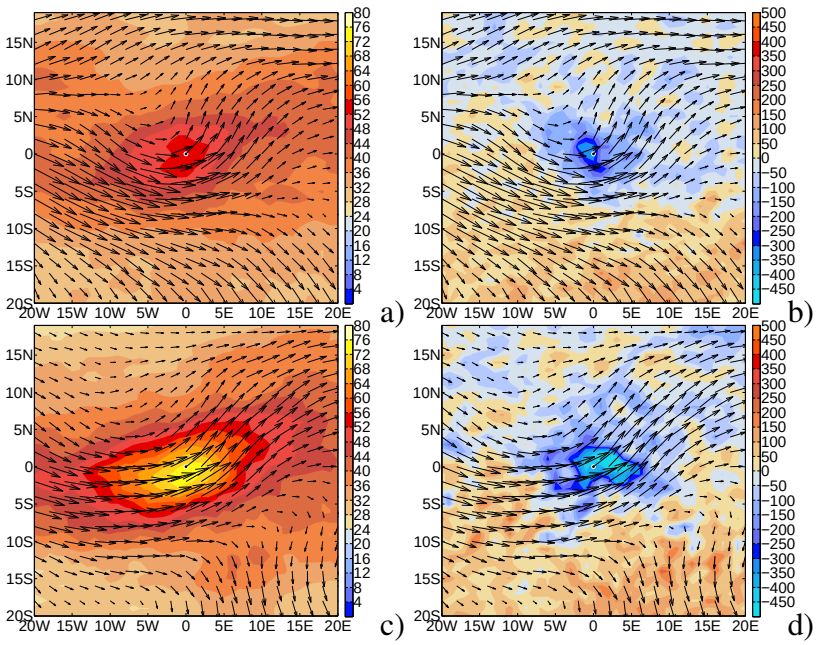

Figure B.40: Comparison between weak (F0) type (upper row) and damaging (F1+) type (lower row) for moisture flux in 10^{-3} kg m s^{-1} on 850 hPa (left side) and moisture flux convergence (negative values) in 10^{-3} kg m s^{-1} on 850 hPa (right side) during the event. The black dots mark the position of the tornado events.

B.3 Case studies

B.3.1 Cut-off case

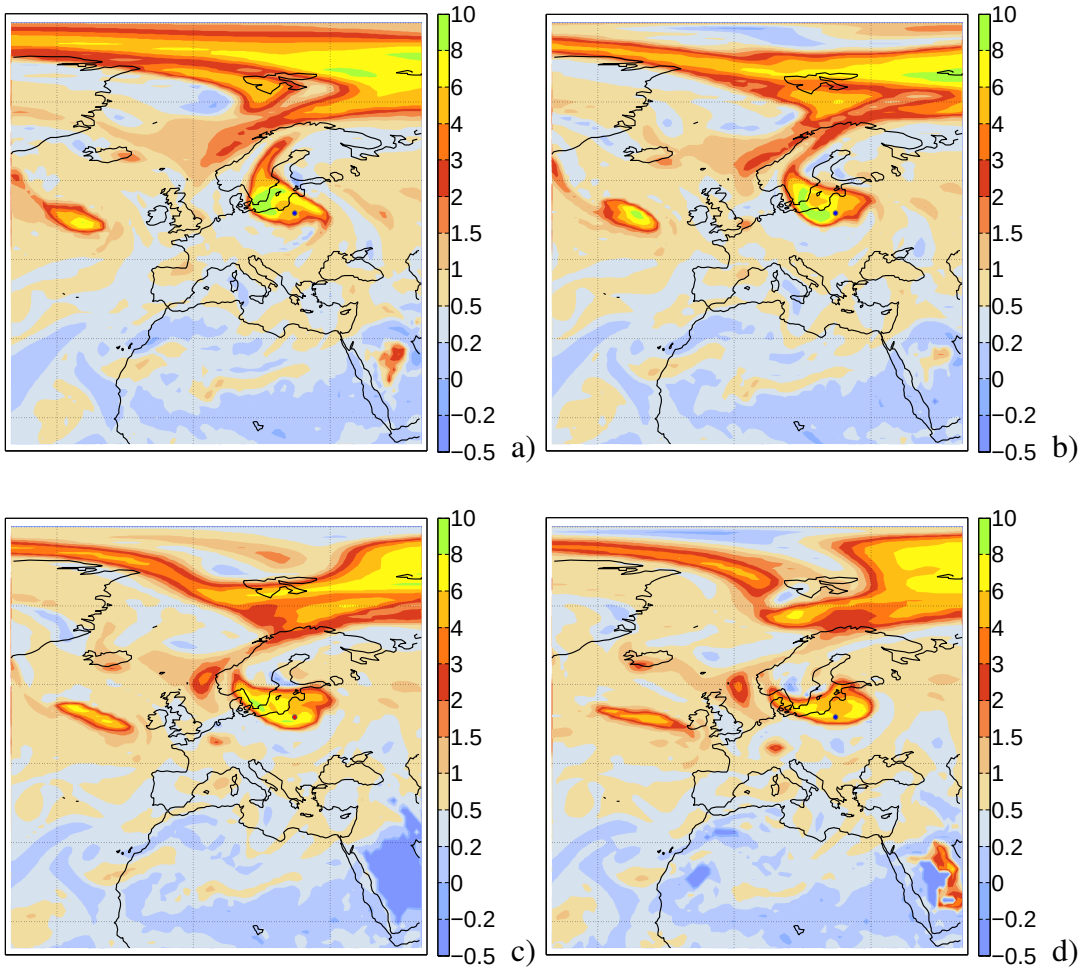

Figure B.41: Temporal evolution of potential vorticity (PV) on 320 K in [PVU] a) 12 h before, b) 6 h before, c) during and d) 6 h after the tornado event. The blue respectively red point (during the tornado event) marks the position of the tornado.

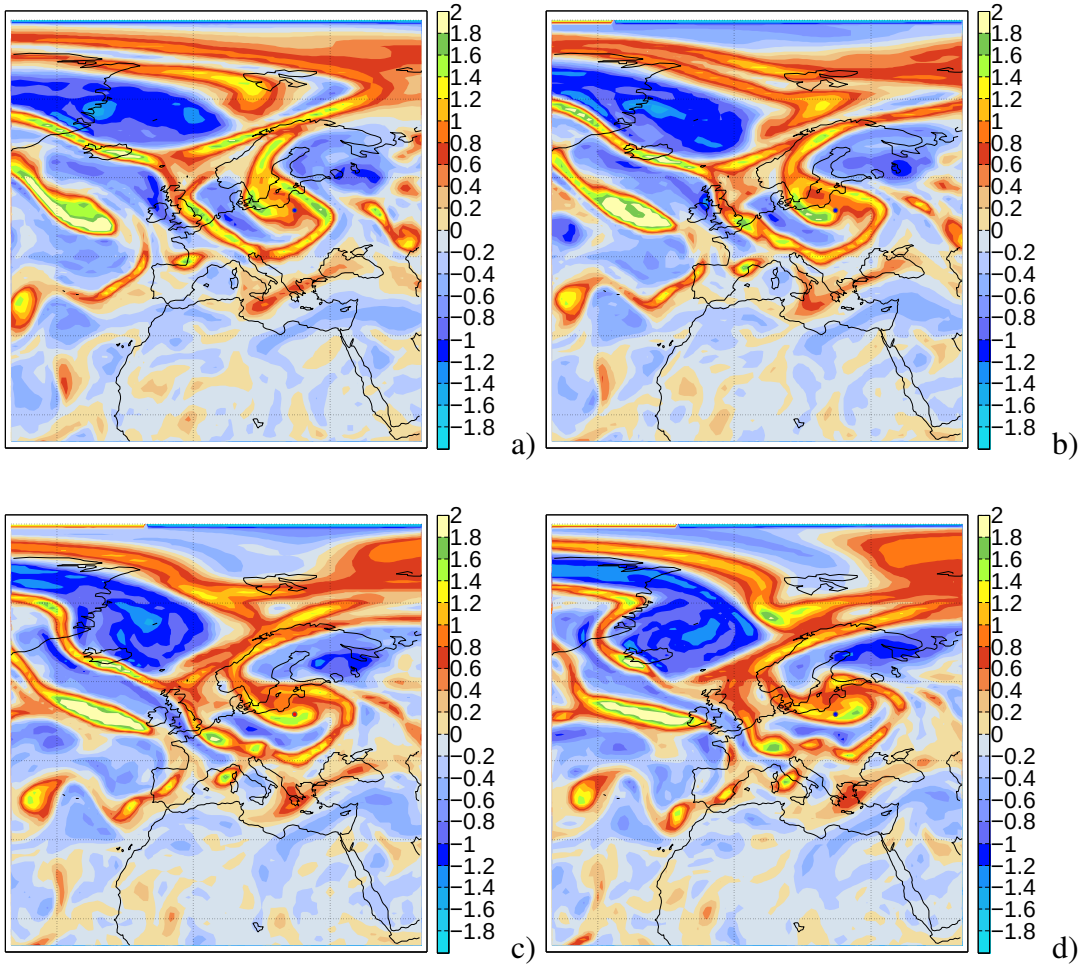

Figure B.42: Temporal evolution of vorticity on 250 hPa in [10^{-4} s^{-1}] a) 12 h before, b) 6 h before, c) during and d) 6 h after the tornado event. The blue respectively red point (during the tornado event) marks the position of the tornado.

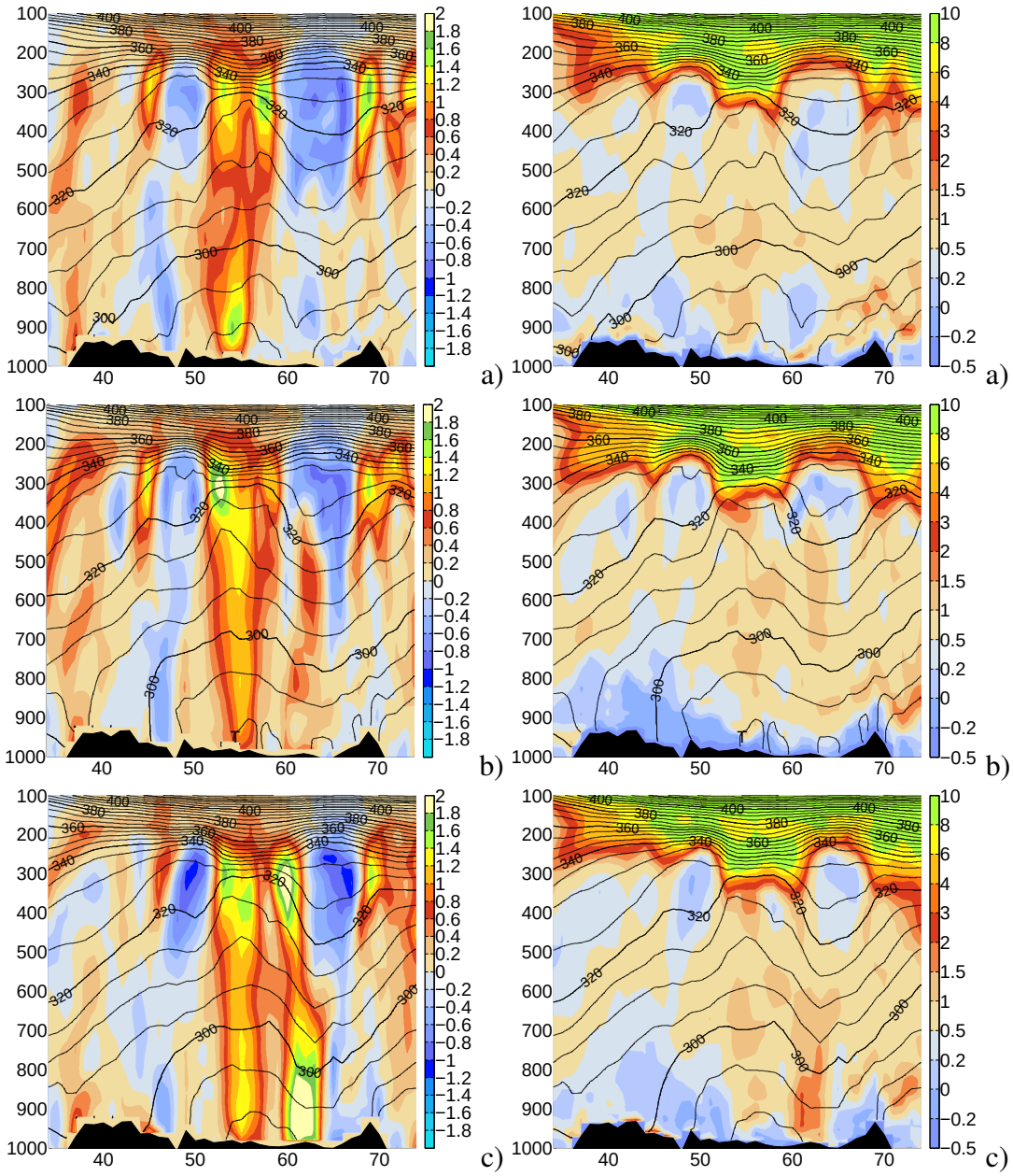

Figure B.43: Vertical cross section of vorticity in [10^{-4} s^{-1}] (left side) and PV in [PVU] (right side) in north-south direction a) 6 h before, b) during and c) 6 h after the tornado event. Solid contours denote isentropic levels in K.

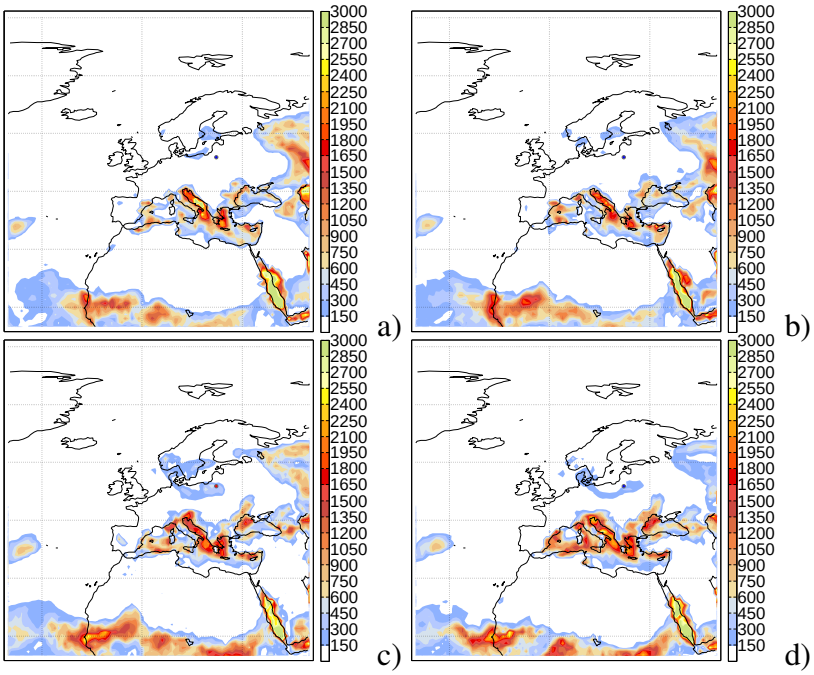

Figure B.44: Temporal evolution of most unstable CAPE in [J kg^{-1}] a) 12 h before, b) 6 h before, c) during and d) 6 h after the tornado event. The blue respectively red point (during the tornado event) marks the position of the tornado.

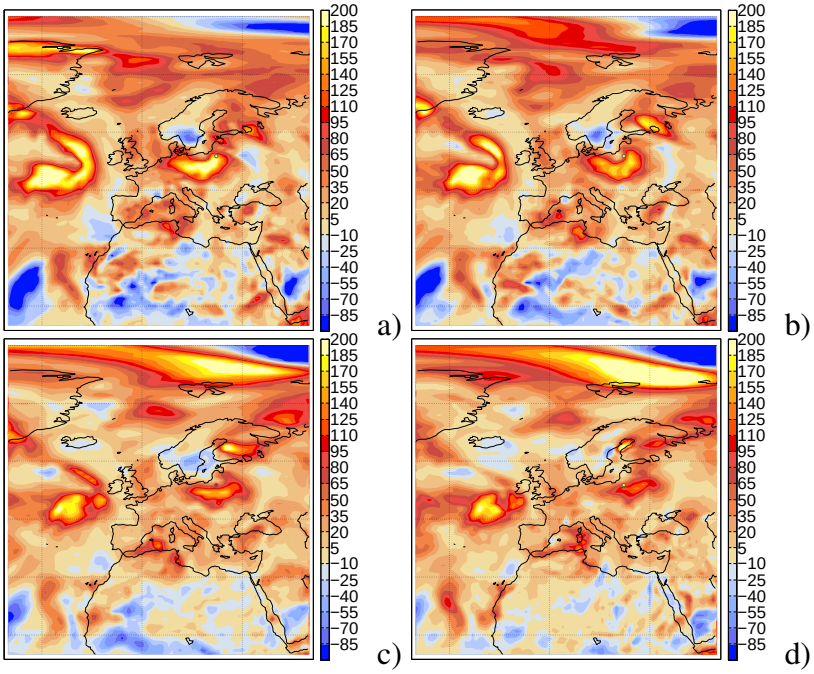

Figure B.45: Temporal evolution of storm-relative helicity (SRH) in [J kg^{-1}] a) 12 h before, b) 6 h before, c) during and d) 6 h after the tornado event. The yellow respectively red point (during the tornado event) marks the position of the tornado.

B.3.2 PV streamer case

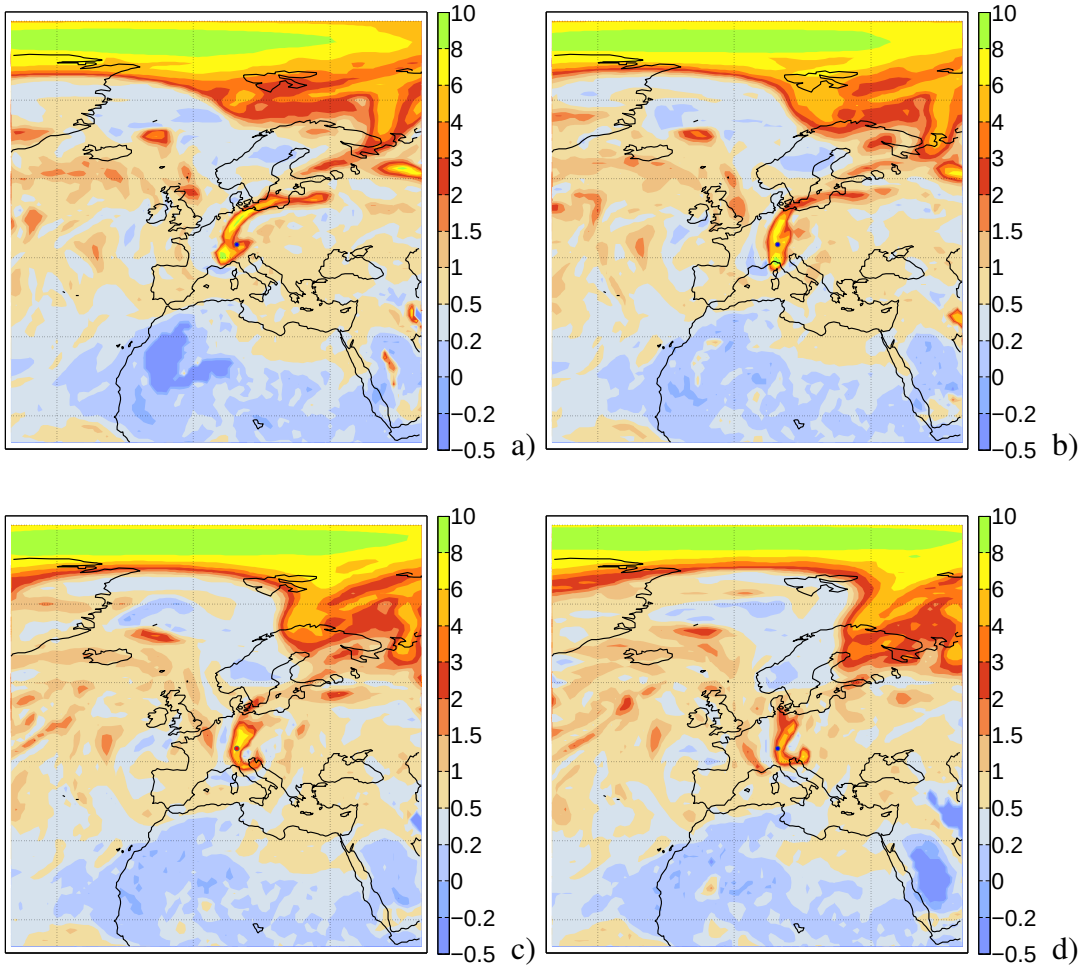

Figure B.46: Temporal evolution of potential vorticity (PV) on 320 K in [PVU] a) 12 h before, b) 6 h before, c) during and d) 6 h after the tornado event. The blue respectively red point (during the tornado event) marks the position of the tornado.

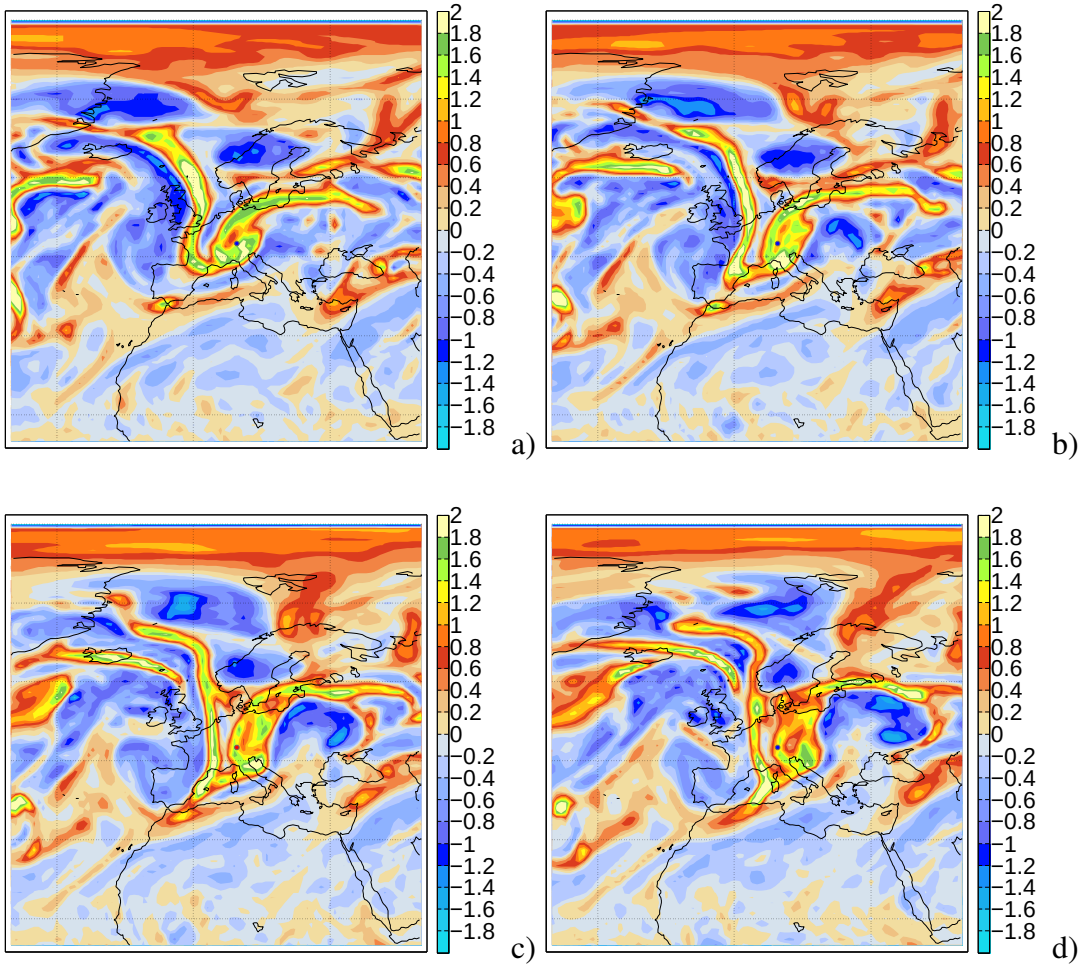

Figure B.47: Temporal evolution of vorticity on 250 hPa in [10^{-4} s^{-1}] a) 12 h before, b) 6 h before, c) during and d) 6 h after the tornado event. The blue respectively red point (during the tornado event) marks the position of the tornado.

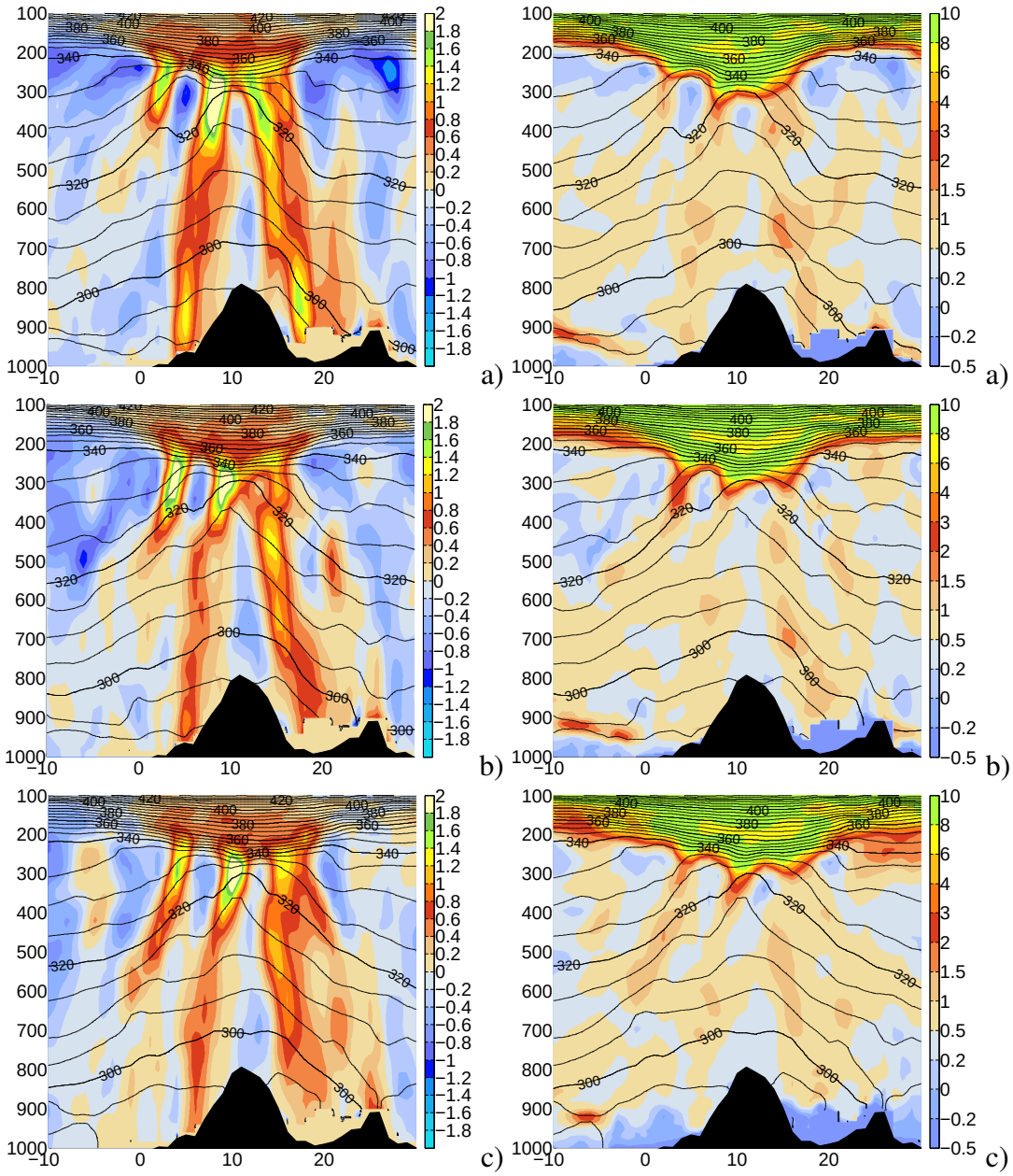

Figure B.48: Vertical cross section of vorticity (left side) in [10^{-4} s^{-1}] and PV (right side) in [PVU] in west-east direction a) 6 h before, b) during and c) 6 h after the tornado event. Solid contours denote isentropic levels in K.

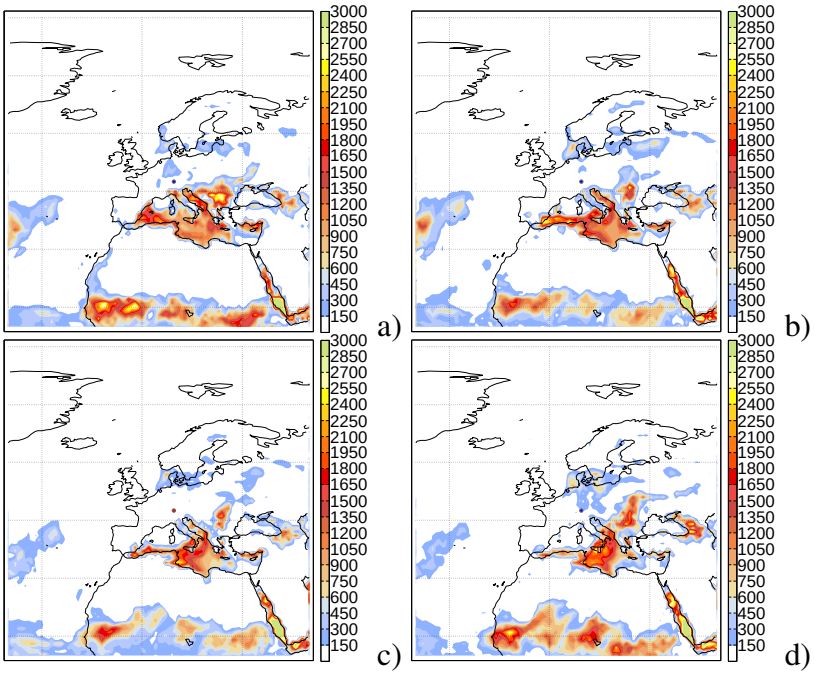

Figure B.49: Temporal evolution of most unstable CAPE in [J kg^{-1}] a) 12 h before, b) 6 h before, c) during and d) 6 h after the tornado event. The blue respectively red point (during the tornado event) marks the position of the tornado.

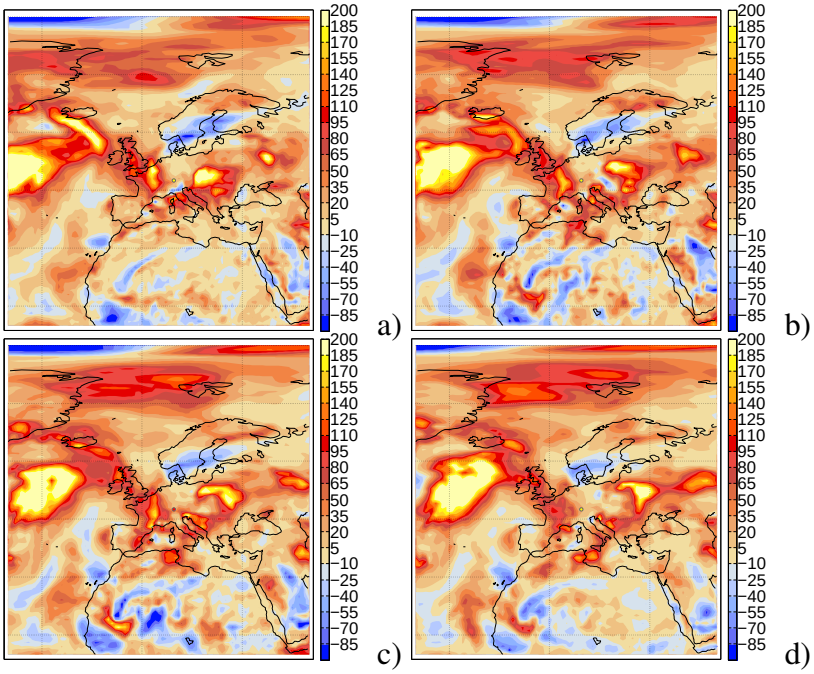

Figure B.50: Temporal evolution of storm-relative helicity (SRH) in [J kg^{-1}] a) 12 h before, b) 6 h before, c) during and d) 6 h after the tornado event. The yellow respectively red point (during the tornado event) marks the position of the tornado.

B.3.3 MCS case

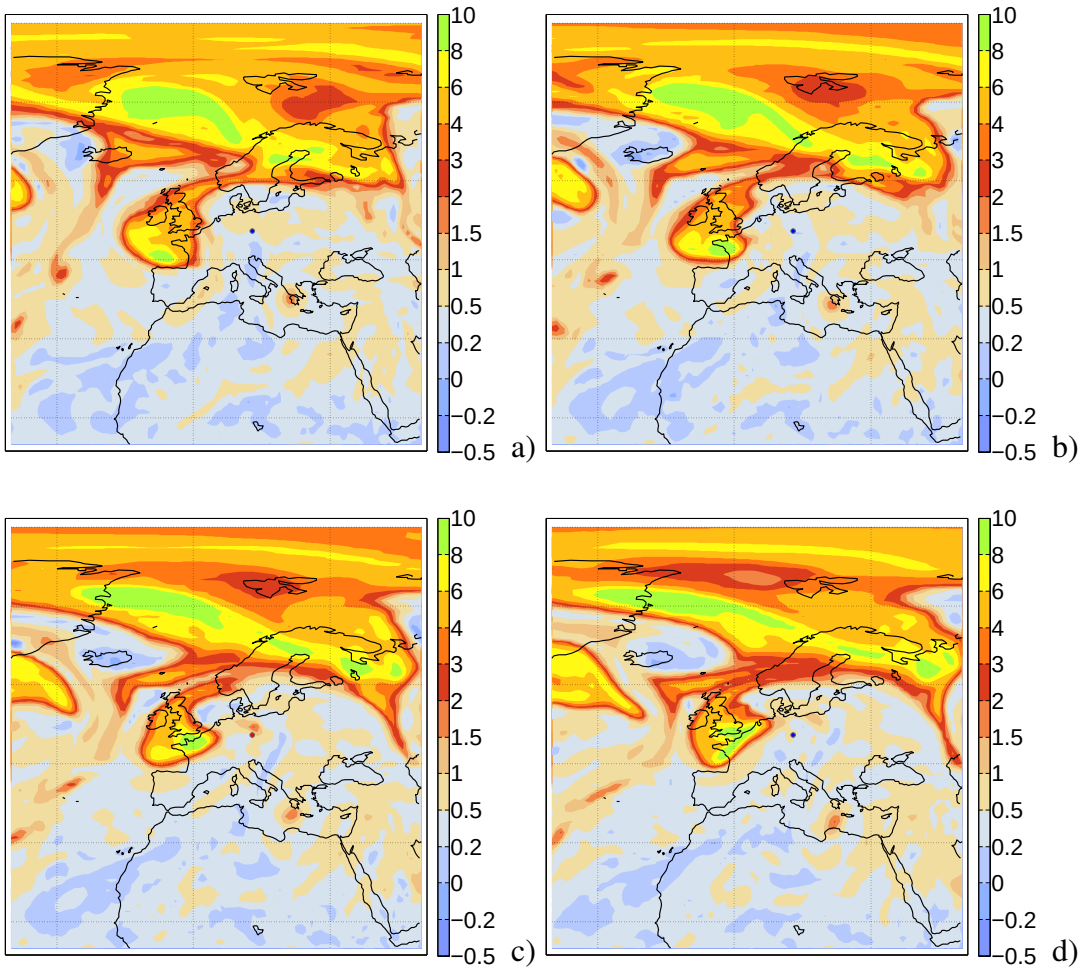

Figure B.51: Temporal evolution of potential vorticity (PV) on 325 K in [PVU] a) 12 h before, b) 6 h before, c) during and d) 6 h after the tornado event. The blue respectively red point (during the tornado event) marks the position of the tornado.

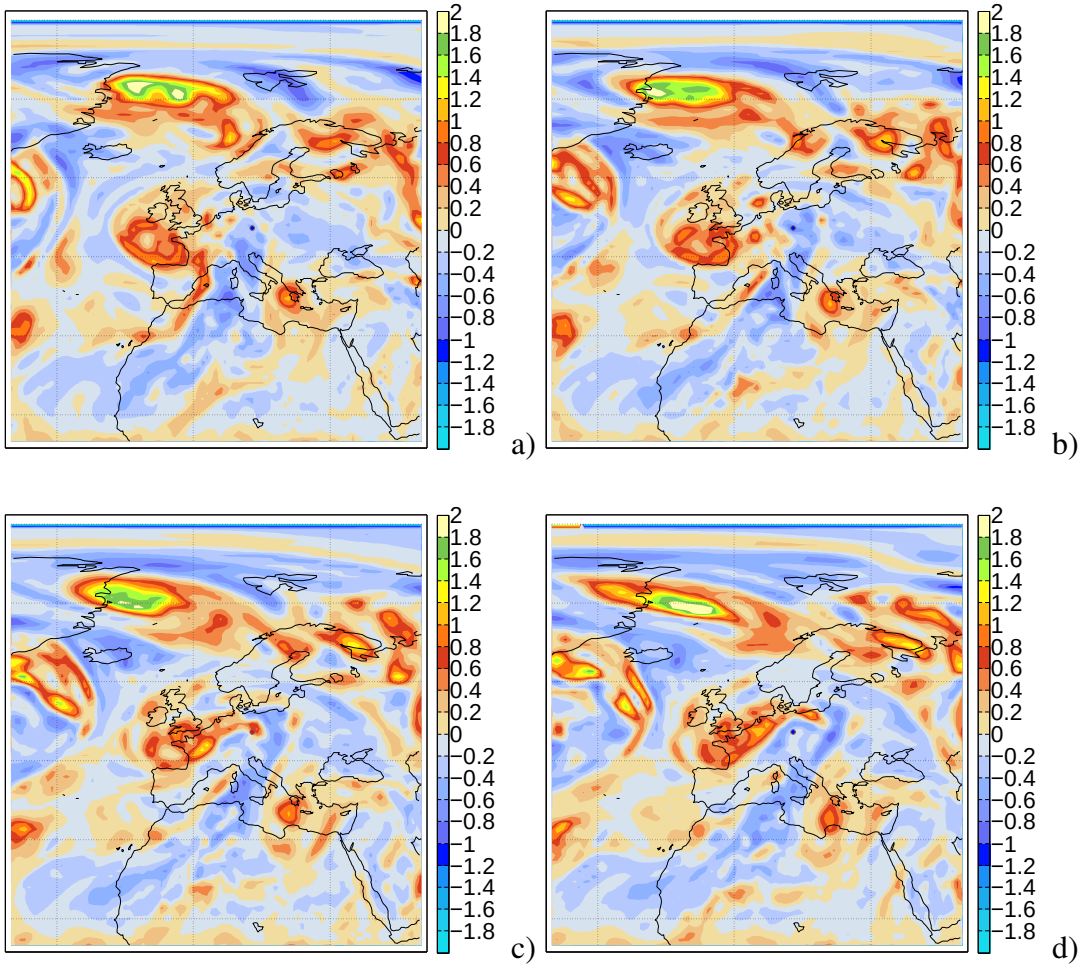

Figure B.52: Temporal evolution of vorticity on 500 hPa in [10^{-4} s^{-1}] a) 12 h before, b) 6 h before, c) during and d) 6 h after the tornado event. The blue respectively red point (during the tornado event) marks the position of the tornado.

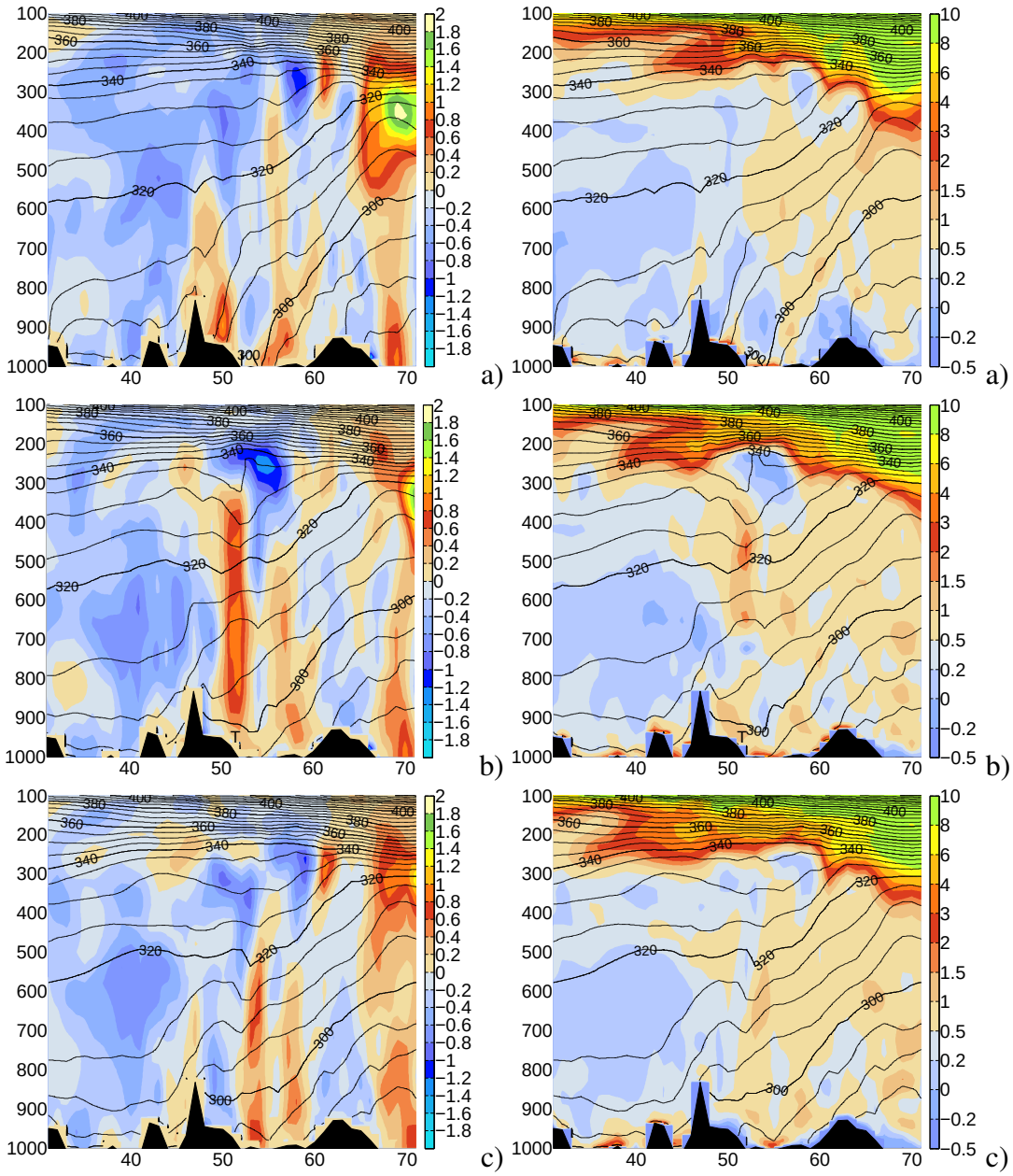

Figure B.53: Vertical cross section of vorticity (left side) in [10^{-4} s^{-1}] and PV (right side) in [PVU] in north-south direction a) 6 h before, b) during and c) 6 h after the tornado event. Solid contours denote isentropic levels in K.

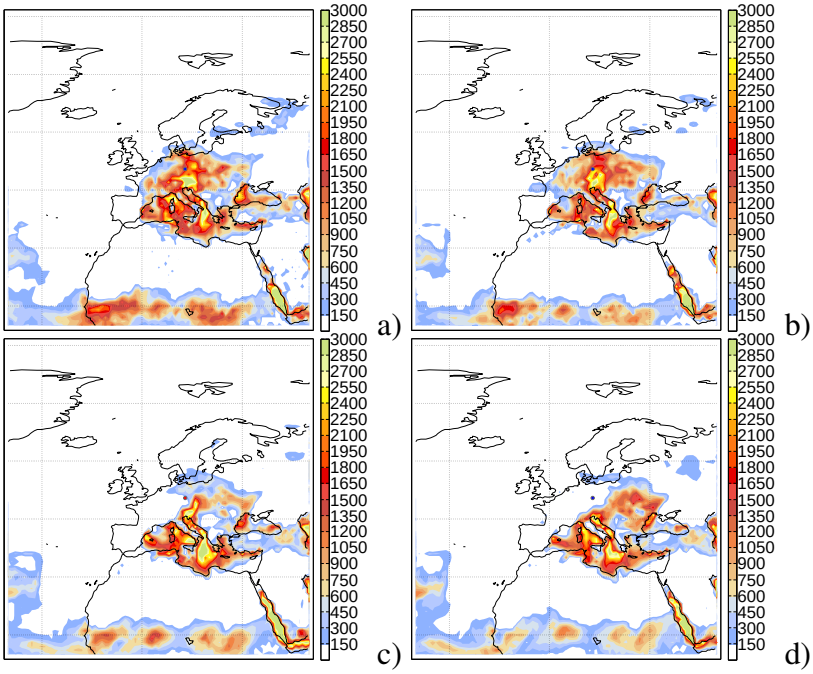

Figure B.54: Temporal evolution of most unstable CAPE in [J kg^{-1}] a) 12 h before, b) 6 h before, c) during and d) 6 h after the tornado event. The blue respectively red point (during the tornado event) marks the position of the tornado.

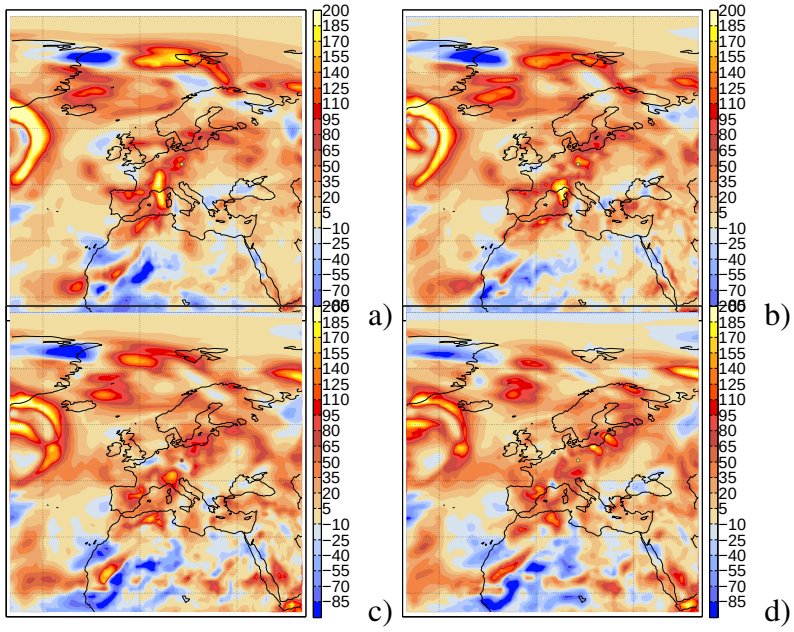

Figure B.55: Temporal evolution of storm-relative helicity (SRH) in [J kg^{-1}] a) 12 h before, b) 6 h before, c) during and d) 6 h after the tornado event. The yellow respectively red point (during the tornado event) marks the position of the tornado.